



January 2012

# Computation Of The Response Of Thin Piezoelectric Films

Marc Cierzan

Follow this and additional works at: <https://commons.und.edu/theses>

---

## Recommended Citation

Cierzan, Marc, "Computation Of The Response Of Thin Piezoelectric Films" (2012). *Theses and Dissertations*. 1279.  
<https://commons.und.edu/theses/1279>

This Thesis is brought to you for free and open access by the Theses, Dissertations, and Senior Projects at UND Scholarly Commons. It has been accepted for inclusion in Theses and Dissertations by an authorized administrator of UND Scholarly Commons. For more information, please contact [zeinebyousif@library.und.edu](mailto:zeinebyousif@library.und.edu).

COMPUTATION OF THE RESPONSE OF THIN PIEZOELECTRIC FILMS

by

Marc A. Cierzan  
Bachelor of Mechanical Engineering, University of North Dakota, 2008

A Thesis

Submitted to the Graduate Faculty

of the

University of North Dakota

in partial fulfillment of the requirements

for the degree of

Master of Science

Grand Forks, North Dakota

August

2012

Copyright 2012 Marc Cierzan

This thesis, submitted by Marc A. Cierzan in partial fulfillment of the requirements for the Degree of Master of Science from the University of North Dakota, has been read by the Faculty Advisory Committee under whom the work has been done and is hereby approved.

---

Dr. Marcellin Zahui, Chairperson

---

Dr. George Bibel

---

Dr. Matthew Cavalli

This thesis meets the standards for appearance, conforms to the style and format requirements of the Graduate School of the University of North Dakota, and is hereby approved.

---

Dr. Wayne Swisher  
Dean of the Graduate School

7/25/2012  
Date

## PERMISSION

Title: Computation of the Response of Thin Piezoelectric Films

Department: Mechanical Engineering

Degree: Master of Science

In presenting this thesis in partial fulfillment of the requirements for a graduate degree from the University of North Dakota, I agree that the library of this University shall make it freely available for inspection. I further agree that permission for extensive copying for scholarly purposes may be granted by the professor who supervised my thesis work or, in his absence, by the chairperson of the department or the dean of the Graduate School. It is understood that any copying or publication or other use of this thesis or part thereof for financial gain shall not be allowed without my written permission. It is also understood that due recognition shall be given to me and to the University of North Dakota in any scholarly use which may be made of any material in my thesis.

Signature \_\_\_\_\_  
Marc Cierzan

Date 7/25/2012

## TABLE OF CONTENTS

LIST OF FIGURES .....	ix
LIST OF TABLES .....	xii
LIST OF VARIABLES .....	xiii
ACKNOWLEDGMENTS .....	xvii
ABSTRACT .....	xviii
CHAPTER	
I.    INTRODUCTION .....	1
1.1 Literature Review .....	1
1.2 Thesis Objectives and Significance .....	6
1.3 Approach .....	7
1.4 Thesis Layout .....	9
II.   PIEZOELECTRIC SHELL VIBRATION THEORY .....	11
2.1 Fundamentals .....	11
2.2 Distributed Sensing of Elastic Shells .....	25
2.2.1 Generic Shape .....	26
2.2.2 Spatial Thickness Shaping .....	28
2.2.3 Spatial Surface Shaping .....	30
2.3 Cylindrical Shell .....	31
2.4 Plate Substrate .....	34
2.3 Beam Substrate .....	36

III.	INTRODUCTION TO FINITE ELEMENT ANALYSIS AND SIMULATION .....	38
	3.1 Analysis Methods .....	38
	3.2 ANSYS Element Characteristics.....	39
	3.2.1 Element Type .....	39
	3.2.2 Element Degrees of Freedom.....	39
	3.2.3 Element Real Constants.....	40
	3.2.4 Element Material Properties .....	40
	3.2.5 Node and Element Loads.....	40
	3.2.6 Element KEYOPT Options.....	41
	3.3 Structural Elements.....	41
	3.3.1 BEAM4.....	41
	3.3.2 SHELL63 .....	45
	3.4 ANSYS Verication Manual Test Examples .....	50
	3.4.1 VM19: Random Vibration Analysis of a Deep Simply-Supported Beam.....	50
	3.4.2 VM203: Dynamic Load Effect on Supported Thick Plate .....	52
IV.	ANALYSES FORMULATION.....	56
	4.1 Analyses Procedures.....	56
	4.1.1 Mode Frequency Analysis .....	56
	4.1.2 Spectrum Analysis.....	57
	4.1.3 Harmonic Response Analysis .....	57
	4.2 Mode Frequency Analysis .....	58
	4.2.1 Formulation.....	58
	4.3 Spectrum Analysis.....	63

4.3.1	Response Spectrum .....	63
4.3.2	Dynamic Design Analysis Method (DDAM) .....	64
4.3.3	Power Spectral Density (PSD) Approach.....	64
4.3.4	Single Point Response Random Vibration Analysis .....	64
4.3.5	Random Vibration Method Formulation .....	65
4.3.6	Response Power Spectral Densities and Mean Square Response .....	67
4.4	Harmonic Response Analysis.....	69
4.4.1	Formulation.....	69
4.4.2	Complex Displacement Output.....	70
4.4.3	Nodal and Reaction Load Computation .....	71
4.4.4	Mode Superposition Method.....	72
V.	MODELING AND SIMULATION .....	78
5.1	ANSYS Parametric Design Language.....	78
5.2	Beam Modeling .....	79
5.3	Beam Simulation .....	81
5.3.1	Mode Frequency Analysis .....	81
5.3.2	Single Point PSD Spectrum Random Vibration Analysis .....	82
5.3.3	Harmonic Response Analysis .....	83
5.4	Processing of ANSYS Results of Beam in Matlab.....	84
5.5	Plate Modeling .....	88
5.6	Plate Simulation.....	91
5.6.1	Mode Frequency Analysis .....	92
5.6.2	Single Point PSD Spectrum Random Vibration Analysis .....	94



5.6.3 Harmonic Response Analysis .....	95
5.7 Processing of ANSYS Results of Plate in Matlab.....	96
5.8 Cylindrical Shell Modeling .....	103
5.9 Cylindrical Shell Simulation .....	106
5.9.1 Mode Frequency Analysis .....	106
5.9.2 Single Point PSD Spectrum Random Vibration Analysis .....	108
5.9.3 Harmonic Response Analysis .....	108
5.10 Processing of ANSYS Results of Cylindrical Shell in Matlab .....	109
5.11 Conclusions and Future Scope .....	116
APPENDICES .....	118
APPENDIX A.....	119
APPENDIX B.....	123
APPENDIX C.....	129
APPENDIX D.....	132
APPENDIX E .....	140
APPENDIX F .....	143
APPENDIX G.....	155
APPENDIX H.....	158
APPENDIX I.....	175
REFERENCES .....	181

## LIST OF FIGURES

Figure	Page
2.1. A Piezoelectric Sensor Bonded to Shell Structure	12
2.2. Spatial Thickness Shaping	29
2.3. Spatial Surface Shaping	30
2.4. Cylindrical Shell with a Shaped Sensor Adhered	32
2.5. A Rectangular Plate Bonded with a Piezoelectric Sensor	36
2.6. Top View of Beam with PVDF Sensor	37
3.1. BEAM4 Geometry	42
3.2. BEAM4 Stress Output	44
3.3. SHELL63 Geometry	46
3.4. SHELL63 Stress Output	49
3.5. Simply-Supported Beam Problem Sketch	51
3.6. Thick Square Plate Problem Sketch	53
3.7. Harmonic Response to Uniform PSD Force	54
4.1. (a) Single-Point and (b) Multi-Point Response Spectra	63
5.1. Node Creation using APDL Code	80
5.2. Element Creation using APDL Code	80
5.3. Clamped-Free Aluminum Beam	81
5.4. First Mode Shape of Cantilevered Beam (28.057 Hz)	81
5.5. Second Mode Shape of Cantilevered Beam (175.81 Hz)	82

5.6. Third Mode Shape of Cantilevered Beam (492.18 Hz)	82
5.7. FRF Plot of Clamped-Free Beam	83
5.8. FRF Plot of Clamped-Free Beam	85
5.9. Generic Film Shape of Beam	86
5.10. Shaped Film of Beam	86
5.11. Frequency Response of Beam vs. Generic Sensor Output Charge	87
5.12. Frequency Response of Beam vs. Shaped Sensor Output Charge	88
5.13. Node Creation using APDL Code	90
5.14. Element Creation using APDL Code	90
5.15. Clamped-Free Aluminum Plate	91
5.16. First Mode Shape of Cantilevered Plate (10.881 Hz)	92
5.17. Second Mode Shape of Cantilevered Plate (40.363 Hz)	92
5.18. Third Mode Shape of Cantilevered Plate (67.644 Hz)	93
5.19. Fourth Mode Shape of Cantilevered Plate (134.34 Hz)	93
5.20. FRF Plot of Clamped-Free Plate	96
5.21. FRF Plot of Plate	98
5.22. Generic Film Shape for Plate	99
5.23. Shaped Film for Plate	100
5.24. Film Shape in Matrix Form	100
5.25. Frequency Response of Plate vs. Generic Sensor Output Charge	101
5.26. Frequency Response of Plate vs. Shaped Sensor Output Charge	102
5.27. Node on Beam Example	103
5.28. Node Creation using APDL Code	104

5.29. Element Creation using APDL Code	105
5.30. Clamped-Free Aluminum Cylindrical Shell	105
5.31. First Mode Shape of Cantilevered Cylinder (452.46 Hz)	106
5.32. Second Mode Shape of Cantilevered Cylinder (452.46 Hz)	107
5.33. Third Mode Shape of Cantilevered Cylinder (1247.6 Hz)	107
5.34. Fourth Mode Shape of Cantilevered Cylinder (1247.6 Hz)	107
5.35. Fifth Mode Shape of Cantilevered Cylinder (1550.7 Hz)	107
5.36. Sixth Mode Shape of Cantilevered Cylinder (1550.7 Hz)	108
5.37. FRF Plot of Clamped-Free Cylindrical Shell	109
5.38. FRF Plot of the Cylindrical Shell	111
5.39. Generic Film Shape for Cylindrical Shell	112
5.40. Shaped Film for Cylindrical Shell	113
5.41. Film Shape in Matrix Form	113
5.42. Frequency Response of Generic Shaped Sensor	114
5.43. Frequency Response of Shaped Sensor	115

## LIST OF TABLES

Table	Page
3.1. BEAM4 Real Constants	43
3.2. KEYOPT Options for BEAM4	44
3.3. SHELL63 Real Constants	46
3.4. KEYOPT Options for SHELL63	48
3.5. Results Comparison for VM19	52
3.6. Results Comparison for VM203	54
5.1. Geometrical and Material Properties for Cantilevered Beam	79
5.2. Frequencies at the First Six Modes	82
5.3. Geometrical and Material Properties for Cantilevered Plate	89
5.4. Frequencies at the First Six Modes	93
5.5. Natural Frequency Convergence	94
5.6. Geometrical and Material Properties for Aluminum Cylindrical Shell	103
5.7. Frequencies at the First Six Modes	108

## LIST OF VARIABLES

$\alpha_1 \alpha_2 \alpha_3$		curvilinear coordinate system
$\beta_1, \beta_2$		angles related to displacement
$\beta_{33}$		impermeability coefficient of the piezoelectric sensor
$\delta$		variation
$\varepsilon_{ij}$		strain of the $i^{th}$ surface and the $j^{th}$ direction
$\varepsilon_{ij}^{\circ}$		membrane strain of the $i^{th}$ surface and the $j^{th}$ direction
$[\epsilon]$		dielectric constant matrix
$\theta$		theta direction in cylindrical coordinates
$\kappa_{ij}$		bending strain of the $i^{th}$ surface and the $j^{th}$ direction
$\xi_j$		fraction of critical damping for mode $j$
$\rho$		mass density
$\sigma_{ij}$		mechanical stress of the $i^{th}$ surface and the $j^{th}$ direction
$\sigma$		surface charge density
$\nu$		Poisson's ratio
$\phi$		electric potential
$\phi_3^S$		total signal output in the 3 direction
$\{\phi\}_i$		eigenvector representing the mode shape of the $i^{th}$ natural frequency
$\omega$		natural frequency
$\omega_i$		$i^{th}$ natural circular frequency

$A_1$ and $A_2$	-----	Lamé parameters
$B$	-----	thickness of cylindrical shell
$[c]$	-----	elastic constant matrix
$[C]$	-----	structural damping matrix
$D$	-----	electric displacement
$\{D_j\}$	-----	electric displacement vector
$E$	-----	modulus of elasticity
$E_j$	-----	electric field strength in the $\alpha_j$ direction
$E_i^e$	-----	electric field induced by an electric displacement
$[e]$	-----	piezoelectric constant matrix
$e_{31}$	-----	PVDF sensor strain/charge coefficients in the 1 direction
$e_{32}$	-----	PVDF sensor strain/charge coefficients in the 2 direction
$F$	-----	force
$\{F\}$	-----	force vector
$F(x, y)$	-----	shape function of the sensor
$F_x$	-----	first derivative of the shape function of the sensor with respect to $x$
$F_{xx}$	-----	second derivative of the shape function of the sensor with respect to $x$
$F_y$	-----	first derivative of the shape function of the sensor with respect to $y$
$F_{yy}$	-----	second derivative of the shape function of the sensor with respect to $y$
$(f)$	-----	natural frequency
$H$	-----	enthalpy
$h^s$	-----	thickness of the sensor

$h_{ij}$  ----- strain charge coefficient of the piezoelectric sensor  
 $i, j$  ----- stress tensors: surface and direction, respectively  
 $\hat{K}$  ----- kinetic energy  
 $[K]$  ----- structural stiffness matrix  
 $L_x$  ----- dimension of the plate in the  $x$  direction  
 $L_y$  ----- dimension of the plate in the  $y$  direction  
 $[M]$  ----- mass matrix  
 $P, P'$  ----- initial and end points, respectively  
 $Q$  ----- surface charge per unit area  
 $q$  ----- charge output of PVDF film  
 $R$  ----- radius of cylindrical shell  
 $R_1$  and  $R_2$  ----- radii of curvatures in the 1 and 2 directions  
 $r_1, r_2$  - distance measured from the neutral surface to the top and bottom of the sensor layer  
 $S$  ----- surface over the volume  
 $S_{ij}$  ----- mechanical strain of the  $i^{th}$  surface and the  $j^{th}$  direction  
 $S^e$  ----- effective surface electrode area  
 $\text{sgn}(\cdot)$  ----- signum function  
 $\text{sgn}[U_3(\alpha_1, \alpha_2)]$  ----- polarity function  
 $t$  ----- surface traction  
 $t_0, t_1$  ----- initial and end time, respectively  
 $\{T_{ij}\}$  ----- stress vector  
 $U_1, U_2,$  and  $U_3$  ----- generic deflections



$U_x, U_y, \text{ and } U_z$  -----displacements in the x, y, and z directions  
 $\hat{U}$  ----- potential energy  
 $\{u\}$  ----- nodal displacement vector  
 $V$  ----- piezoelectric volume  
 $W_s(\alpha_1, \alpha_2)$  ----- weighting shape function  
 $W_t(\alpha_1, \alpha_2)$  -----spatial function  
 $w_x$  -- first partial derivative of the plate surface displacement field  $w(x,y)$  with respect to  $x$   
 $w_y$  -- first partial derivative of the plate surface displacement field  $w(x,y)$  with respect to  $y$   
 $w_{xx}$  -----second partial derivative of the plate surface displacement  
field  $w(x,y)$  with respect to  $x$   
 $w_{yy}$  -----second partial derivative of the plate surface displacement  
field  $w(x,y)$  with respect to  $y$   
 $Z$  -----length of cylindrical shell

## ACKNOWLEDGMENTS

This work would not have been possible without the support from my advisor Dr. Zahui. With the direction provided by Dr. Zahui, I learned a great deal about FEA, Vibrations and Active Noise Control. I am deeply indebted to my advisory committee for their confidence, tolerance and support during last two years. I would also like to thank the Mechanical Engineering Department at the University of North Dakota for providing the space and means to complete this research. Finally, I would like to thank my family members and fiancée, Aynsley for their support during this project.

## ABSTRACT

This work shows that a mix of Finite Element Analysis (FEA) and numerical differentiation and integration methods can be used in order to calculate the output charge of a thin piezoelectric film bonded to a shell structure. The method is applied to cases of a cylindrical shell structure, as well as a beam and plate for both generic and shaped piezoelectric films. An overview of the fundamentals of shell vibration theory is presented where the development of the piezoelectric film equation is reviewed and applied to the three different structure cases. The FEA process used is discussed in terms of mode frequency, harmonic, and spectrum analysis. The structural analysis data of the shell substrate is imported into Matlab for further processing using numerical differentiation and integration. The processed data is then used to calculate the film output charge assuming that the piezoelectric film is perfectly coupled with the structure continuum, but does not change its dynamic characteristics i.e. natural frequencies and mode shapes. The results presented herein indicate that the film correctly captures the modes of the structure. However, further investigation is needed for the film output to better predict other structural dynamic properties such as displacement, velocity, or acceleration. The proposed method can be applied to calculate the output charge of films attached to complex structures or structures with complex boundary conditions. Another application is cases where close form equations cannot be derived and the only data available are discrete or experimental. Moreover, in sensor design applications where the film is often shaped so that its output charge corresponds to a specific structural dynamic property, the proposed method greatly simplifies the design process.

# **CHAPTER I**

## **INTRODUCTION**

### **1.1 Literature Review**

Piezoelectricity is described as the appearance of positive electric charge on one side of certain nonconducting crystals and negative charge on the opposite side when the crystals are subjected to mechanical pressure. Piezoelectricity was discovered in 1880 by Paul-Jacques and Pierre Curie, who found that when they compressed certain types of crystals including quartz, tourmaline, and Rochelle salt, along certain axes, a voltage was produced on the surface of the crystal. In 1881, they observed the converse effect, the elongation of such crystals upon the application of an electric current [1]. Basically, when a piezoelectric material expands or contracts, an electric charge collects on its surface. Conversely, when a piezoelectric material is subjected to a voltage change, it mechanically deforms. Many crystalline materials exhibit piezoelectric behavior. A few materials exhibit the phenomenon strongly enough to be used in applications that take advantage of their properties. One such material is barium titanate, the first piezoceramic discovered. It is a dielectric ceramic used for capacitors and it is a piezoelectric material used for microphone and other transducers.

Now, lead zirconate titanate (PZT) is the most commonly used piezoceramic today due to its higher Curie temperature, which is the temperature above which a piezoelectric material loses its piezoelectric characteristics. Another piezoelectric material, which is not a ceramic, but a polymer, is Polyvinylidene Fluoride (PVDF).

In polymers, the polymer chains attract and repel each other when an electric field is applied, dissimilar to ceramics where its crystal structure creates the piezoelectric effect. In 1969, it was observed that PVDF had strong piezoelectric properties; having a piezoelectric coefficient of thin films as high as ten times that of any other polymer [2]. This makes it a better material for sensor applications. The electromechanical coupling of PVDF is lower than that of piezoceramics, but since the foil thickness can be as small as 10 micrometers the vibration mass is extremely small. PVDF has a low density and low cost compared to other fluoropolymers. PVDF also has greater damping than ceramics, and the resulting dynamic characteristics allow very short pulses to be generated. This means that it is possible to measure shorter ranges using PVDF than is possible with piezoceramic transducers. PVDF is more frequently being used in aeronautics and aerospace applications.

It was discovered near the beginning of the 20<sup>th</sup> century that piezoelectric materials could be used in practical applications. One such application is in the area of electrical sensing devices, also known as sensors, or more specifically, piezoelectric sensors [3]. A piezoelectric sensor is a device that uses the piezoelectric effect to measure pressure, acceleration, strain, or force by converting them to an electrical charge.

Piezoelectric materials have inherent advantages: their modulus of elasticity is comparable to that of metals, the sensing elements have almost no deflection, have high natural frequencies, and have an extreme stability even at high temperatures [4].

Applications of sensing include: medical, automotive, communication, and aerospace.

In a paper by Hurlebaus et al. [5], PVDF film was used for sensors and actuators in an automotive application. They investigated active vibration control of more complex

geometries than beams and plates. They could not evaluate modal parameters from numerical calculations of local modes, because of the complications involved with proper boundary conditions. Therefore, they identified the modal data using experimental modal analysis. The objective of their work was to demonstrate the successful implementation of modal control to arbitrary curved panels using experimentally evaluated mode shapes. The applied modal formulation for the dynamics of the considered structure was advantageous, because it allowed for control of a small set of chosen modes. Also, they significantly reduced structural vibrations, which also lead to a reduction in acoustic radiation. However, their proposed concept has some drawbacks: the limitation of the frequency band limitation of the modal analysis, and the performance of the control method was compromised by modal spillover, and curve fitting to the experimental mode shapes.

Other research, done by Xu et al. [6], has also shown that PVDF film is being used in sensing applications. Their work was focused on the development of an acoustic pressure sensor with high sensitivity for aero-acoustic and clinical applications. They proposed a sensor design consisting of micron-sized PVDF pillars and patterned electrodes in which the pillars generated a charge when subjected to normal stresses associated with acoustic waves. The pillars are sandwiched between an electrode plate and a rigid membrane. They developed a constrained optimization algorithm as a function of geometric parameters and electrical parameters of the sensor and conditioning amplifier. One potential application for their proposed micro-acoustic sensor would be vehicle positioning. It would be able to provide localization of objects around the vehicle which would create safer driving conditions.

The objective of research done by Choi et al. [7] was to enhance the damping performance for vibration suppression of rotating composite thin-walled beams using macro fiber composite actuators and PVDF sensors. They based their formulation on a thin-walled beam, including a warping function, centrifugal force, Coriolis acceleration and piezoelectric effect. They used a negative velocity feedback control algorithm to acquire adaptive capability of the beam. They performed numerical analysis using finite element method and Newmark time integration method was used to calculate the time response of the model. They observed that the feedback control gain had a linear effect on damping performance; hence, vibrations could be damped out quicker when a higher feedback control gain was applied within the limit of actuator voltage. The damping effect could be increased through structural tailoring. Furthermore, the position and distributed area of the sensor/actuator pair was an important factor in obtaining effective damping performance.

Very recent work by Song and Li [8] studied the aeroelastic flutter characteristics and active vibration control of supersonic beams. In their paper, they do further research applied to a supersonic composite laminated plate with piezoelectric actuator/sensor pairs. They used Hamilton's principle with the assumed mode method to develop the governing equation of the structural system. The impulse responses of the structural system were calculated by using the Houbolt numerical algorithm to study the active aeroelastic vibration control. From the numerical results, they observed that the aeroelastic flutter characteristics of the supersonic composite laminated plate can be improved and that the aeroelastic vibration response amplitudes can be reduced,

especially at the flutter points, by the velocity feedback control algorithm using the piezoelectric actuator/sensor pairs.

Other recent work was aimed to improve the efficiency of harvesting and reduce grain losses. Zhao et al. [9] designed a grain impact sensor utilizing PVDF films and a floating raft damping structure to monitor grain losses in the field. Through the analysis of a mathematical model of the sensor and the vibration characteristics of installation position, the sensor resonances were calculated. The performance of the sensor was verified by field experiments. They found that by using a floating raft damping structure, the acceleration amplitude and corresponding frequency spectrum of the PVDF films could be suppressed.

Saviz and Mohammedpourfard [10] presented work on the dynamic analysis of a laminated cylindrical shell with piezoelectric layers under dynamic loads. A cylindrical shell with finite length was simply supported at both ends and elasticity approach was used. The highly coupled partial differential equations are reduced to ordinary differential equations by means of trigonometric function expansion in plane directions. The resulting equations are solved by finite element method. Stress analysis and vibrational behavior are presented for different shell thicknesses and are compared for four different ring loads widths. Their worked showed that the dynamic elasticity solution provided an accurate analysis of active shell with piezoelectric layer as sensor and actuator.

In another recent paper, Benedetti et al. [11] presented a fast boundary element method for the analysis of three-dimensional solids with cracks and adhesively bonded piezoelectric patches used as strain sensors. Both the sensors and adhesive layer were modeled using a finite element approach, taking into account the full electromechanical



coupling in the piezoelectric layer. They utilize a generalized minimal residual method (GMRES) iterative solver with a preconditioner for the solution of the system of equations. They performed numerical experiments which showed that the sensor model offers accurate predictions of the output voltage.

In a paper by Alibeigloo and Kani [12], they address the free vibration problem of multilayered shells with embedded piezoelectric layers. The variable of the governing differential equation were changed to constant, and obtained the natural frequencies from the state equations. They investigated the effect of edges conditions, mid-radius to thickness ratio, length to mid-radius ratio, and the piezoelectric thickness on vibration behavior of a cylindrical shell. They consider simply-supported and clamped-clamped boundary conditions. Analytical solution was presented for the case of the simply-supported edges, whereas for the clamped-clamped boundary condition, differential quadrature method is used. They also focused on the influence of the electromechanical coupling on the free vibration response of multilayered shells. The relevance of the effectiveness of the method in predicting the exact natural frequencies of vibration was checked by comparing numerical results for the shell without the piezoelectric layer and simply-supported boundary condition with corresponding numerical results from previous literature.

## **1.2 Thesis Objectives and Significance**

The vibration response of PVDF piezoelectric film in the context of sensor or actuator application is often investigated for structures with infinite radii of curvatures such as beams and plates. The objective is to develop a method to calculate the piezoelectric film output charge on any type of structure. In this research, a mix of finite

element and numerical differentiation and integration methods are utilized in order to calculate the output charge of a thin piezoelectric film which is bonded to a shell structure. Due to the complexity of structures, simple structures: a beam, a plate, and a cylindrical shell are used in this investigation. Generic and shaped films of the aforementioned structures are discussed. The proposed method can be applied to calculate the output charge of films attached to complex structures or structures with complex boundary conditions. An application is cases where close-form equations cannot be derived and the only data available are discrete or experimental. Furthermore, the proposed method greatly simplifies the design process in sensor design applications where the film is often shaped so that its output charge corresponds to a specific structural dynamic property.

### **1.3 Approach**

An approach to providing a way to calculate the output charge of a piezoelectric sensor can be found by looking at the generic output charge equation as described in Chapter II. In the equation, if the displacements are known, then the first and second partial derivatives of those displacements can be found, and therefore, the equation can be solved numerically. The displacement field can be obtained through measurement or finite element analysis. Then, another program, like Matlab, can be used to accomplish numerical differentiation and integration required by the piezoelectric charge equation. The results of the output charge equation are then obtained. This process is applied to the three structures: beam, plate, and cylindrical shell. The generic output charge equation is reduced for these structures to find their respective output charge equations, and a shaping function is added for the use of a shaped sensor to verify that the proposed

method can be applied to non-generic shaped sensors which can be designed to monitor specific nodes, such as a quadratic shape which was applied in this present work. This research employs ANSYS, a finite element analysis program, in order to model and simulate all three of the structures mentioned. Numerical differentiation and integration processes are then used with the program, Matlab, to determine the generic and shaped sensor output charges corresponding to the displacement frequency response of the coupled films' structures. The dynamic responses, i.e. natural frequencies and mode shapes of the film are finally compared to that of the structure.

In contrast to [5], the work in this thesis is focused on simple geometries: beams, plates, and cylindrical shells. Also, they use PVDF film as a point sensor, whereas here it covers the whole surface; hence, spillover may be reduced in this thesis by the implementation of a shaping function. In [6], they do not cover an entire surface with thin PVDF film, instead they use pillars of PVDF sandwiched between 2 rigid plates. Different from [7], the geometries used here do not include a thin-walled beam, do not include an actuator, and the sensor spans the entire length of the substrate. In [8], they used a simply supported composite plate; in contrast to work done here, the main focus is on a clamped-free aluminum beam, plate, and cylindrical shell. They are also interested in active vibration control, so they include an actuator and control algorithms in their analysis. In [9], they used three rectangularly-shaped sensors to measure vibration, whereas in this work, one sensor will be used which will cover an entire surface of a structure and also quadratically-shaped. In contrast to [10], they analyze rings, whereas in this work a beam, plate, and cylindrical shell are analyzed. Different from [11], they modeled a beam with small rectangularly-shaped sensors all along the length of the beam

instead of a sensor which covers the entire surface of a beam. Although, in [12] they investigate the vibration of a cylindrical shell, they focus on comparing different boundary conditions. They solved an eigenfrequency equation to obtain natural frequencies and then obtained state equations. However, they did not use dynamic output to numerically solve a film output charge equation in order to capture the dynamic of the substrate.

#### **1.4 Thesis Layout**

In Chapter II of this thesis, piezoelectric shell vibration theory is introduced. This theory employs Love's equations of motion, which are used to derive the generic film output charge equations for arbitrary curved shells. These equations are simplified for cylindrical shells, plates, and beams. Then, a shaping function is added to the generic film output charge equation in order to verify that a shaped film can correctly capture the dynamic of the substrate. The sensors are assumed to span the entire length of the substrates. ANSYS is introduced in Chapter III, discussing the different element types involved in this study. Two verification manual test examples are performed and discussed which pertain to the simulation of the structures. In Chapter IV, a general procedure for the analyses and formulations used in this process are presented from ANSYS. In Chapter V, the structures of the aluminum beam, plate, and cylindrical shell are modeled and simulated using ANSYS. A random excitation force is applied to the structures and the nodal displacements of the structure are exported to Matlab for numerical differentiation and integration of the displacements. The output charges of the sensors are calculated using the output charge equation for the three structures. The modes of the output charge equations are compared to the frequency responses of the

structure substrates. This research shows that the proposed method can be an effective tool for correctly capturing the modes of a given structure for a given film.

## CHAPTER II

### PIEZOELECTRIC SHELL VIBRATION THEORY

In order to obtain the output charge of a given structure, the development of the output charge equation must be the first task. In the equation, if the displacements are known, then the first and second derivatives of those displacements can be found, and therefore, the equation can be solved numerically. The displacement field can be obtained through measurement or finite element analysis. Then, another program, like Matlab, can be used to accomplish numerical differentiation and integration required by the equation. The results of the output charge equation are then obtained. This chapter discusses the general piezoelectric shell vibration theory and a general output charge equation is developed. The generic output charge equation is applied to these structures to find their respective output charge equations, and a shaping function is added for the use of a shaped sensor to verify the method can be applied to non-generic shaped sensors which can be designed to monitor specific nodes.

#### 2.1 Fundamentals

In this section, derivations of generic piezoelectric shell theories are reviewed based on linear piezoelectricity and Hamilton's principle presented by Tzou [13]. Figure 2.1 depicts a generic piezoelectric shell continuum defined in a tri-orthogonal curvilinear coordinate system with  $\alpha_1$  and  $\alpha_2$  defining the shell neutral surface and  $\alpha_3$  the normal direction. The shell sensor has a constant thickness  $h^S$  which is much thinner than the shell structure and its radii of curvatures,  $R_1$  and  $R_2$ , such that the strains in the film are

assumed constant and equal to the outer surface strains of the shell. Generic deflections:  $U_1$ ,  $U_2$ , and  $U_3$ , in three principal directions, respectively:  $\alpha_1$ ,  $\alpha_2$ , and  $\alpha_3$ , are assumed to be small. The piezoelectric sensor is perfectly coupled with the shell continuum, but does not change its dynamic characteristics.

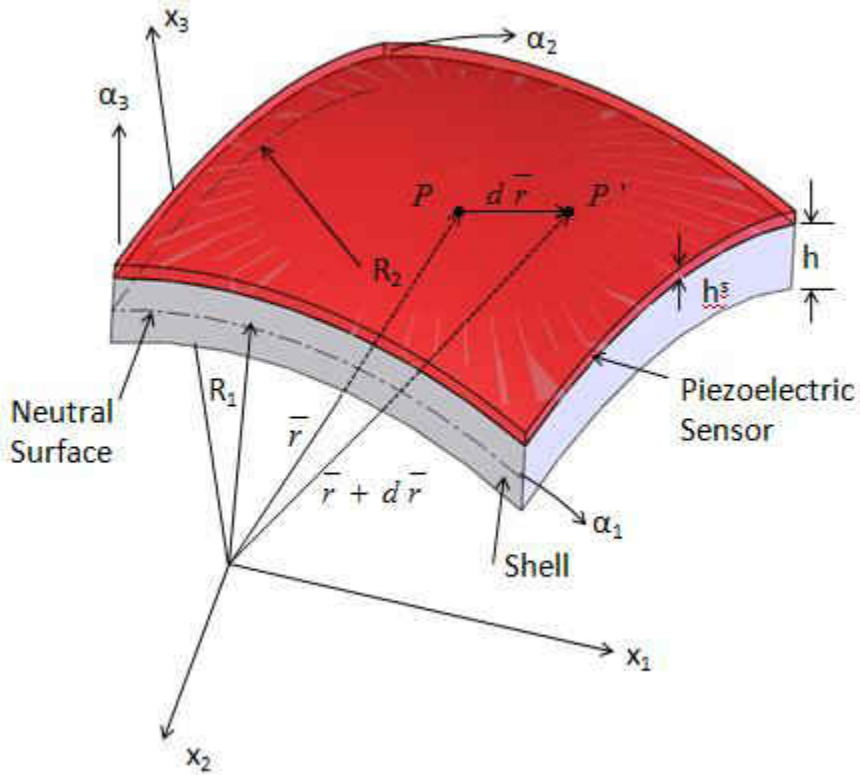


Figure 2.1: A Piezoelectric Sensor Bonded to a Shell Structure

In this section, some fundamental physical laws are defined, including Hamilton's principle which is the fundamental basis of all theoretical derivations performed.

Hamilton's principle is written as:

$$\delta \int_{t_0}^{t_1} dt [\hat{K} - \hat{U}] = 0 \quad (2.1)$$

where  $\hat{K}$  is the kinetic energy;  $\hat{U}$  is the total potential energy (including the mechanical energy, electric energy, and work done by externally applied forces and charge);  $\delta$  is the variation with respect to the variable that follows, in this case kinetic energy and total

potential energy. For a piezoelectric continuum subjected to a prescribed surface traction  $t$  and a surface charge per unit area  $Q$ , Hamilton's principle states:

$$\delta \int_{t_0}^{t_1} dt \int_V \left[ \frac{1}{2} \rho \dot{U}_j \dot{U}_j \right] dV - \left\{ \int_{t_0}^{t_1} dt \int_V [H(S_{ij}, E_j)] dV - \int_{t_0}^{t_1} dt \int_S (t_j \delta U_j - Q_j \delta \phi) dS \right\} = 0 \quad (2.2)$$

where  $H(S_{ij}, E_j)$  is the electric enthalpy;  $\rho$  is the mass density;  $U_j$  is the deflection in the  $\alpha_j$  direction;  $S_{ij}$  is the mechanical strain of the  $i^{th}$  surface and the  $j^{th}$  direction;  $E_j$  is the electric field strength in the  $\alpha_j$  direction;  $Q_j$  is the surface charge;  $\phi$  is the electric potential;  $V$  is the piezoelectric volume considered;  $S$  is the surface over the volume.

Electric field  $E_j$  and potential  $\phi$  relations in the curvilinear coordinate system are defined as:

$$E_1 = \frac{1}{A_1 \left( 1 + \frac{\alpha_3}{R_1} \right)} \frac{\partial \phi}{\partial \alpha_1} \quad (2.3)$$

$$E_2 = \frac{1}{A_2 \left( 1 + \frac{\alpha_3}{R_2} \right)} \frac{\partial \phi}{\partial \alpha_2} \quad (2.4)$$

$$E_3 = - \frac{\partial \phi}{\partial \alpha_3} \quad (2.5)$$

where  $A_1$  and  $A_2$  are the Lamé parameters from the fundamental equation:

$$(ds)^2 = A_1^2 (d\alpha_1)^2 + A_2^2 (d\alpha_2)^2 \quad (2.6)$$

$A_1$  and  $A_2$  may also be referred to as the fundamental form parameters and  $R_1$  and  $R_2$  are the radii of curvatures of  $\alpha_1$  and  $\alpha_2$  axes, respectively. The Lamé parameters are



named after the French mathematician, Gabriel Lamé, well known for his work of curvilinear coordinates. From Figure 2.1, the infinitesimal distance between points  $P$  and  $P'$  can be defined on the neutral surface. The differential change  $d\bar{r}$  of the vector  $\bar{r}$  moving from  $P$  to  $P'$  is  $d\bar{r} = \frac{d\bar{r}}{\partial\alpha_1}d\alpha_1 + \frac{d\bar{r}}{\partial\alpha_2}d\alpha_2$  [14]. The magnitude  $ds$  of  $d\bar{r}$  is

obtained by  $(ds)^2 = d\bar{r} \cdot d\bar{r}$ . The following can be defined which produces Eq. 2.6:

$$\frac{\partial\bar{r}}{\partial\alpha_1} \cdot \frac{\partial\bar{r}}{\partial\alpha_1} = \left| \frac{\partial\bar{r}}{\partial\alpha_1} \right|^2 = A_1^2 \quad \text{and} \quad \frac{\partial\bar{r}}{\partial\alpha_2} \cdot \frac{\partial\bar{r}}{\partial\alpha_2} = \left| \frac{\partial\bar{r}}{\partial\alpha_2} \right|^2 = A_2^2.$$

In general, linear piezoelectric relations of a piezoelectric continuum can be described as:

$$\begin{aligned} \{T_{ij}\} &= [c]\{S_{ij}\} - [e]^T \{E_j\} \\ \{D_j\} &= [e]\{S_{ij}\} + [\epsilon]\{E_j\} \end{aligned} \quad (2.7)$$

where  $\{T_{ij}\}$  is the stress vector induced by two effects: mechanical and electrical [13].

$[c]$  is the elastic constant matrix;  $[e]$  is the piezoelectric constant matrix;  $\{S_{ij}\}$  is the mechanical strain of the  $i^{\text{th}}$  surface in the  $j^{\text{th}}$  direction;  $\{E_j\}$  is the electric field strength in the  $\alpha_j$  direction;  $\{D_j\}$  is the electric displacement vector;  $[\epsilon]$  is the dielectric constant matrix. Eq. (2.7) denotes the converse piezoelectric effect and the direct piezoelectric effect. The direct piezoelectric effect is the internal generation of electrical charge which is the result of an applied mechanical force. Whereas the converse piezoelectric effect is the internal generation of a mechanical strain due to an applied electrical field [4]. A piezoelectric material with a symmetrical hexagonal structure ( $C_{6v} = 6mm$ ) is isotropic in the transverse  $\alpha_3$  but is anisotropic in the  $\alpha_1$  and  $\alpha_2$

directions. When an electric field having the same polarity and orientation as the original polarization field is placed across the thickness of a piezoelectric shell, the material expands along the axis of polarization (thickness direction) and contracts perpendicular to the axis of polarization. If it is polarized in the thickness direction,  $[c]$ ,  $[e]$ , and  $[\epsilon]$  matrices are defined as [13]:

$$[c] = \begin{bmatrix} c_{11} & c_{12} & c_{13} & 0 & 0 & 0 \\ c_{12} & c_{11} & c_{13} & 0 & 0 & 0 \\ c_{13} & c_{13} & c_{33} & 0 & 0 & 0 \\ 0 & 0 & 0 & c_{44} & 0 & 0 \\ 0 & 0 & 0 & 0 & c_{44} & 0 \\ 0 & 0 & 0 & 0 & 0 & c_{66} \end{bmatrix} \quad (2.8)$$

$$[e] = \begin{bmatrix} 0 & 0 & 0 & 0 & e_{15} & 0 \\ 0 & 0 & 0 & e_{24} & 0 & 0 \\ e_{31} & e_{32} & e_{33} & 0 & 0 & 0 \end{bmatrix} \quad (2.9)$$

$$[\epsilon] = \begin{bmatrix} \epsilon_{11} & 0 & 0 \\ 0 & \epsilon_{11} & 0 \\ 0 & 0 & \epsilon_{33} \end{bmatrix} \quad (2.10)$$

where  $c_{66} = (c_{11} - c_{12})/2$ . Note  $e_{31} = e_{32}$  for the 6 mm structure. If a piezoelectric material is electrically polarized, but is not mechanically stretched in the process,  $e_{24} = e_{15}$ .

Based on these matrices, enthalpy H can be written as:

$$\begin{aligned} H = & \frac{1}{2} (\sigma_{11} S_{11} + \sigma_{22} S_{22} + \sigma_{12} S_{12} + \sigma_{13} S_{13} + \sigma_{23} S_{23} + \sigma_{33} S_{33}) \\ & - (e_{15} E_1 S_{13} + e_{15} E_2 S_{23} + e_{31} E_3 S_{11} + e_{31} E_3 S_{22} + e_{33} E_3 S_{33}) \\ & - \frac{1}{2} (\epsilon_{11} E_1^2 + \epsilon_{11} E_2^2 + \epsilon_{33} E_3^2) \end{aligned} \quad (2.11)$$

The strain-displacement relationships as defined in [14]:

$$\varepsilon_{11} = \frac{1}{1 + \alpha_3/R_1} (\varepsilon_{11}^\circ + \alpha_3 \kappa_{11}) \quad (2.12)$$

$$\varepsilon_{22} = \frac{1}{1 + \alpha_3/R_2} (\varepsilon_{22}^\circ + \alpha_3 \kappa_{22}) \quad (2.13)$$

$$\varepsilon_{12} = \frac{1}{(1 + \alpha_3/R_1)(1 + \alpha_3/R_2)} \cdot \left[ \left( 1 - \frac{\alpha_3^2}{R_1 R_2} \right) \varepsilon_{12}^\circ + \alpha_3 \left( 1 + \frac{\alpha_3}{2R_1} + \frac{\alpha_3}{2R_2} \right) \kappa_{12} \right] \quad (2.14)$$

where the membrane strains are

$$\varepsilon_{11}^\circ = \frac{1}{A_1} \frac{\partial u_1}{\partial \alpha_1} + \frac{u_2}{A_1 A_2} \frac{\partial A_1}{\partial \alpha_2} + \frac{u_3}{R_1} \quad (2.15)$$

$$\varepsilon_{22}^\circ = \frac{1}{A_2} \frac{\partial u_2}{\partial \alpha_2} + \frac{u_1}{A_1 A_2} \frac{\partial A_2}{\partial \alpha_1} + \frac{u_3}{R_2} \quad (2.16)$$

$$\varepsilon_{12}^\circ = \frac{A_2}{A_1} \frac{\partial}{\partial \alpha_1} \left( \frac{u_2}{A_2} \right) + \frac{A_1}{A_2} \frac{\partial}{\partial \alpha_2} \left( \frac{u_1}{A_1} \right) \quad (2.17)$$

and where the change-in-curvature terms (bending strains) are

$$\kappa_{11} = \frac{1}{A_1} \frac{\partial \beta_1}{\partial \alpha_1} + \frac{\beta_2}{A_1 A_2} \frac{\partial A_1}{\partial \alpha_2} \quad (2.18)$$

$$\kappa_{22} = \frac{1}{A_2} \frac{\partial \beta_2}{\partial \alpha_2} + \frac{\beta_1}{A_1 A_2} \frac{\partial A_2}{\partial \alpha_1} \quad (2.19)$$

$$\kappa_{12} = \frac{A_2}{A_1} \frac{\partial}{\partial \alpha_1} \left( \frac{\beta_2}{A_2} \right) + \frac{A_1}{A_2} \frac{\partial}{\partial \alpha_2} \left( \frac{\beta_1}{A_1} \right) \quad (2.20)$$

where  $\beta_1$  and  $\beta_2$  represent angles

$$\beta_1 = \frac{u_1}{R_1} - \frac{1}{A_1} \frac{\partial u_3}{\partial \alpha_1} \quad (2.21)$$

$$\beta_2 = \frac{u_2}{R_2} - \frac{1}{A_2} \frac{\partial u_3}{\partial \alpha_2} \quad (2.22)$$

Substituting Eq. (2.21) and Eq. (2.22) into Eq. (2.18) gives:

$$\kappa_{11} = \frac{1}{A_1} \frac{\partial}{\partial \alpha_1} \left[ \frac{u_1}{R_1} - \frac{1}{A_1} \frac{\partial u_3}{\partial \alpha_1} \right] + \frac{1}{A_1 A_2} \left[ \frac{u_2}{R_2} - \frac{1}{A_2} \frac{\partial u_3}{\partial \alpha_2} \right] \frac{\partial A_1}{\partial \alpha_2} \quad (2.23)$$

Since  $S_{11}$  is equivalent to  $\varepsilon_{11}$ , when substituting Eqs. (2.15) and (2.23) into Eq. (2.12)

gives:

$$S_{11} = \frac{1}{1 + \alpha_3/R_1} \left( \frac{1}{A_1} \frac{\partial u_1}{\partial \alpha_1} + \frac{u_2}{A_1 A_2} \frac{\partial A_1}{\partial \alpha_2} + \frac{u_3}{R_1} \right. \\ \left. + \alpha_3 \left\{ \frac{1}{A_1} \frac{\partial}{\partial \alpha_1} \left[ \frac{u_1}{R_1} - \frac{1}{A_1} \frac{\partial u_3}{\partial \alpha_1} \right] + \frac{1}{A_1 A_2} \left[ \frac{u_2}{R_2} - \frac{1}{A_2} \frac{\partial u_3}{\partial \alpha_2} \right] \frac{\partial A_1}{\partial \alpha_2} \right\} \right) \quad (2.24)$$

Simplifying further:

$$S_{11} = \frac{1}{A_1 (1 + \alpha_3/R_1)} \left( \frac{\partial u_1}{\partial \alpha_1} + \frac{u_2}{A_2} \frac{\partial A_1}{\partial \alpha_2} + u_3 \frac{A_1}{R_1} \right) \quad (2.25)$$

Similarly,  $S_{22}$  and  $S_{33}$ , the normal strain components become:

$$S_{11} = \frac{1}{A_1 (1 + \alpha_3/R_1)} \left[ \frac{\partial U_1}{\partial \alpha_1} + \frac{U_2}{A_2} \frac{\partial A_1}{\partial \alpha_2} + U_3 \frac{A_1}{R_1} \right] \quad (2.26)$$

$$S_{22} = \frac{1}{A_2 (1 + \alpha_3/R_2)} \left[ \frac{\partial U_2}{\partial \alpha_2} + \frac{U_1}{A_1} \frac{\partial A_2}{\partial \alpha_1} + U_3 \frac{A_2}{R_2} \right] \quad (2.27)$$

$$S_{33} = \frac{\partial U_3}{\partial \alpha_3} \quad (2.28)$$

Substituting Eqs. (2.9) and (2.10) into (2.7) gives:

$$E_1 = \frac{1}{\epsilon_{11}} D_1 - \frac{e_{15}}{\epsilon_{11}} S_{13} = E_1^e + E_1^d \quad (2.29)$$

$$E_2 = \frac{1}{\epsilon_{11}} D_2 - \frac{e_{15}}{\epsilon_{11}} S_{23} = E_2^e + E_2^d \quad (2.30)$$

$$E_3 = \frac{1}{\epsilon_{33}} D_3 - \frac{e_{31} S_{11} + e_{31} S_{22} + e_{33} S_{33}}{\epsilon_{33}} = E_3^e + E_3^d \quad (2.31)$$

where  $E_i^e$  denotes the electric field induced by an electric displacement;  $E_i^d$  denotes the electric field induced by the direct piezoelectric effect ( $i = 1, 2, 3$ ). These two separate effects are further defined as:

$$E_i^e = \frac{D_i}{\epsilon_{ii}}, \quad (i = 1, 2, 3) \quad (2.32)$$

$$E_1^d = \frac{e_{15}}{\epsilon_{11}} S_{13} \quad (2.33)$$

$$E_2^d = -\frac{e_{15}}{\epsilon_{11}} S_{23} \quad (2.34)$$

$$E_3^d = -\frac{e_{31} S_{11} + e_{31} S_{22} + e_{33} S_{33}}{\epsilon_{33}} \quad (2.35)$$

These fundamental definitions and mechanical/electric relations will be used in derivations of piezoelectric shell theories. In order to derive the system electromechanical equations and mechanical/electric boundary conditions of the piezoelectric shell continuum, all variations in Eq. (2.2) need to be calculated. To find these, the first thing that must be looked at is the variation of kinetic energy and followed by energies associated with electric enthalpy  $H$ , and electric charge  $Q$ . A final variational equation is derived, which leads to all electromechanical system equations and boundary conditions [13]. The variation of kinetic energy  $\hat{K}$  is

$$\begin{aligned}
\delta \int_{t_0}^{t_1} dt \int_{\alpha_1} \int_{\alpha_2} \int_{\alpha_3} \hat{K} dv &= \delta \int_{t_0}^{t_1} dt \int_{\alpha_1} \int_{\alpha_2} \int_{\alpha_3} \left[ \frac{1}{2} \rho \dot{U}_j \dot{U}_j \right] A_1 A_2 \left( 1 + \frac{\alpha_3}{R_1} \right) \left( 1 + \frac{\alpha_3}{R_2} \right) d\alpha_1 d\alpha_2 d\alpha_3 \\
&= -p \int_{t_0}^{t_1} dt \int_v \left( \ddot{U}_1 \delta U_1 + \ddot{U}_2 \delta U_2 + \ddot{U}_3 \delta U_3 \right) A_1 A_2 \left( 1 + \frac{\alpha_3}{R_1} \right) \left( 1 + \frac{\alpha_3}{R_2} \right) d\alpha_1 d\alpha_2 d\alpha_3
\end{aligned} \tag{2.36}$$

Note that integration by parts was used in the kinetic energy variation.

Next, the variation of electric enthalpy includes two components: mechanical strains,  $S_{ij}$ ,

and electric fields,  $E_j$ . The variation of electric-field energy is derived:

$$\begin{aligned}
&\frac{\partial H}{\partial E_k} \delta E_k \\
&= (e_{15} S_{13} + \epsilon_{11} E_1) \frac{1}{A_1 \left( 1 + \frac{\alpha_3}{R_1} \right)} \frac{\partial(\delta\phi)}{\partial\alpha_1} \\
&+ (e_{15} S_{23} + \epsilon_{11} E_2) \frac{1}{A_2 \left( 1 + \frac{\alpha_3}{R_2} \right)} \frac{\partial(\delta\phi)}{\partial\alpha_2} \\
&+ (e_{31} S_{11} + e_{31} S_{22} + e_{33} S_{33} + \epsilon_{33} E_3) \frac{\partial(\delta\phi)}{\partial\alpha_3}
\end{aligned} \tag{2.37}$$

Using integration by parts, the first term becomes:

$$\begin{aligned}
& \int_{t_0}^{t_1} dt \int_{\alpha_1} \int_{\alpha_2} \int_{\alpha_3} (e_{15}S_{13} + \epsilon_{11} E_1) \frac{1}{A_1 \left(1 + \frac{\alpha_3}{R_1}\right)} \frac{\partial(\delta\phi)}{\partial\alpha_1} A_1 A_2 \left(1 + \frac{\alpha_3}{R_2}\right) d\alpha_1 d\alpha_2 d\alpha_3 \\
&= \int_{t_0}^{t_1} dt \int_{\alpha_2} \int_{\alpha_3} (e_{15}S_{13} + \epsilon_{11} E_1) A_2 \left(1 + \frac{\alpha_3}{R_2}\right) \delta\phi d\alpha_2 d\alpha_3 \\
& - \int_{t_0}^{t_1} dt \int_{\alpha_1} \int_{\alpha_2} \int_{\alpha_3} \frac{\partial \left[ (e_{15}S_{13} + \epsilon_{11} E_1) A_2 \left(1 + \frac{\alpha_3}{R_2}\right) \right]}{\partial\alpha_1} \delta\phi d\alpha_1 d\alpha_2 d\alpha_3
\end{aligned} \tag{2.38}$$

Proceeding with all terms in Eq. (2.37) yields:

$$\begin{aligned}
& \int_{t_0}^{t_1} dt \int_v \frac{\partial H}{\partial E_k} \delta E_k dv \\
&= \int_{t_0}^{t_1} dt \int_{\alpha_2} \int_{\alpha_3} (e_{15}S_{13} + \epsilon_{11} E_1) A_2 \left(1 + \frac{\alpha_3}{R_2}\right) \delta\phi d\alpha_2 d\alpha_3 \\
& + \int_{t_0}^{t_1} dt \int_{\alpha_1} \int_{\alpha_3} (e_{15}S_{23} + \epsilon_{11} E_2) A_1 \left(1 + \frac{\alpha_3}{R_1}\right) \delta\phi d\alpha_1 d\alpha_3 \\
& + \int_{t_0}^{t_1} dt \int_{\alpha_1} \int_{\alpha_2} (e_{31}S_{11} + e_{31}S_{22} + e_{33}S_{33} + \epsilon_{33} E_3) A_1 A_2 \left(1 + \frac{\alpha_3}{R_1}\right) \left(1 + \frac{\alpha_3}{R_2}\right) \delta\phi d\alpha_1 d\alpha_2 \\
& - \int_{t_0}^{t_1} dt \int_{\alpha_1} \int_{\alpha_2} \int_{\alpha_3} \left\{ \frac{\partial \left[ (e_{15}S_{13} + \epsilon_{11} E_1) A_2 \left(1 + \frac{\alpha_3}{R_2}\right) \right]}{\partial\alpha_1} \right. \\
& + \frac{\partial \left[ (e_{15}S_{23} + \epsilon_{11} E_2) A_1 \left(1 + \frac{\alpha_3}{R_1}\right) \right]}{\partial\alpha_2} \\
& \left. + \frac{\partial \left[ (e_{31}S_{11} + e_{31}S_{22} + e_{33}S_{33} + \epsilon_{33} E_3) A_1 A_2 \left(1 + \frac{\alpha_3}{R_1}\right) \left(1 + \frac{\alpha_3}{R_2}\right) \right]}{\partial\alpha_3} \right\} \delta\phi d\alpha_1 d\alpha_2 d\alpha_3
\end{aligned} \tag{2.39}$$

Carrying out the variation of electrical potential energy in the variational equation gives:

$$\begin{aligned}
& \int_{t_0}^{t_1} dt \int_S Q \delta \phi dS \\
&= \int_{t_0}^{t_1} dt \int_{\alpha_2} \int_{\alpha_3} Q_1 A_2 \left( 1 + \frac{\alpha_3}{R_2} \right) \delta \phi d\alpha_2 d\alpha_3 \\
&+ \int_{t_0}^{t_1} dt \int_{\alpha_1} \int_{\alpha_3} Q_2 A_1 \left( 1 + \frac{\alpha_3}{R_1} \right) \delta \phi d\alpha_1 d\alpha_3 \\
&+ \int_{t_0}^{t_1} dt \int_{\alpha_1} \int_{\alpha_2} Q_3 A_1 A_2 \left( 1 + \frac{\alpha_3}{R_1} \right) \left( 1 + \frac{\alpha_3}{R_2} \right) \delta \phi d\alpha_1 d\alpha_2
\end{aligned} \tag{2.40}$$

Thus, the electric components of variations were carried out. Derivations of system equations of the piezoelectric shell continuum can be proceeded.

To obtain the charge equation, Eq. (2.41), simply take the fourth term of Eq. (2.39) inside the integral.

$$\begin{aligned}
& \partial \left[ \frac{(e_{15} S_{13} + \epsilon_{11} E_1) A_2 \left( 1 + \frac{\alpha_3}{R_2} \right)}{\partial \alpha_1} \right] + \partial \left[ \frac{(e_{15} S_{23} + \epsilon_{11} E_2) A_1 \left( 1 + \frac{\alpha_3}{R_1} \right)}{\partial \alpha_2} \right] \\
&+ \partial \left[ \frac{(e_{31} S_{11} + e_{31} S_{22} + e_{33} S_{33} + \epsilon_{33} E_3) A_1 A_2 \left( 1 + \frac{\alpha_3}{R_1} \right) \left( 1 + \frac{\alpha_3}{R_2} \right)}{\partial \alpha_3} \right] = 0
\end{aligned} \tag{2.41}$$

Substituting all energy variational terms into Hamilton's equation (but only observing the electric boundary conditions) yields the last three terms of the electromechanical equations.

$$\begin{aligned}
& \int_{t_0}^{t_1} dt \int_{S_1} (e_{15} S_{13} + \epsilon_{11} E_1 + Q_1) A_2 \left( 1 + \frac{\alpha_3}{R_2} \right) \delta \phi d\alpha_2 d\alpha_3 \\
&+ \int_{t_0}^{t_1} dt \int_{S_2} (e_{15} S_{23} + \epsilon_{11} E_2 + Q_2) A_1 \left( 1 + \frac{\alpha_3}{R_1} \right) \delta \phi d\alpha_1 d\alpha_3 \\
&+ \int_{t_0}^{t_1} dt \int_{S_3} (e_{31} S_{11} + e_{31} S_{22} + e_{33} S_{33} + \epsilon_{33} E_3 + Q_3) A_1 A_2 \left( 1 + \frac{\alpha_3}{R_1} \right) \left( 1 + \frac{\alpha_3}{R_2} \right) \delta \phi d\alpha_1 d\alpha_2 = 0
\end{aligned} \tag{2.42}$$



Electric boundary conditions are defined on the outside surfaces of the piezoelectric shell, that is, the electric field value is defined along the material interface.

$$(e_{15}S_{13} + \epsilon_{11} E_1 + Q_1)A_2 \left(1 + \frac{\alpha_3}{R_2}\right) = 0 \quad (2.43a)$$

$$(e_{15}S_{23} + \epsilon_{11} E_2 + Q_2)A_1 \left(1 + \frac{\alpha_3}{R_1}\right) = 0 \quad (2.43b)$$

$$(e_{31}S_{11} + e_{31}S_{22} + e_{33}S_{33} + \epsilon_{33} E_3 + Q_3)A_1A_2 \left(1 + \frac{\alpha_3}{R_1}\right) \left(1 + \frac{\alpha_3}{R_2}\right) = 0 \quad (2.43c)$$

Note that the electric boundary conditions in Eqs. (2.43-a,b,c) indicate that the electric displacements  $D$  on the surfaces are equal to the densities of surface charges  $\sigma$ , which is defined as the amount of electric charge  $q$  that is present on a surface of given area  $A$ .

All  $A_i \left(1 + \frac{\alpha_3}{R_i}\right)$  and  $A_1A_2 \left(1 + \frac{\alpha_3}{R_1}\right) \left(1 + \frac{\alpha_3}{R_2}\right)$  terms can be removed since  $A_i \left(1 + \frac{\alpha_3}{R_i}\right) \neq 0$

and  $A_1A_2 \left(1 + \frac{\alpha_3}{R_1}\right) \left(1 + \frac{\alpha_3}{R_2}\right) \neq 0$ , because  $A_i$  cannot be zero, and  $\alpha_3$  nor  $R_i$  can be a

negative number. Thus,

$$(e_{15}S_{13} + \epsilon_{11} E_1 + Q_1) = 0 \quad (2.44a)$$

$$(e_{15}S_{23} + \epsilon_{11} E_2 + Q_2) = 0 \quad (2.44b)$$

$$(e_{31}S_{11} + e_{31}S_{22} + e_{33}S_{33} + \epsilon_{33} E_3 + Q_3) = 0 \quad (2.44c)$$

Since the piezoelectric shell continuum is thin, the transverse shear deformations and rotary inertias are neglected. The transverse shear strains are also negligible, i.e.,  $S_{13} = 0$  and  $S_{23} = 0$ . Also, the in-plane electric fields  $E_1$  and  $E_2$  are neglected and only the

transverse electric field  $E_3$  is discernible; Eq. (2.41), the charge equation of electrostatics, becomes [15]:

$$\frac{\partial}{\partial \alpha_3} (e_{31}S_{11} + e_{32}S_{22} + \epsilon_{33} E_3) A_1 A_2 \left(1 + \frac{\alpha_3}{R_1}\right) \left(1 + \frac{\alpha_3}{R_2}\right) = 0 \quad (2.45)$$

$\alpha_3 \ll R_i$ , curvature effect can be neglected:

$$\left(1 + \frac{\alpha_3}{R_i}\right) \cong 1 \quad (2.46)$$

In sensor applications, it is assumed there are no externally applied electric boundary conditions in an open-circuit condition:

$$e_{31}S_{11} + e_{32}S_{22} + \epsilon_{33} E_3 = 0 \quad (2.47)$$

Integrating over the piezoelectric layer thickness yields:

$$\int_{\alpha_3} (e_{31}S_{11} + e_{32}S_{22}) d\alpha_3 + \epsilon_{33} \int_{\alpha_3} E_3 d\alpha_3 = 0 \quad (2.48)$$

Integrating the electric field  $E_3$  gives the electric potential:

$$\int_{\alpha_3} E_3 d\alpha_3 = \phi_3 \quad (2.49)$$

$$\phi_3 = -\frac{1}{\epsilon_{33}} \int_{\alpha_3} (e_{31}S_{11} + e_{32}S_{22}) d\alpha_3 \quad (2.50)$$

For spatially distributed piezoelectric shell sensor continuum with an effective surface electrode area  $S^e$ , the total signal output  $\phi_3^S$  is:

$$\begin{aligned} & \int_{S^e} \phi_3^S A_1 A_2 \left(1 + \frac{\alpha_3}{R_1}\right) \left(1 + \frac{\alpha_3}{R_2}\right) d\alpha_1 d\alpha_2 \\ &= -\frac{1}{\epsilon_{33}} \int_{S^e} \int_{\alpha_3} (e_{31}S_{11} + e_{32}S_{22}) A_1 A_2 \left(1 + \frac{\alpha_3}{R_1}\right) \left(1 + \frac{\alpha_3}{R_2}\right) d\alpha_1 d\alpha_2 d\alpha_3 \end{aligned} \quad (2.51)$$

Note:  $\frac{\alpha_3}{R_1} \ll 1, \frac{\alpha_3}{R_2} \ll 1$

Taking the surface average over the entire electrode area  $S^e$ , neglecting curvature effect:

$$\phi_3^S = - \frac{\int_{S^e} \int_{\alpha_3} (e_{31}S_{11} + e_{32}S_{22}) A_1 A_2 d\alpha_1 d\alpha_2 d\alpha_3}{\epsilon_{33} S^e} \quad (2.52)$$

Note that  $\int_{S^e} A_1 A_2 \left(1 + \frac{\alpha_3}{R}\right) \left(1 + \frac{\alpha_3}{R}\right) d\alpha_1 d\alpha_2 = S^e$ , the effective electrode area. For a thin

shell continuum, normal strains can be further divided into two strain components:

membrane strains,  $S_{ii}^\circ$  and bending strains,  $\kappa_{ii}$ :

$$S_{11} = S_{11}^\circ + \alpha_3 \kappa_{11} \quad (2.53)$$

$$S_{22} = S_{22}^\circ + \alpha_3 \kappa_{22} \quad (2.54)$$

Membrane strain is defined as average strain throughout the thickness of a shell, plate, or beam and occurs during in-plane expansion and contraction. Bending strain occurs during bending applications and is calculated by determining the relationship between the force and the amount of bending which results from it. For distributed sensors made of symmetrical hexagonal piezoelectric materials, the piezoelectric constants  $e_{31} = e_{32}$ . Thus, the sensor output signal becomes:

$$\phi_3^S = - \frac{1}{\epsilon_{33} S^e} \int_{S^e} \int_{\alpha_3}^{h^s} \left[ e_{31} (S_{11}^\circ + S_{22}^\circ) + \alpha_3 (\kappa_{11} + \kappa_{22}) \right] A_1 A_2 d\alpha_1 d\alpha_2 d\alpha_3 \quad (2.55)$$

The membrane strains  $S_{ii}^\circ$  and bending strains  $\kappa_{ii}$  can be further expressed as a function of three neutral-surface displacements,  $u_1$ ,  $u_2$ , and  $u_3$ , in the three axial directions:

$$S_{11}^\circ = \frac{1}{A_1} \frac{\partial u_1}{\partial \alpha_1} + \frac{u_2}{A_1 A_2} \frac{\partial A_1}{\partial \alpha_2} + \frac{u_3}{R_1} \quad (2.56)$$

$$S_{22}^{\circ} = \frac{1}{A_2} \frac{\partial u_2}{\partial \alpha_2} + \frac{u_1}{A_1 A_2} \frac{\partial A_2}{\partial \alpha_1} + \frac{u_3}{R_2} \quad (2.57)$$

$$\kappa_{11} = \frac{1}{A_1} \frac{\partial}{\partial \alpha_1} \left( \frac{u_1}{R_1} - \frac{1}{A_1} \frac{\partial u_3}{\partial \alpha_1} \right) + \frac{1}{A_1 A_2} \left( \frac{u_2}{R_2} - \frac{1}{A_2} \frac{\partial u_3}{\partial \alpha_2} \right) \frac{\partial A_1}{\partial \alpha_2} \quad (2.58)$$

$$\kappa_{22} = \frac{1}{A_2} \frac{\partial}{\partial \alpha_2} \left( \frac{u_2}{R_2} - \frac{1}{A_2} \frac{\partial u_3}{\partial \alpha_2} \right) + \frac{1}{A_1 A_2} \left( \frac{u_1}{R_1} - \frac{1}{A_1} \frac{\partial u_3}{\partial \alpha_1} \right) \frac{\partial A_2}{\partial \alpha_1} \quad (2.59)$$

Substituting Eqs. (2.56), (2.57), (2.58), and (2.59) into Eq. (2.55) gives the general sensor equation:

$$\begin{aligned} \phi_3^S = & -\frac{1}{\epsilon_{33} S^e} \int_{S^e} \int_{\alpha_3}^{h^s} \left\{ e_{31} \left[ \frac{1}{A_1} \frac{\partial u_1}{\partial \alpha_1} + \frac{u_2}{A_1 A_2} \frac{\partial A_1}{\partial \alpha_2} + \frac{u_3}{R_1} \right. \right. \\ & \left. \left. + \alpha_3 \left( \frac{1}{A_1} \frac{\partial}{\partial \alpha_1} \left( \frac{u_1}{R_1} - \frac{1}{A_1} \frac{\partial u_3}{\partial \alpha_1} \right) + \frac{1}{A_1 A_2} \left( \frac{u_2}{R_2} - \frac{1}{A_2} \frac{\partial u_3}{\partial \alpha_2} \right) \frac{\partial A_1}{\partial \alpha_2} \right) \right] \right. \\ & \left. + e_{32} \left[ \frac{1}{A_2} \frac{\partial u_2}{\partial \alpha_2} + \frac{u_1}{A_1 A_2} \frac{\partial A_2}{\partial \alpha_1} + \frac{u_3}{R_2} \right. \right. \\ & \left. \left. + \alpha_3 \left( \frac{1}{A_2} \frac{\partial}{\partial \alpha_2} \left( \frac{u_2}{R_2} - \frac{1}{A_2} \frac{\partial u_3}{\partial \alpha_2} \right) + \frac{1}{A_1 A_2} \left( \frac{u_1}{R_1} - \frac{1}{A_1} \frac{\partial u_3}{\partial \alpha_1} \right) \frac{\partial A_2}{\partial \alpha_1} \right) \right] \right\} A_1 A_2 d\alpha_1 d\alpha_2 d\alpha_3 \end{aligned} \quad (2.60)$$

Note that the Lamé parameters, the  $A_i$ s, and radii of curvatures, the  $R_i$ s, are geometry dependent, e.g.,  $A_1 = A_2 = 1$  and  $R_1 = R_2 = \infty$  for a rectangular plate;  $A_1 = 1$ ,  $A_2 = R$ ,  $R_1 = \infty$ , and  $R_2 = R$  for a cylindrical shell, etc. Thus, the sensor equation can be further simplified based on these four parameters defined for the geometries. The next section introduces shaping functions to the sensor equation which can be used to specify a certain sensor shape.

## 2.2 Distributed Sensing of Elastic Shells

Observation spillover in a control system can give unwanted dynamic responses, thus, it is beneficial that sensors only monitor those modes which need to be controlled,

so that spillover is prevented. However, sensors respond to the uncontrolled residual modes as well as the controlled modes. There are techniques which can reduce this occurrence; one such method is to use spatially distributed modal sensors which only respond to a structural mode or group of modes. In this section, detailed electromechanics of generic distributed shell sensors/actuators for modal sensing and control are studied.

### 2.2.1 Generic Shape

A piezoelectric film is bonded to a flexible shell continuum. In a generic case, the film covers the entire surface of the structure. The piezoelectric film is perfectly coupled with the shell continuum, but does not change its dynamic characteristics, such as natural frequencies and mode shapes. The top piezoelectric layer on the generic shell distributed sensor/actuator system serves as a distributed sensor. In this section, a distributed sensing theory based on the direct piezoelectric effect and the shell strains/deformations is presented. It is assumed that the distributed piezoelectric layer is much thinner than that of the shell structure. Therefore, the piezoelectric strains are the same as the outer surface strains of the shell. For such thin film, only the transverse electric field  $E_3$  is considered and thus the voltage across the electrodes can be obtained by integrating the electric field over the thickness of the piezoelectric sensor layer as shown in Eq. (2.61).

$$\phi = -\int^{h^s} E_3 d\alpha_3 \quad (2.61)$$

where  $h^s$  is the piezoelectric sensor thickness. Using Figure 2.1, Eq. (2.61) can be expressed in terms of normal strains in the sensor:  $S_{11}^S$  and  $S_{22}^S$  in the direction of  $\alpha_1$  and  $\alpha_2$ , respectively, and dielectric displacement  $D_3$ .

$$\phi_3 = h^s (h_{31} S_{11}^S + h_{32} S_{22}^S - \beta_{33} D_3) \quad (2.62)$$

where  $\beta_{33}$  and  $h_{ij}$  denote respectively the impermeability and the strain charge coefficients of the piezoelectric sensor. It is assumed that the piezoelectric material is not sensitive to in-plane twisting shear strain  $S_{12}$ . Also, since the shell is thin, the transverse shear strains  $S_{13}$  and  $S_{23}$  are neglected. The piezoelectric sensor layer is coupled with the elastic shell; thus, the normal strains in the sensor layer can be estimated by:

$$S_{11}^S = \left\{ \left[ \frac{1}{A_1} \frac{\partial u_1}{\partial \alpha_1} + \frac{u_2}{A_1 A_2} \frac{\partial A_1}{\partial \alpha_2} + \frac{u_3}{R_1} \right] + r_1^S \left[ \frac{1}{A_1} \frac{\partial}{\partial \alpha_1} \left( \frac{u_1}{R_1} - \frac{1}{A_1} \frac{\partial u_3}{\partial \alpha_1} \right) + \frac{1}{A_1 A_2} \frac{\partial A_1}{\partial \alpha_2} \left( \frac{u_2}{R_2} - \frac{1}{A_2} \frac{\partial u_3}{\partial \alpha_2} \right) \right] \right\} \quad (2.63)$$

$$S_{22}^S = \left\{ \left[ \frac{1}{A_2} \frac{\partial u_2}{\partial \alpha_2} + \frac{u_1}{A_1 A_2} \frac{\partial A_2}{\partial \alpha_1} + \frac{u_3}{R_2} \right] + r_2^S \left[ \frac{1}{A_2} \frac{\partial}{\partial \alpha_2} \left( \frac{u_2}{R_2} - \frac{1}{A_2} \frac{\partial u_3}{\partial \alpha_2} \right) + \frac{1}{A_1 A_2} \frac{\partial A_2}{\partial \alpha_1} \left( \frac{u_1}{R_1} - \frac{1}{A_1} \frac{\partial u_3}{\partial \alpha_1} \right) \right] \right\} \quad (2.64)$$

where  $r_1^S$  and  $r_2^S$  denote the distances measured from the neutral surface to the mid-plane of the sensor layer. Rearranging Eq. (2.62), the electric displacement  $D_3^S$  can be written as:

$$D_3^S = \frac{1}{\beta_{33}} \left( h_{31} S_{11}^S + h_{32} S_{22}^S - \frac{\phi_3}{h^S} \right) \quad (2.65)$$

Since  $D_3^S$  is defined as the charge per unit area, Eq. (2.64) can be integrated over the electrode surface  $S^e$  to estimate a total surface charge. An open-circuit voltage  $\phi^S$  condition can be obtained by setting the charge zero:

$$\begin{aligned}
\phi^S &= \frac{h^S}{S^e} \int_{S^e} (h_{31}S_{11}^S + h_{32}S_{22}^S) dS^e \\
&= \frac{h^S}{S^e} \int_{S^e} (h_{31}S_{11}^S + h_{32}S_{22}^S) A_1 A_2 d\alpha_1 d\alpha_2
\end{aligned} \tag{2.66}$$

Substituting the strains into Eq. (2.65) yields the distributed sensor output  $\phi^S(\alpha_1, \alpha_2)$  in terms of displacements and other system parameters.

$$\begin{aligned}
\phi^S(\alpha_1, \alpha_2) &= \frac{h^S}{S^e} \int_{S^e} \left\{ h_{31} \left[ \left( \frac{1}{A_1} \frac{\partial u_1}{\partial \alpha_1} + \frac{u_2}{A_1 A_2} \frac{\partial A_1}{\partial \alpha_2} + \frac{u_3}{R_1} \right) \right. \right. \\
&+ r_1^S \left[ \frac{1}{A_1} \frac{\partial}{\partial \alpha_1} \left( \frac{u_1}{R_1} - \frac{1}{A_1} \frac{\partial u_3}{\partial \alpha_1} \right) + \frac{1}{A_1 A_2} \frac{\partial A_1}{\partial \alpha_2} \left( \frac{u_2}{R_2} - \frac{1}{A_2} \frac{\partial u_3}{\partial \alpha_2} \right) \right] \left. \right\} \\
&+ h_{32} \left\{ \left( \frac{1}{A_2} \frac{\partial u_2}{\partial \alpha_2} + \frac{u_1}{A_1 A_2} \frac{\partial A_2}{\partial \alpha_1} + \frac{u_3}{R_2} \right) + r_2^S \left[ \frac{1}{A_2} \frac{\partial}{\partial \alpha_2} \left( \frac{u_2}{R_2} - \frac{1}{A_2} \frac{\partial u_3}{\partial \alpha_2} \right) \right. \right. \\
&+ \left. \left. \frac{1}{A_1 A_2} \frac{\partial A_2}{\partial \alpha_1} \left( \frac{u_1}{R_1} - \frac{1}{A_1} \frac{\partial u_3}{\partial \alpha_1} \right) \right] \right\} dS^e
\end{aligned} \tag{2.67}$$

Eq. (2.67) relates the piezoelectric film output charge to the dynamic of the substrate shell structure. From this equation, many sensors and actuators have been developed using experimental, simplified analytical, and finite element approaches. The goal here is to develop a technique that uses a combination of numerical and experimental methods for sensors or actuators design.

### 2.2.2 Spatial Thickness Shaping

Distributed piezoelectric shell layers can be either embedded or surface bonded with a flexible elastic shell, and the layers are used as distributed sensors. For a spatially distributed piezoelectric shell convolving sensor, a weighting function  $W(\alpha_1, \alpha_2)$  and a polarity function  $\text{sgn}[U_3(\alpha_1, \alpha_2)]$  can be added to the generic shell sensor equation, Eq. (2.67). Also, a  $\text{sgn}(\cdot)$  denotes a signum function can be used to change the piezoelectric

polarity, in which  $\text{sgn}(\cdot) = 1$  when  $(\cdot) > 0$ ,  $0$  when  $(\cdot) = 0$  and  $-1$  when  $(\cdot) < 0$ .

$U_3(\alpha_1, \alpha_2)$  denotes a transverse modal function, mode shape function. Two weighting functions are discussed: thickness shaping and surface shaping. In thickness shaping, it is assumed that the thickness of the piezoelectric shell is a spatial function.

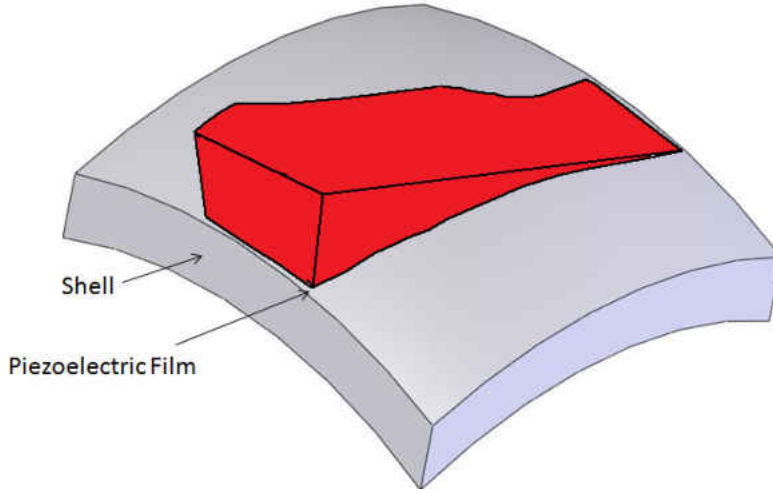


Figure 2.2: Spatial Thickness Shaping

In spatial thickness shaping, the sensor thickness varies over the effective sensor area.

Figure 2.2 illustrates the thickness shaping of distributed shell sensors. The piezoelectric shell sensor thickness is a spatial function  $W_t(\alpha_1, \alpha_2)$ . Thus, the sensor equation, Eq.

(2.51), becomes:

$$\begin{aligned}
 & \int_{S^e} \phi_3^S A_1 A_2 \left(1 + \frac{\alpha_3}{R_1}\right) \left(1 + \frac{\alpha_3}{R_2}\right) d\alpha_1 d\alpha_2 \\
 &= -\frac{e_{31}}{\epsilon_{33}} \int_{\alpha_1} \int_{\alpha_2} \text{sgn}[U_3(\alpha_1, \alpha_2)] [W_t(\alpha_1, \alpha_2) (S_{11}^\circ + S_{22}^\circ) \\
 &+ \int_{r_1}^{W_t(\alpha_1, \alpha_2) + r_1} \alpha_3 (\kappa_{11} + \kappa_{22}) d\alpha_3] \left(1 + \frac{\alpha_3}{R_1}\right) \left(1 + \frac{\alpha_3}{R_2}\right) A_1 A_2 d\alpha_1 d\alpha_2
 \end{aligned} \tag{2.68}$$

where  $S^e$  denotes the effective sensor area or electrode area and  $r_1$  is the distance measured from the shell neutral surface to the bottom of the piezoelectric sensor layer.



Note that the first term inside the second set of square brackets is contributed by the membrane strains and the second by the bending strains. The total output signal is contributed by the sum of membrane and bending strains.

### 2.2.3 Spatial Surface Shaping

In the second case, the piezoelectric shell thickness is assumed constant. The piezoelectric film does not usually cover the entire surface of the substrate flexible shell structure. The film is shaped such that the output charge represents the desired dynamic characteristics of the structure. Figure 2.3 illustrates the surface shaping of a shell sensor.

Sensor shape can be designed by using the weighting shape function  $W_s(\alpha_1, \alpha_2)$ .

$$\begin{aligned}
 & \int_{\alpha_1} \int_{\alpha_2} \phi_3^S \left( 1 + \frac{\alpha_3}{R_1} \right) \left( 1 + \frac{\alpha_3}{R_2} \right) A_1 A_2 d\alpha_1 d\alpha_2 \\
 &= -\frac{1}{\epsilon_{33}} \int_{\alpha_1} \int_{\alpha_2} W_s(\alpha_1, \alpha_2) \cdot \text{sgn}[U_3(\alpha_1, \alpha_2)] \int_{S^e} (e_{31} S_{11} + e_{31} S_{22}) \\
 & \cdot \left( 1 + \frac{\alpha_3}{R_1} \right) \left( 1 + \frac{\alpha_3}{R_2} \right) A_1 A_2 d\alpha_1 d\alpha_2 d\alpha_3
 \end{aligned} \tag{2.69}$$

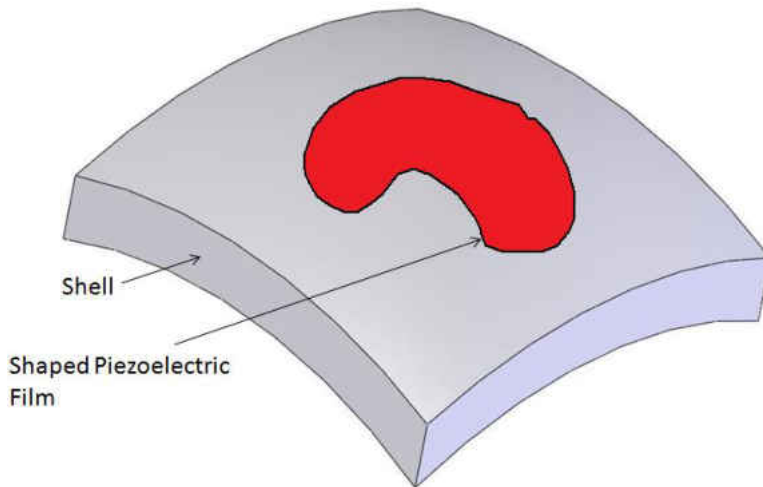


Figure 2.3: Spatial Surface Shaping

Hence, the generic sensor equation does not include a shape function, so the film covers the whole structure. As for the shaped sensor equation, it does have a shape

function, so the film covers a certain area of the structure. For this thesis, a surface shaped sensor will be utilized along with the generic shape of all three of the named structures. Considering Eq. (2.67) as the output of the piezoelectric film can be calculated analytically for simple structures such as beams, plates, and cylinders if  $u_1$ ,  $u_2$ ,  $u_3$  are known. However, for complicated structures and boundary conditions, analytical solution is impossible, but using numerical integration, the charge  $\phi$  could be calculated. In this approach, it is assumed that the structure displacement field can be obtained either experimentally or with finite element analysis. The spatial double derivatives are then computed before the numerical integration. Next, the generic sensor output charge equation is reduced for a cylindrical shell, plate, and beam.

### 2.3 Cylindrical Shell

The generic sensor theory can be applied to other geometries with curvature, such as a cylinder, sphere, ring, cylindrical shell, etc. Here, a cylindrical shell is discussed. A cylindrical shell is a special case of the generic shell continuum defined by a three tri-orthogonal axes  $\alpha_1$ ,  $\alpha_2$ , and  $\alpha_3$ . The cylindrical shell can be defined in a cylindrical coordinate system where the z-axis ( $\alpha_1$ ) is aligned with the length, the second axis  $\theta$  ( $\alpha_2$ ) defines the circumferential direction and the third axis ( $\alpha_3$ ) is normal to the neutral surface. For a generic sensor case, the sensor would cover the entire outer surface of the shell; Figure 2.4 shows the cylindrical shell with a piezoelectric shaped sensor adhered to the top half of it.

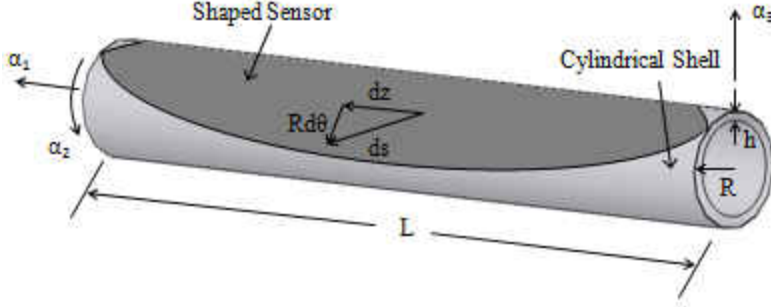


Figure 2.4: Cylindrical Shell with a Shaped Sensor Adhered

It has Lamé parameters:  $A_1 = 1$  and  $A_2 = R$ , and radii of curvatures:  $R_1 = \infty$  and  $R_2 = R$ .

Substituting these four parameters into the generic shell sensor equation Eq. (2.67) gives:

$$\begin{aligned}
\phi^S(\alpha_1, \alpha_2) = & \frac{h^S}{S^e} \int_{S^e} \left( h_{31} \left\{ \left[ \frac{1}{(1)} \frac{\partial u_1}{\partial \alpha_1} + \frac{u_2}{(1)(R)} \frac{\partial(1)}{\partial \alpha_2} + \frac{u_3}{(\infty)} \right] \right. \right. \\
& + r_1^S \left[ \frac{1}{(1)} \frac{\partial}{\partial \alpha_1} \left( \frac{u_1}{(\infty)} - \frac{1}{(1)} \frac{\partial u_3}{\partial \alpha_1} \right) + \frac{1}{(1)(R)} \frac{\partial(1)}{\partial \alpha_2} \left( \frac{u_2}{(R)} - \frac{1}{(R)} \frac{\partial u_3}{\partial \alpha_2} \right) \right] \left. \right\} \\
& + h_{32} \left\{ \left[ \frac{1}{(R)} \frac{\partial u_2}{\partial \alpha_2} + \frac{u_1}{(1)(R)} \frac{\partial(R)}{\partial \alpha_1} + \frac{u_3}{(R)} \right] + r_2^S \left[ \frac{1}{(R)} \frac{\partial}{\partial \alpha_2} \left( \frac{u_2}{(R)} - \frac{1}{(R)} \frac{\partial u_3}{\partial \alpha_2} \right) \right. \right. \\
& \left. \left. + \frac{1}{(1)(R)} \frac{\partial(R)}{\partial \alpha_1} \left( \frac{u_1}{(\infty)} - \frac{1}{(1)} \frac{\partial u_3}{\partial \alpha_1} \right) \right] \right\} \right) dS^e
\end{aligned} \tag{2.70}$$

Simplifying Eq. (2.70), where  $\frac{\partial(1)}{\partial \alpha_2} = 1, \frac{u_{1,3}}{(\infty)} = 0$  gives:

$$\begin{aligned}
\phi^S(\alpha_1, \alpha_2) = & \frac{h^S}{S^e} \int_{S^e} \left( h_{31} \left\{ \left[ \frac{\partial u_1}{\partial \alpha_1} + \frac{u_2}{R} \right] \right. \right. \\
& + r_1^S \left[ \frac{\partial}{\partial \alpha_1} \left( -\frac{\partial u_3}{\partial \alpha_1} \right) + \frac{1}{R} \left( \frac{u_2}{R} - \frac{1}{R} \frac{\partial u_3}{\partial \alpha_2} \right) \right] \left. \right\} \\
& + h_{32} \left\{ \left[ \frac{1}{R} \frac{\partial u_2}{\partial \alpha_2} + \frac{u_1}{R} \frac{\partial R}{\partial \alpha_1} + \frac{u_3}{R} \right] + r_2^S \left[ \frac{1}{R} \frac{\partial}{\partial \alpha_2} \left( \frac{u_2}{R} - \frac{1}{R} \frac{\partial u_3}{\partial \alpha_2} \right) \right. \right. \\
& \left. \left. + \frac{1}{R} \frac{\partial R}{\partial \alpha_1} \left( -\frac{\partial u_3}{\partial \alpha_1} \right) \right] \right\} \right) dS^e
\end{aligned} \tag{2.71}$$

Converting from curvilinear to cylindrical coordinates gives:

$$\begin{aligned}
\phi^S(z, \theta) = & \frac{-h^s}{S^e} \int_{S^e} \left( h_{31} \left\{ \left( \frac{\partial u_z}{\partial z} + \frac{u_\theta}{R} \right) \right. \right. \\
& + r_z^s \left[ \frac{\partial}{\partial z} \left( -\frac{\partial u_R}{\partial z} \right) + \frac{1}{R} \left( \frac{u_\theta}{R} - \frac{1}{R} \frac{\partial u_R}{\partial \theta} \right) \right] \left. \right\} \\
& + h_{32} \left\{ \left( \frac{1}{R} \frac{\partial u_\theta}{\partial \theta} + \frac{u_z}{R} \frac{\partial R}{\partial z} + \frac{\partial u_R}{\partial z} \right) + r_\theta^s \left[ \frac{1}{R} \frac{\partial}{\partial \theta} \left( \frac{u_\theta}{R} - \frac{1}{R} \frac{\partial u_R}{\partial \theta} \right) \right. \right. \\
& \left. \left. + \frac{1}{R} \frac{\partial R}{\partial z} \left( -\frac{\partial u_R}{\partial z} \right) \right] \right\} \right) dS^e
\end{aligned} \tag{2.72}$$

Where  $\frac{u_\theta}{R} = 0$ ,  $\frac{\partial u_R}{\partial z} = 0$  and multiplying through gives:

$$\begin{aligned}
\phi^S(z, \theta) = & \frac{-h^s}{S^e} \int_{S^e} \left( h_{31} \left\{ \left( \frac{\partial u_z}{\partial z} \right) + r_z^s \left( -\frac{\partial}{\partial z} \frac{\partial u_R}{\partial z} \right) + \left( -\frac{1}{R^2} \frac{\partial u_R}{\partial \theta} \right) \right\} \right. \\
& \left. + h_{32} \left\{ \left( \frac{1}{R} \frac{\partial u_\theta}{\partial \theta} + \frac{u_z}{R} \frac{\partial R}{\partial z} + \frac{\partial u_R}{\partial z} \right) + r_\theta^s \left( \frac{1}{R} \frac{\partial}{\partial \theta} \frac{u_\theta}{R} - \frac{1}{R^2} \frac{\partial}{\partial \theta} \frac{\partial u_R}{\partial \theta} \right) \right\} \right) dS^e
\end{aligned} \tag{2.73}$$

$$\begin{aligned}
\phi^S(z, \theta) = & \frac{-e_{31} h^s}{e_{33} S^e} \int_{S^e} \left\{ e_{31} \left( \frac{\partial u_z}{\partial z} - r_z^s \frac{\partial^2 u_R}{\partial z^2} \right) \right. \\
& \left. + e_{32} \left( \frac{\partial u_\theta}{R \partial \theta} + \frac{u_R}{R^2} + r_\theta^s \frac{\partial u_\theta}{R^2 \partial \theta} - r_\theta^s \frac{\partial^2 u_R}{R^2 \partial \theta^2} \right) \right\} dS^e
\end{aligned} \tag{2.74}$$

Which can be expanded to:

$$\begin{aligned}
\phi^S(z, \theta) = & \frac{-e_{31} h^s}{e_{33} S^e} \int_0^z \int_{\theta=0}^{\theta=\pi} \int_{r-t}^r \left\{ e_{31} (z'(z) - r_z^s z''(R)) \right. \\
& \left. + e_{32} \left( \frac{1}{R} \theta'(\theta) + \frac{u_R}{R^2} + r_\theta^s \frac{1}{R^2} \theta'(\theta) - r_\theta^s \frac{1}{R^2} \theta''(R) \right) \right\} r dr d\theta dz
\end{aligned} \tag{2.75}$$

It is observed that the transverse direction, when the cylindrical shell is under loading, exhibits greater displacement than that of the other two directions. Therefore, it is proposed that the cylindrical shell can be observed as the shape of a plate in order to visualize the shape of the sensor. Hence,  $F = k(x^2 - Lx)$  for a beam by Lee and Moon

[16], is also used for the shaping function of the piezoelectric sensor for a cylindrical shell, because of existing previous research on the shaped film in order to verify that a shaping function can correctly capture the dynamic of the structure [16].

## 2.4 Plate Substrate

The next case is a zero-curvature shell, a plate. The general sensor equation can be applied here as well. In this section, the development of the generic sensor output charge equation for a plate is presented.

The Lamé parameters are derived from the fundamental equation

$(ds)^2 = (1)^2 (dx)^2 + (1)^2 (dy)^2$  and therefore  $A_1 = A_2 = 1$  and  $R_1 = R_2 = \infty$ . Substituting these values into Eq. (2.67) gives the piezoelectric film output charge as:

$$\begin{aligned}
\phi^S(\alpha_1, \alpha_2) = & \frac{h^S}{S^e} \int_{S^e} \left\{ h_{31} \left[ \left( \frac{1}{(1)} \frac{\partial u_1}{\partial \alpha_1} + \frac{u_2}{(1)(1)} \frac{\partial(1)}{\partial \alpha_2} + \frac{u_3}{(\infty)} \right) \right. \right. \\
& + r_1^S \left[ \frac{1}{(1)} \frac{\partial}{\partial \alpha_1} \left( \frac{u_1}{(\infty)} - \frac{1}{(1)} \frac{\partial u_3}{\partial \alpha_1} \right) + \frac{1}{(1)(1)} \frac{\partial(1)}{\partial \alpha_2} \left( \frac{u_2}{(\infty)} - \frac{1}{(1)} \frac{\partial u_3}{\partial \alpha_2} \right) \right] \left. \right\} \\
& + h_{32} \left\{ \left[ \frac{1}{(1)} \frac{\partial u_2}{\partial \alpha_2} + \frac{u_1}{(1)(1)} \frac{\partial(1)}{\partial \alpha_1} + \frac{u_3}{(\infty)} \right] + r_2^S \left[ \frac{1}{(1)} \frac{\partial}{\partial \alpha_2} \left( \frac{u_2}{(\infty)} - \frac{1}{(1)} \frac{\partial u_3}{\partial \alpha_2} \right) \right. \right. \\
& \left. \left. + \frac{1}{(1)(1)} \frac{\partial(1)}{\partial \alpha_1} \left( \frac{u_1}{(\infty)} - \frac{1}{(1)} \frac{\partial u_3}{\partial \alpha_1} \right) \right] \right\} dS^e
\end{aligned} \tag{2.76}$$

Simplifying Eq. (2.76), where  $\frac{u_{1,2,3}}{(\infty)} = 0$  gives:

$$\begin{aligned}
\phi^S(\alpha_1, \alpha_2) = & \frac{h^S}{S^e} \int_{S^e} \left\{ h_{31} \left[ \left( \frac{\partial u_1}{\partial \alpha_1} + \frac{\partial u_2}{\partial \alpha_2} \right) + r_1^S \left[ \frac{\partial}{\partial \alpha_1} \left( -\frac{\partial u_3}{\partial \alpha_1} \right) + \frac{\partial}{\partial \alpha_2} \left( -\frac{\partial u_3}{\partial \alpha_2} \right) \right] \right] \right\} \\
& + h_{32} \left\{ \left[ \frac{\partial u_2}{\partial \alpha_2} + \frac{\partial u_1}{\partial \alpha_1} \right] + r_2^S \left[ \frac{\partial}{\partial \alpha_2} \left( -\frac{\partial u_3}{\partial \alpha_2} \right) + \frac{\partial}{\partial \alpha_1} \left( -\frac{\partial u_3}{\partial \alpha_1} \right) \right] \right\} dS^e
\end{aligned} \tag{2.77}$$

The plate can be defined in a coordinate system where the x-axis ( $\alpha_1$ ) is aligned with the length, the y-axis ( $\alpha_2$ ) defines the width and the third axis ( $\alpha_3$ ) is normal to the neutral surface. Eq. (2.77) can further be simplified, where the plate, shown in Figure 2.6, experiences only a transverse vibration, where  $\frac{\partial u_1}{\partial \alpha_1} = \frac{\partial u_2}{\partial \alpha_2} = 0$ .

$$\phi^S(\alpha_1, \alpha_2) = \frac{h^S}{S^e} \int_{S^e} \left( h_{31} \left\{ r_x^S \left[ -\frac{\partial^2 u_3}{\partial x^2} - \frac{\partial^2 u_3}{\partial y^2} \right] \right\} + h_{32} \left\{ r_y^S \left[ -\frac{\partial^2 u_3}{\partial y^2} - \frac{\partial^2 u_3}{\partial x^2} \right] \right\} \right) dS^e \quad (2.78)$$

The generic sensor output charge equation for a plate becomes:

$$\phi^S = -\frac{h^S}{S^e} \int_{S^e} \left[ h_{31} r_x^S \frac{\partial^2 u_3}{\partial x^2} + h_{32} r_y^S \frac{\partial^2 u_3}{\partial y^2} \right] dS^e \quad (2.79)$$

Research has been done on known film shapes for a plate. Zahui and Wendt [17] proposed the following equation:

$$\phi^S = \int_0^{L_y} \int_0^{L_x} (-h) W_s(x, y) \left[ h_{31} \frac{\partial^2 u_3}{\partial x^2} + h_{32} \frac{\partial^2 u_3}{\partial y^2} \right] dx dy \quad (2.80)$$

Where  $L_x$  and  $L_y$  are the dimensions of the plate in the  $x$  and  $y$  directions, respectively.  $W_s(x, y)$  is the surface shaping function of the plate and  $h$  is given by the following equation:

$$h = \frac{h_p + h_s}{2} \quad (2.81)$$

Where  $h_p$  and  $h_s$  define the plate and sensor thicknesses, respectively.

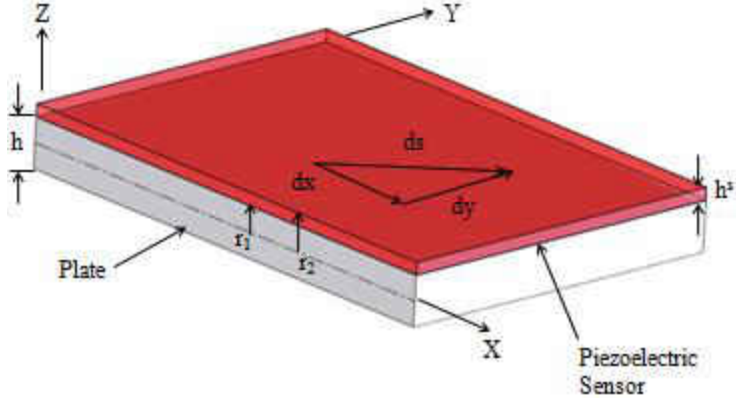


Figure 2.5: A Rectangular Plate Bonded with a Piezoelectric Sensor

As for the shaped sensor for the plate, the equation for the shape of a beam as proposed by Lee and Moon [16], can be applied for a plate. Hence, in this research, the shape in Figure 2.6 will be used in this method, because of previous research done on the known film shape.

### 2.3 Beam Substrate

The general sensor equation can be applied to a beam structure. In this section, the generic and shaped sensor output charge equations for a beam are presented [13].

Note that the plate can be reduced to a beam by considering only one effective axis, in this case, the x direction. Thus, the generic sensor output equation, Eq. (2.67) becomes:

$$\phi^S = -\frac{bh^S}{S^e} \int_x \left( h_{31} r_x^S \frac{\partial^2 u_3}{\partial x^2} \right) dx \quad (2.82)$$

where  $b$  is the beam width and  $x$  defines the sensor length in the x direction.

In a paper by Lee and Moon [16], it is reported that the electrical charge of an arbitrarily shaped PVDF sensor applied to a beam of length as

$$\phi^S = -(h_b + h_s) h_{31} \int_0^l W(x) z''(x) dx \quad (2.83)$$

where here,  $h_b$  and  $h_s$  are the beam and the PVDF sensor thicknesses, respectively.  $h_{31}$  is the PVDF sensor stress/charge coefficient,  $z''(x)$  is the second derivative of the displacement field, and  $W(x)$  represents the function describing the shape of the PVDF sensor. This shape covers the beam surface between  $-W(x)$  and  $+W(x)$  as pictured in Figure 2.5.

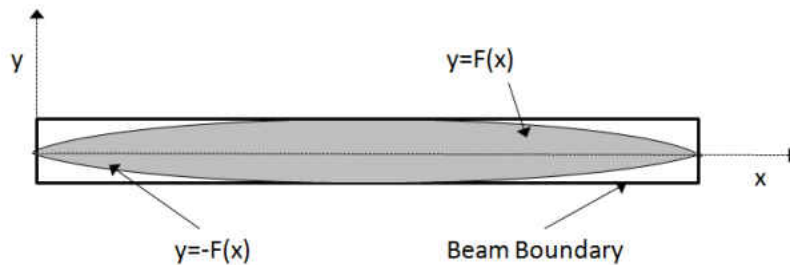


Figure 2.6: Top View of Beam with Shaped PVDF Sensor

The shape of the PVDF film is defined as  $W(x)$  to be quadratic in the  $x$  direction and to be independent of  $y$ . Hence, the shape in Figure 2.6 will be used in this method, because of previous research done with the known film shape [18] [19].

The equation from which the frequency response and sensor output charge are compared, Equation 2.67, is used in conjunction with the aforementioned sensor shape function. In Chapter V, a beam, a plate, and a cylindrical shell are modeled and simulated in ANSYS. Their displacements are then read into Matlab, numerical differentiation and integration are performed in which the results are used in the generic and shaped sensor equations, and their results are presented. In Chapter III, the finite element program ANSYS is introduced, discussing the different element types involved. Also, two verification manual test examples are performed and discussed which pertain to the simulation of the structures.



## **CHAPTER III**

### **INTRODUCTION TO FINITE ELEMENT ANALYSIS AND SIMULATION**

Finite Element Analysis (FEA) is a numerical technique used to approximate solutions of partial differential equations. ANSYS is an engineering simulation program which uses FEA to simulate interactions of all disciplines of physics, structural, vibration, fluid dynamics, thermal, and electromagnetic. This chapter introduces Frequency Response Function (FRF), ANSYS finite element analysis methods used in this work for analysis and simulation, the different elements involved, and a couple of the verification manual examples are presented [20].

#### **3.1 Analysis Methods**

In order to obtain the required displacements for numerical differentiation and integration, the Frequency Response Function of the structure must first be obtained. FRF is a tool for performing vibration analysis and testing. FRF is defined as the measure of the output spectrum of a system in response to an input. It is used to characterize the dynamic of the system over a range of frequencies. FRF is a transfer function, expressed in the frequency-domain. It can be created from either measured data or analytical functions. FRF expresses the structural response, in this case displacement, to an applied force as a function of frequency. FRF requires three analyses: modal analysis, harmonic analysis, and spectrum analysis. The first step to computing the FRF is to perform a modal analysis, which is used to calculate the natural frequencies and mode shapes of a

structure. Then, a spectrum analysis is performed, which is an extension of the modal analysis; it is used to calculate stresses and strains due to a response spectrum or a Power Spectral Density (PSD) input. Then a harmonic analysis is performed, which is used to determine the response of a structure to harmonically time-varying loads. The final solution of FRF is achieved as the sum of influence from all the involved modes. These analyses are discussed more in depth in Chapter IV.

### **3.2 ANSYS Element Characteristics**

#### **3.2.1 Element Type**

There are many types of elements within ANSYS. Element types may be defined in input files with the ANSYS command “ET” where the element type is defined in the element library. Information derived from the element type is used for succeeding commands. An element type may be identified by an element name or a number which is given in the element library. The elements used in these simulations are BEAM4 and SHELL63, which will be further discussed later.

#### **3.2.2 Element Degrees of Freedom**

Each element type has a set of degrees of freedom, which are the primary nodal unknown values of the field variable. These may be displacements, rotations, temperatures, pressures, voltages, etc. Results, such as stresses, strains, heat flows, etc., may be derived from these degree of freedom results. Degrees of freedom are not defined on the nodes explicitly by the user, but rather are implied by the element types attached to them. Hence, it is important which element type is chosen.

### **3.2.3 Element Real Constants**

Element real constants are properties that depend on the element type, such as cross-sectional properties of a beam element. Each element type has a different set of real constants. Real constants are required values of data used for calculations. The real constant command in ANSYS for input files is given by “R”. Real constant values may be interpreted as area, thickness, stiffness, moment of inertia, etc.

### **3.2.4 Element Material Properties**

An element type may have various material properties. These may include Young’s Modulus of elasticity, density, coefficient of thermal expansion, thermal conductivity, etc. Each property is referenced by an ANSYS label; for example, EX, EY and EZ are for the directional components of Young’s Modulus. Material properties may be accessed by the command “MP” when using an input file.

### **3.2.5 Node and Element Loads**

There are two types of loadings: nodal and element. Nodal loads are defined at the nodes and are not directly related to the elements. These nodal loads are associated with the degrees of freedom at the node and are typically entered with the commands “D” and “F”, which specify nodal constraints and nodal force loads, respectively. Element loads are surface loads, body loads and inertia loads. Surface loads may be specified as pressures for structural elements, convections for thermal elements, etc. which may be input in a nodal format or an element format. Body loads are temperatures for structural elements, heat generation rates for thermal elements, etc. Either the nodal or the element loading format may be used for an element, with the element format taking precedence.

### **3.2.6 Element KEYOPT Options**

Each element type may also have additional options, known as KEYOPTs, which are the key options specified according to each element type and can be switched on or off, whichever is required. Some element types have many key options, including element stiffness, stiffness matrix, extra displacement shapes, printouts, reduced or consistent pressure loading, etc. KEYOPT(1) indicates the first key option, KEYOPT(2) for the second, and so forth. From KEYOPTS (1) to (6), the ET command may be used; after that, KEYOPT(7) or greater must use the “KEYOPT” command. For example, KEYOPT(9) for BEAM4 allows the user to choose results to be calculated at intermediate locations on each element, and KEYOPT(3) for SHELL63 allows the user to suppress extra displacement shapes.

## **3.3 Structural Elements**

In this present work, when modeling the beam, plate, and shell in ANSYS, two element types are utilized: BEAM4 and SHELL63. BEAM 4 is used in the beam application, whereas SHELL63 is used in the plate and cylindrical shell applications. Before these elements can be used, an understanding of their element characteristics must first be gained. In the following sections, each will be discussed.

### **3.3.1 BEAM4**

BEAM4 is a uniaxial element with tension, compression, torsion, and bending capabilities. The BEAM4 element has six degrees of freedom at each node: translations in the x, y, and z directions and rotations about the x, y, and z axes. It also includes stress stiffening and large deflection capabilities. A consistent tangent stiffness matrix option is available for use in large deflection analyses. This matrix is used in nonlinear problems;

it is comprised of the main tangent stiffness matrix, the initial displacement matrix, initial stress matrix, and the initial load matrix. The geometry, node locations, and coordinate system for this element are shown in Figure 3.1.

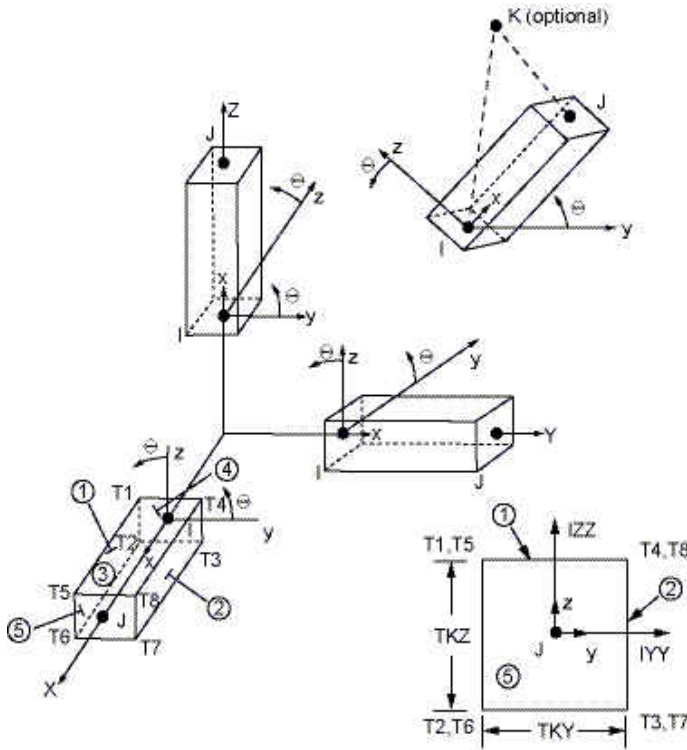


Figure 3.1: BEAM4 Geometry

The element is defined by two or three nodes, the cross sectional area, two area moments of inertia, two thicknesses, an angle of orientation about the element x-axis, the torsional moment of inertia, and the material properties. The element x-axis is oriented from node I toward node J.

**Element Loads:** Most loads can either be applied on the solid model, on keypoints, lines, and areas, or on the finite element model, on nodes and elements. For example, forces can be specified at a keypoint or a node. Similarly, surface loads can be specified on lines and areas or on nodes and element faces. Pressures may be input as surface loads on

element faces as shown in Figure 3.1. Positive normal pressures act into the element.

Lateral pressures are input as a force per unit length. End “pressures” are input as a force.

Table 3.1: BEAM4 Real Constants

No.	Name	Description
1	AREA	Cross-sectional area
2	IZZ	Area moment of inertia
3	IYY	Area moment of inertia
4	TKZ	Thickness along Z axis
5	TKY	Thickness along Y axis
6	THETA	Orientation about X-axis
7	ISTRN	Initial Strain
8	IXX	Torsional moment of inertia
9	SHEARZ	Shear deflection constant Z
10	SHEARY	Shear deflection constant Y
11	SPIN	Rotational frequency
12	ADDMAS	Added mass/unit length

**Special Features:** The BEAM4 element has special features of stress stiffening, large deflection, and element birth and death. Stress stiffening is the stiffening of a structure due to its stress state. This effect usually needs to be considered for thin structures with bending stiffness very small compared to axial stiffness, such as cables, thin beams and shells. The stress stiffening effect also changes the regular nonlinear stiffness matrix produced by large strain or large deflection effects. Element birth and death options may

be used to deactivate or reactivate selected elements if certain elements in a model may become existent or nonexistent when material is added or removed from a system.

Table 3.2: KEYOPT Options for BEAM4

<p>KEYOPT (2) Stress stiffening option 0: Use only the main tangent stiffness matrix when large deflection is ON. 1: Use the consistent tangent stiffness matrix when large deflection is ON. 2: Use to turn off consistent tangent stiffness matrix.</p>	<p>KEYOPT(7) Gyroscopic damping matrix 0: No gyroscopic damping matrix 1: Compute gyroscopic damping matrix. Real constant SPIN must be greater than zero. IYY must equal IZZ.</p>
<p>KEYOPT(6) Member force and moment output 0: No printout of member forces or moments 1: Print out member forces and moments in the element coordinate system</p>	<p>KEYOPT(9) Output at intermediate points between ends I and J N: Output at N intermediate locations (N= 0, 1, 3, 5, 7, 9)</p>

### Output Data

The maximum stress is computed as the direct stress plus the absolute values of both bending stresses. The minimum stress is the direct stress minus the absolute value of both bending stresses. The stress output of the BEAM4 element is illustrated in Figure 3.2.

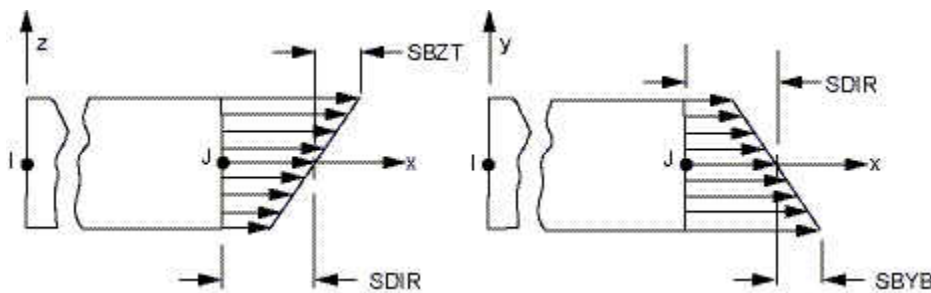


Figure 3.2: BEAM4 Stress Output

## **Assumptions**

The BEAM4 element has some assumptions associated with it. The beam must not have a zero length or area. However, the moments of inertia may be zero if large deflections are not used. The beam can have any cross-sectional shape for which the moments of inertia can be computed. However, the stresses will be determined as if the distance between the neutral axis and extreme fiber is one-half of the corresponding thickness. The element thicknesses are used only in the bending and thermal stress calculations. The applied thermal gradients are assumed to be linear across the thickness in both directions and along the length of the element. If the consistent tangent stiffness matrix is used, element real constants should be realistic, because the consistent stress-stiffening matrix is based on the calculated stress in the element; hence, the calculated stress will become inaccurate. Eigenvalues calculated in a gyroscopic modal analysis can be very sensitive to changes in the initial shift value, leading to potential error in either or both the real or imaginary parts of the eigenvalues.

## **Restrictions**

There are also restrictions associated with ANSYS Professional using the BEAM4 element. The SPIN real constant is not available. The damp material property is not allowed. The only special features allowed are stress stiffening and large deflections. KEYOPT(2) and (7) can only be set to 0, the default.

### **3.3.2 SHELL63**

SHELL63 is a shell structural element which has both bending and membrane capabilities. When modeled, it has the appearance of a thin sheet; Figure 3.3 gives a visualization of the SHELL63 geometry. Both in-plane and normal loads are permitted.



SHELL63 has six degrees of freedom at each node: displacements in the nodal x, y and z directions and rotations about the nodal x, y and z axes. Stress stiffening and large deflection capabilities are included. A consistent stiffness matrix option is available for use in large deflection analyses.

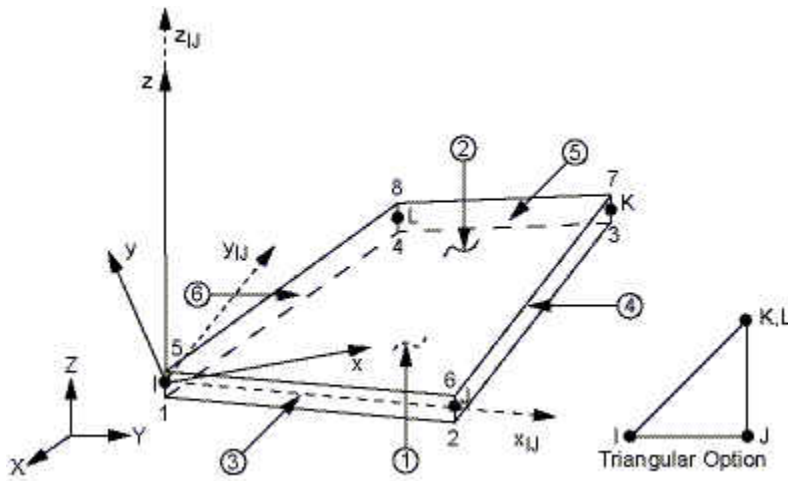


Figure 3.3: SHELL63 Geometry

$x_{ij}$  = Element x-axis if ESYS (Element Coordinate System) is not supplied.

$X$  = Element x-axis if ESYS is supplied.

SHELL63 element is defined by four nodes: I, J, K and L, each with a thickness. The thickness is assumed to vary smoothly over the area of the element, with the thickness input at the four nodes. If the element has a constant thickness, only TK(I) needs to be input. Conversely, if the thickness is not constant, then all four thicknesses need input.

**Element Loads:** Pressures may be input as surface loads on the element faces as shown on Figure 3.3. Positive pressures act into the element. Because shell edge pressures are input on a per-unit-area basis, per-unit-area quantities must be multiplied by the shell thickness.

Table 3.3: SHELL63 Real Constants

No.	Name	Description
1	TK(I)	Shell thickness at node I
2	TK(J)	Shell thickness at node J
3	TK(K)	Shell thickness at node K
4	TK(L)	Shell thickness at node L
5	EFS	Elastic foundation stiffness
6	THETA	Element X-axis rotation
7	RMI	Bending moment of inertia ratio
8	CTOP	Distance from mid surface to top
9	CBOT	Distance from mid surface to bottom
10,...,18	(Blank)	--
19	ADMSUA	Added mass/unit area

**Special Features:** The SHELL63 element has the features of stress stiffening, large deflection and element birth and death. Stress stiffening is the stiffening of a structure due to its stress state. This effect usually needs to be considered for thin structures with bending stiffness very small compared to axial stiffness, such as cables, thin beams and shells. The stress stiffening effect also changes the regular nonlinear stiffness matrix produced by large strain or large deflection effects. Element birth and death options may be used to deactivate or reactivate selected elements if certain elements in a model may become existent or nonexistent when material is added or removed from a system.

Table 3.4: KEYOPT Options for SHELL63

<p>KEYOPT (1) Element stiffness 0: Bending and membrane stiffness 1: Membrane stiffness only 2: Bending stiffness only</p>	<p>KEYOPT(7) Mass matrix 0: Consistent mass matrix 1: Reduced mass matrix</p>
<p>KEYOPT (2) Stress stiffening option 0: Use only the main tangent stiffness matrix when large deflection is ON. 1: Use the consistent tangent stiffness matrix when large deflection is ON. 2: Use to turn off consistent tangent stiffness matrix.</p>	<p>KEYOPT(8) Stress stiffness matrix 0: “Nearly” consistent stress stiffness matrix (default) 1: Reduced stress stiffness matrix</p>
<p>KEYOPT(3) 0: Include extra displacement shapes 1: Suppress extra displacement shapes 2: Include extra displacement shapes</p>	<p>KEYOPT(9) Element coordinate system defined 0: No user subroutine to define element coordinate system. 4: Element x-axis located by user subroutine.</p>
<p>KEYOPT(5) Extra stress output 0: Basic element printout 1: Nodal stress printout</p>	<p>KEYOPT (11) Specify data storage 0: No user subroutine to define element coordinate system 2: Store data for TOP, BOTTOM, and MID surfaces.</p>
<p>KEYOPT(6) Pressure loading 0: Reduced pressure loading 1: Consistent pressure loading</p>	

### Output Data

The solution printout includes the moments about the x face, the moments about the y face, and the twisting moment. The moments are calculated per unit length in the element coordinate system. The element stress directions are parallel to the element coordinate system. The stress output of the SHELL63 element is shown in Figure 3.4.

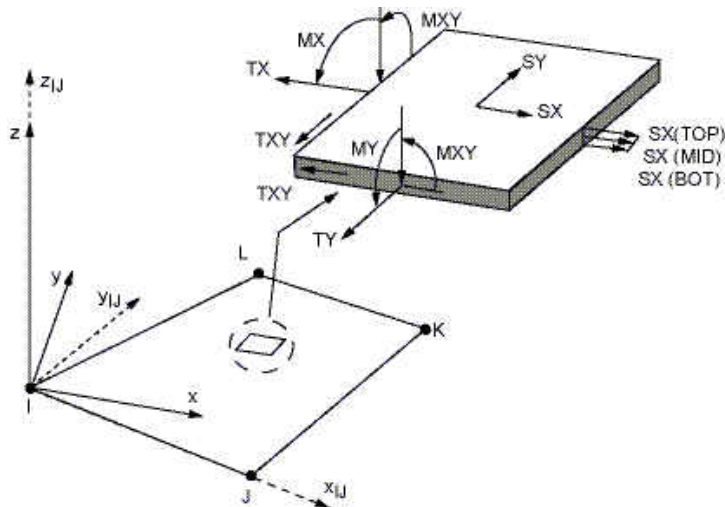


Figure 3.4: SHELL63 Stress Output

### Assumptions

There are some assumptions associated with the SHELL63 element. Zero area elements are not allowed; this occurs most often whenever the elements are not numbered properly. Also, zero thickness elements or elements tapering down to a zero thickness at any corner are not allowed. The applied transverse thermal gradient is assumed to vary linearly through the thickness and vary bilinearly over the shell surface. An assemblage of flat shell elements can produce a good approximation of a curved shell surface provided that each flat element does not extend over more than a  $15^\circ$  arc. If an elastic foundation stiffness is input, one-fourth of the total is applied at each node. Shear deflection is not included in this thin-shell element. A triangular element may be formed by defining duplicate K and L node numbers. The extra shapes are automatically deleted for triangular elements so that the membrane stiffness reduces to a constant strain formulation. For  $KEYOPT(1) = 0$  or  $2$ , the four nodes defining the element should lie as close as possible to a flat plane for maximum accuracy; however, a moderate amount of warping is permitted. For  $KEYOPT(1) = 1$ , the warping limit is very restrictive. In either

case, an excessively warped element may produce a warning or error message. If the lumped mass matrix formulation is specified, the effect of the implied offsets on the mass matrix is ignored for warped SHELL63 elements.

### **Restrictions**

There are also restrictions associated with ANSYS Professional using the SHELL63 element. The damp material property is not allowed. The only special features allowed are stress stiffening and large deflection. KEYOPT(2) and (9) can only be set to 0, the default.

## **3.4 ANSYS Verification Manual Test Examples**

The primary purpose of this manual is to demonstrate a wide range of ANSYS elements and capabilities in straightforward problems which have readily-obtainable theoretical solutions. Furthermore, the close agreement of the ANSYS solutions to the theoretical results in the verification manual is intended to provide confidence in the ANSYS solution. These problems are served as the basis for additional validation and qualification of ANSYS capabilities for the application of interest in this work [20].

### **3.4.1 VM19: Random Vibration Analysis of a Deep Simply-Supported Beam**

#### **Power Spectral Density (PSD)**

The power spectral density (PSD) describes how the power of a signal or time series is distributed with frequency. Mathematically, it is defined as the Fourier Transform of the autocorrelation sequence of the time series. An equivalent definition of PSD is the squared modulus of the Fourier transform of the time series, scaled by a proper constant term. The Fourier transform and PSD are defined as in Eq. (3.1). Mathematically, the definition of the complex spectrum of a sound  $x(t)$  in the time range  $(t_1, t_2)$  is given by Eq. (3.1).

$$X(f) = \int_{t_1}^{t_2} x(t)e^{-2\pi ift} dt \quad (3.1)$$

For a sound  $x(t)$ , defined for all times  $t$  in the domain  $(t_1, t_2)$  the complex spectrum  $X(f)$  for any frequency  $f$  is the Fourier transform of  $x(t)$ , in the two-sided frequency domain  $(-F, +F)$ , with a negative exponent is defined in Eq. (3.1). If  $x(t)$  is expressed in units of Pascal,  $X(f)$  is expressed in units of Pa/Hz. From the complex spectrum the one-sided power spectral density in  $Pa^2 / Hz$  can be computed as

$$PSD(f) = 2|X(f)|^2 / (t_2 - t_1) \quad (3.2)$$

where the factor 2 is due to adding the contributions from positive and negative frequencies.

### Test Example

In this test example, a deep simply-supported square beam is reviewed. The ANSYS input log file for VM19 is listed in Appendix A. The beam is of length  $\ell = 10m$  and has a square cross-sectional area of thickness  $t = 2.0m$ . The beam is subjected to random force power spectral density. There are three analysis types used: Mode-Frequency, Spectrum Analysis and Harmonic Analysis. The element type used is 3-D Elastic Beam, or BEAM4. The peak response PSD value is to be determined. The simply-supported beam finite element model and PSD is shown in Figure 3.5.

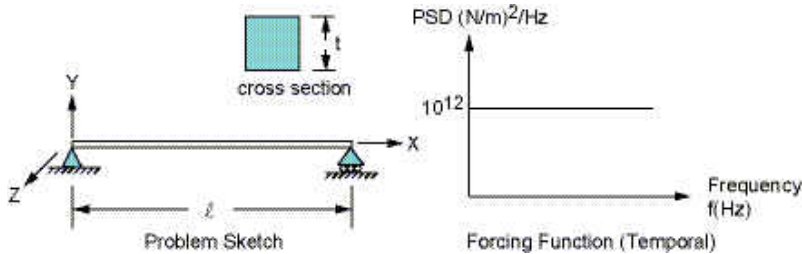


Figure 3.5: Simply-Supported Beam Problem Sketch

## Material Properties and Loading

Young's Modulus  $E = 200 \times 10^9 \text{ N} / \text{m}^2$

Poisson's Ratio  $\nu = 0.3$

Mass Density  $m = 8000 \text{ kg} / \text{m}^3$

$PSD = (10^6 \text{ N} / \text{m}^2)^2 / \text{Hz}$

Damping  $\delta = 0.02$

## Analysis Assumptions and Modeling

All degrees of freedom in the Y direction are selected as master degrees of freedom. A frequency range of  $0.1 \text{ Hz}$  to  $70 \text{ Hz}$  is used as an approximation of the white noise PSD forcing function frequency. White noise is a random signal with a flat power spectral density. The signal contains equal power within a fixed bandwidth at any center frequency.

Table 3.5: Result Comparison for VM19

Description	Analytical	ANSYS	Ratio
Modal Frequency $f$ (Hz)	42.65	42.66	1.00
PSD Freq (Hz)	42.66	42.64	1.00
Peak Deflection PSD ( $\text{mm}^2/\text{Hz}$ )	180.9	179.36	0.99
Peak Stress PSD ( $\text{N}/\text{mm}^2$ ) <sup>2</sup> /Hz	58516.	58533.	1.00

### 3.4.2 VM203: Dynamic Load Effect on Supported Thick Plate

In this ANSYS test case, a simply-supported thick square plate is subject to random uniform pressure power spectral density in order to determine the peak one-sigma, or one standard deviation, displacement at undamped natural frequency. The results follow a Gaussian distribution; 68.3% of the time the response will be less than the standard deviation value. The dimensions of the plate are  $\ell = 10 \text{ m}$  and  $t = 1.0 \text{ m}$ . The

analysis types used are Mode-Frequency, Spectrum Analysis and Harmonic Analysis. A modal analysis of the structure should be initially performed to provide information about the structure's dynamic behavior; determining the mode frequencies and mode shapes. Then, a harmonic analysis should be performed to analyze the steady-state behavior of a structure subject to cyclic loads. Lastly, a spectral analysis studies the response of a structure under the action of loads with known "spectra," for example, random loading conditions. The element type used is the 8-Node Finite Strain Shell Elements, or SHELL281. The problem sketch is shown in Figure 3.6. The ANSYS input log file for VM203 is listed in Appendix B.

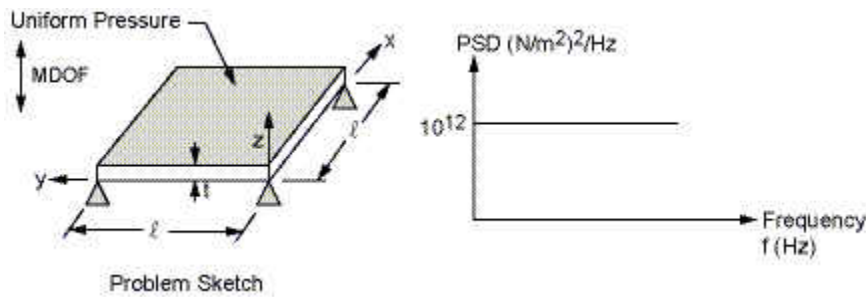


Figure 3.6: Thick Square Plate Problem Sketch

### Material Properties and Loading

Young's Modulus  $E = 200 \times 10^9 \text{ N} / \text{m}^2$

Poisson's Ratio  $\nu = 0.3$

Mass Density  $m = 8000 \text{ kg} / \text{m}^3$

$PSD = (10^6 \text{ N} / \text{m}^2)^2 / \text{Hz}$

Damping  $\delta = 0.02$

### Analysis Assumptions and Modeling

When conducting a modal analysis, an option is to use the reduced mode extraction method; this requires that all degrees of freedom, in this case in the z direction,



are selected as master degrees of freedom. Equivalent nodal forces are obtained from a uniform pressure load by a static run with all UZ degrees of freedom constrained. A frequency range of  $1.0\text{Hz}$  to  $80\text{Hz}$  is used as an approximation of the white noise PSD forcing function frequency. Equivalent analyses are done with Spectrum and Harmonic analyses to compare the peak one-sigma standard deviation. Results from the output are compared to analytical values in Table 3.6, which show that the analytical values are 0.1% and 5.7% off the ANSYS values, respectively. In Figure 3.7, a dynamic analysis of the model is shown, depicting a natural frequency at 45.95 Hz.

Table 3.6: Result Comparison for VM203

Description	Analytical	ANSYS	Ratio
Frequency $f$ (Hz)	45.9	45.95	1.009
Peak Deflection PSD ( $\text{mm}^2/\text{Hz}$ )	340.2	359.5	1.057

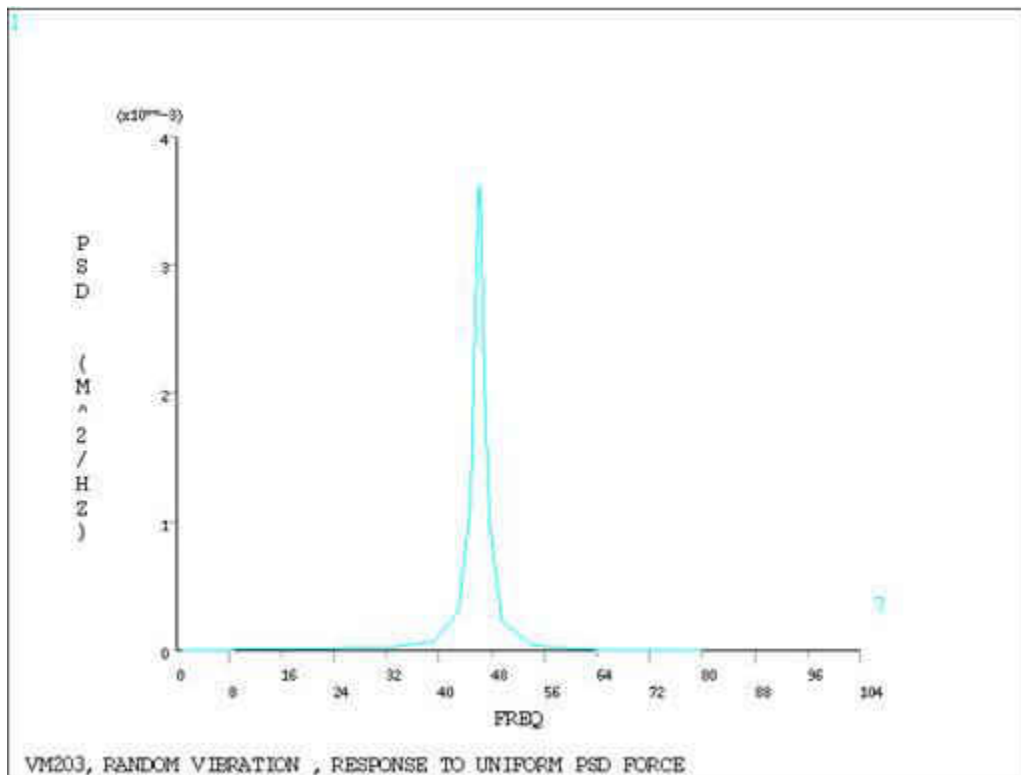


Figure 3.7: Harmonic Response to Uniform PSD Force

This chapter introduced the frequency response function, the finite element analysis methods in terms of mode frequency, harmonic, and spectrum analyses, the different elements involved including BEAM4 and SHELL63, and a couple of the finite element verification manual examples which are referred in the analysis and simulation using ANSYS. The next chapter further discusses the three analyses and their formulations in general.

## **CHAPTER IV**

### **ANALYSES FORMULATION**

Simulations of the beam, plate, and cylindrical shell are carried out by a combination of analysis types. The objective of this chapter is to introduce the three analysis types involved with the FRF: their purpose, and to show a general formulation of the three analysis types. The ultimate purpose is to obtain the nodal complex displacements when a single point excitation force is applied at the opposite end to the support on the structure; on the beam the force is applied at the node at the end, on the plate the force is applied at the node in the center on the end of the plate, and on the cylinder the force is applied at the node in the center of the cylinder on the top end. Three analysis types are used in the simulation: mode-frequency, spectrum, and harmonic. The order in which the analyses are described is also the order in which they are performed in the simulation in order to achieve the required objective of the structure simulation. ANSYS [20] is used for the descriptions and formulations of the analyses in this chapter.

#### **4.1 Analyses Procedures**

##### **4.1.1 Mode Frequency Analysis**

This analysis type is used for natural frequency and mode shape determination of a structure which has no time varying forces, displacements, pressures, or temperatures applied. The modes are extracted and expanded within a specified frequency range, then are written to the results file.

### **4.1.2 Spectrum Analysis**

A spectrum analysis is one in which the results of a modal analysis are used with a known spectrum to calculate displacements and stresses in the model. The spectrum is a graph of spectral values versus frequency that captures the intensity and frequency content of time-history loads, where the values may be displacement, velocity, acceleration, or force. The spectrum analysis must be preceded by a mode-frequency analysis, because a structure's mode shapes and frequencies must be available to calculate the spectrum solution. Also, by performing the spectrum solution before mode expansion, only the significant modes that contribute to the final solution can be expanded.

### **4.1.3 Harmonic Response Analysis**

In a structural system, any sustained cyclic load will produce a sustained cyclic or harmonic response. Harmonic response analysis gives the ability to predict the sustained dynamic behavior of structures, thus giving the ability to verify whether or not a design will successfully overcome resonance, fatigue, and other harmful effects of forced vibrations. This analysis technique calculates only the steady-state, forced vibrations of a structure. The transient vibrations, which occur at the beginning of the excitation, are not accounted for in a harmonic response analysis. In this analysis all loads as well as the structure's response vary sinusoidally at the same frequency. A typical harmonic analysis will calculate the response of the structure to cyclic loads over a frequency range (a sine sweep) and obtain a graph of some response quantity (usually displacements) versus frequency. "Peak" responses are then identified from graphs of response versus frequency and stresses are then reviewed at those peak frequencies.

## 4.2 Mode Frequency Analysis

In modal analyses, vibration characteristics, such as natural frequencies and mode shapes, of a structure or a machine component are determined. It can also serve as an initial point for another, more detailed, dynamic analysis, such as a transient dynamic analysis, a spectrum analysis, or a harmonic analysis. The natural frequencies and mode shapes are important parameters in the design of a structure for dynamic loading conditions. It is required to define stiffness as well as mass in some form. Stiffness may be specified using isotropic and orthotropic elastic material models, for example, Young's modulus and Poisson's ratio. Modal analysis is a linear analysis; any nonlinearity is ignored even if it is defined. The modal solution is needed to calculate the spectrum solution, and there are many mode-extraction methods available: Block Lanczos, Supernode, PCG Lanczos, reduced, unsymmetric, damped, and QR damped. Each method is unique, and which method should be used depends on what the situation requires. If the situation requires the inclusion of the missing mass effect in the spectrum analysis, then the Block Lanczos or PCG Lanczos method should be used. The number of modes extracted should be enough to characterize the structure's response in the frequency range of interest.

### 4.2.1 Formulation

The general equation of motion for a damped system, expressed in matrix notation, and subjected to the force vector  $\{F\}$  is given by Eq. (4.1).

$$[M]\{\ddot{u}\} + [C]\{\dot{u}\} + [K]\{u\} = \{F\} \quad (4.1)$$

$[K]$  is the structural stiffness matrix,  $[C]$  is the structural damping matrix,  $\{u\}$  is the nodal displacement vector and  $[M]$  is the mass matrix. For a linear system, free vibrations are harmonic of the form:

$$\{u\} = \{\phi\}_i \cos \omega_i t \quad (4.2)$$

where,  $\{\phi\}_i$  is an eigenvector representing the mode shape of the  $i^{th}$  natural frequency and  $\omega_i$  is the  $i^{th}$  natural circular frequency (radians per unit time) and  $t$  is the time.

Substituting Eq. (4.2) into Eq. (4.1), Eq. (4.3) becomes:

$$\left(-\omega_i^2 [M] + [K]\right) \{\phi\}_i = \{0\} \quad (4.3)$$

This equality is satisfied if either  $\{\phi\}_i$  is zero or if the determinant of  $\left(-\omega_i^2 [M] + [K]\right)$  is zero. The first option is the trivial one and, therefore, is not of interest. Thus, the second one gives the solution as  $\left|[K] - \omega^2 [M]\right| = 0$ . This is an eigenvalue problem which may be solved for up to  $n$  values of  $\omega_n^2$  and  $n$  eigenvectors  $\{\phi\}_i$  which satisfy Eq. (4.3) where  $n$  is the number of DOFs. Rather than outputting natural circular frequencies  $\{\omega\}$ , the natural frequencies ( $f$ ) are output, where

$$f_i = \frac{\omega_i}{2\pi} \quad (4.4)$$

If normalization of each eigenvector  $\{\phi\}_i$  to the mass matrix is selected,  $\{\phi\}_i$  is normalized such that its largest component is 1.0.

$$\{\phi\}_i^T [M] \{\phi\}_i = 1 \quad (4.5)$$

Eq. (4.2) can also be written in a more general form as a set of modal coordinates,  $y_i$ , is defined such that:

$$\{u\} = \sum_{i=1}^n \{\phi_i\} y_i \quad (4.6)$$

where,  $\{\phi_i\}$  is the mode shape of mode  $i$ , and  $n$  is the number of modes to be used. The inverse relationship does exist for the case where all the displacements are known, but not when only some are known. Substituting Eq. (4.6) into Eq. (4.1) gives Eq. (4.7).

$$[M] \sum_{i=1}^n \{\phi_i\} \ddot{y}_i + [C] \sum_{i=1}^n \{\phi_i\} \dot{y}_i + [K] \sum_{i=1}^n \{\phi_i\} y_i = \{F\} \quad (4.7)$$

Pre-multiplying by a typical mode shape  $\{\phi_j\}^T$  gives Eq. (4.8).

$$\{\phi_j\}^T [M] \sum_{i=1}^n \{\phi_i\} \ddot{y}_i + \{\phi_j\}^T [C] \sum_{i=1}^n \{\phi_i\} \dot{y}_i + \{\phi_j\}^T [K] \sum_{i=1}^n \{\phi_i\} y_i = \{\phi_j\}^T \{F\} \quad (4.8)$$

The orthogonal condition of the natural modes states that

$$\{\phi_j\}^T [M] \{\phi_i\} = 0 \text{ if } i \neq j \quad (4.9)$$

$$\{\phi_j\}^T [K] \{\phi_i\} = 0 \text{ if } i \neq j \quad (4.10)$$

In the mode superposition method using the Lanczos and other extraction methods, only Rayleigh or constant damping is allowed so that:

$$\{\phi_j\}^T [C] \{\phi_i\} = 0 \text{ if } i \neq j \quad (4.11)$$

The Lanczos methods use the Lanczos algorithm, which is an iterative algorithm used to find eigenvalues and eigenvectors of a square matrix. It is useful for finding decompositions of very large sparse matrices (matrices made up of mostly zeros).

Rayleigh's damping is expressed as  $[C] = \alpha[M] + \beta[K]$  where  $\alpha$  and  $\beta$  are constants to be determined from two given damping ratios that correspond to two unequal frequencies

of vibration. It is also known as proportional damping, because  $C$  is proportional to a linear combination of  $[M]$  and  $[K]$ .

Applying these conditions to Eq. (4.8), only the  $i = j$  terms remain:

$$\{\phi_j\}^T [M] \{\phi_j\} \ddot{y}_j + \{\phi_j\}^T [C] \{\phi_j\} \dot{y}_j + \{\phi_j\}^T [K] \{\phi_j\} y_j = \{\phi_j\}^T [F] \quad (4.12)$$

The coefficient of  $\ddot{y}_j$ ,  $\dot{y}_j$ , and  $y_j$  are derived as follows:

Coefficient of  $\ddot{y}_j$ , by the normality condition in Eq. (4.5),

$$\{\phi_j\}^T [M] \{\phi_j\} = 1 \quad (4.13)$$

Coefficient of  $\dot{y}_j$ : The damping term is based on treating the modal coordinate as a single degree of freedom system for which:

$$\{\phi_j\}^T [C] \{\phi_j\} = C_j \phi_j^2 \quad (4.14)$$

$$\{\phi_j\}^T [M] \{\phi_j\} = M_j \phi_j^2 = 1 \quad (4.15)$$

Eq. (4.13) can give a definition of  $\phi_j$ :

$$\phi_j = \frac{1}{\sqrt{M_j}} \quad (4.16)$$

The critical damping constant:

$$C_j = 2\xi_j \sqrt{K_j M_j} \quad (4.17)$$

Where,  $\xi_j$  is the fraction of critical damping for mode  $j$  and,

$$\omega_j = \sqrt{K_j / M_j} \quad (4.18)$$

where,  $\omega_j$  is the natural circular frequency of the mode  $j$ .



Combining Eq. (4.16) through Eq. (4.13) with Eq. (4.14),

$$\{\phi_j\}^T [C]\{\phi_j\} = 2\xi_j \sqrt{K_j M_j} \left( \frac{1}{\sqrt{M_j}} \right)^2 = 2\xi_j \omega_j \quad (4.19)$$

Coefficient of  $y_j$ :

from Eq. (4.3):

$$[K]\{\phi_j\} = \omega_j^2 [M]\{\phi_j\} \quad (4.20)$$

Pre-multiplying Eq. (4.3) by a typical mode shape  $\{\phi_j\}^T$ ,

$$\{\phi_j\}^T [K]\{\phi_j\} = \omega_j^2 \{\phi_j\}^T [M]\{\phi_j\} \quad (4.21)$$

Substituting Eq. (4.7) for the mass term,

$$\{\phi_j\}^T [K]\{\phi_j\} = \omega_j^2 \quad (4.22)$$

For convenient notation, let

$$f_j = \{\phi_j\}^T \{F\} \quad (4.23)$$

represent the right-hand side of Eq. (4.40). Substituting Eq. (4.41), Eq. (4.47), Eq. (4.8) and Eq. (4.9) into Eq. (4.40), the equation of motion of the modal coordinates is obtained in Eq. (4.52).

$$\ddot{y}_j + 2\omega_j \xi_j \dot{y}_j + \omega_j^2 y_j = f_j \quad (4.24)$$

Where,  $y_j$  is modal coordinate,  $\omega_j$  is natural circular frequency of mode  $j$ ,  $\xi_j$  is fraction of critical damping for mode  $j$  and  $f_j$  is force in modal coordinates. Since  $j$  represents any mode, Eq. (4.10) represents  $n$  uncoupled equations in the  $n$  unknowns  $y_j$ .

### 4.3 Spectrum Analysis

Two types of spectrum analyses are supported: the deterministic response spectrum method and the nondeterministic random vibration method. Both the excitation at the support and excitation away from the support are allowed. The three types of spectra are the single-point, multi-point, and dynamic design analysis method. The random vibration method uses the power spectral density, PSD, approach.

#### 4.3.1 Response Spectrum

A response spectrum represents the response of single degree of freedom systems to a time-history loading function. It is a graph of response versus frequency, where the response might be displacement, velocity, acceleration, or force. Two types of response spectrum analysis are possible: single and multi-point response spectra. In a single-point response spectrum analysis, one response spectrum curve is specified, or a family of curves, at a set of points in the model, such as at all supports, as shown in Figure 4.1 (a). In a multi-point response spectrum analysis, different spectrum curves are specified at different sets of points, as shown in Figure 4.2 (b).

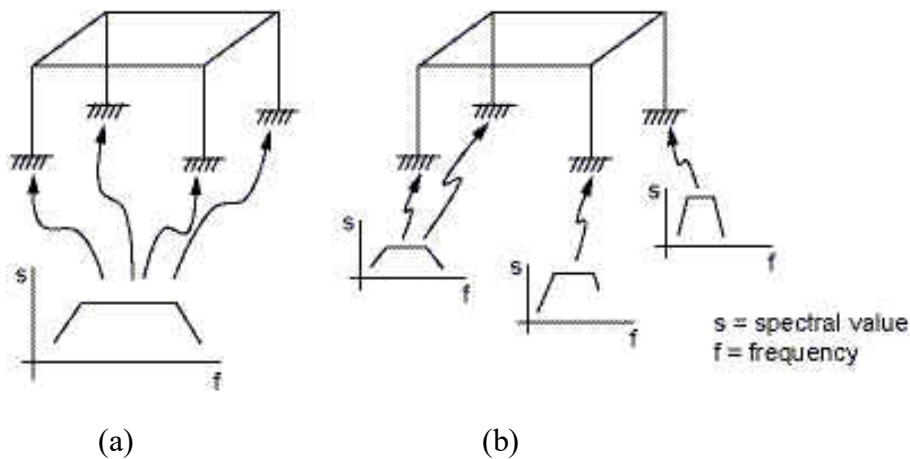


Figure 4.1: (a) Single-Point and (b) Multi-Point Response Spectra

### **4.3.2 Dynamic Design Analysis Method (DDAM)**

The Dynamic Design Analysis Method (DDAM) is a technique used to evaluate the shock resistance of shipboard equipment. The technique is essentially a response spectrum analysis in which the spectrum is obtained from a series of empirical equations and shock design tables provided in the U.S. Naval Research Laboratory Report NRL-1396.

### **4.3.3 Power Spectral Density (PSD) Approach**

Power spectral density, or PSD, is a statistical measure defined as the limiting mean-square value of a random variable. It is used in random vibration analyses in which the instantaneous magnitudes of the response can be specified only by probability distribution functions that show the probability of the magnitude taking a particular value. A PSD is a statistical measure of the response of a structure to random dynamic loading conditions. It is a graph of the PSD value versus frequency, where the PSD may be a displacement PSD, velocity PSD, acceleration PSD, or force PSD. Mathematically, the area under a PSD-versus-frequency curve is equal to the variance. Similar to response spectrum analysis, a random vibration analysis may be single-point or multi-point. In a single-point random vibration analysis, one PSD spectrum is specified at a set of points in the model; whereas in a multi-point random vibration analysis, different PSD spectra are specified at different points in the model.

### **4.3.4 Single Point Response Random Vibration Analysis**

The spectrum analysis must be preceded by a modal analysis. If mode combinations are needed, the required modes must also be expanded. One of the four options available is the single-point response spectrum method. Both excitation at the

support, base excitation, and excitation away from the support, force excitation, is allowed for the single-point response spectrum analysis.

#### 4.3.5 Random Vibration Method Formulation

The random vibration method allows multiple power spectral density (PSD) inputs in which these inputs can be: full correlated, uncorrelated, or partially correlated. The procedure is based on computing statistics of each modal response and then combining them. It is assumed that the excitations are stationary random processes. For partially correlated nodal and base excitations, the complete equations of motion are segregated into the free and the restrained degrees of freedom as:

$$\begin{bmatrix} [M_{ff}] & [M_{fr}] \\ [M_{rf}] & [M_{rr}] \end{bmatrix} \begin{Bmatrix} \ddot{\{u_f\}} \\ \ddot{\{u_r\}} \end{Bmatrix} + \begin{bmatrix} [C_{ff}] & [C_{fr}] \\ [C_{rf}] & [C_{rr}] \end{bmatrix} \begin{Bmatrix} \dot{\{u_f\}} \\ \dot{\{u_r\}} \end{Bmatrix} + \begin{bmatrix} [K_{ff}] & [K_{fr}] \\ [K_{rf}] & [K_{rr}] \end{bmatrix} \begin{Bmatrix} \{u_f\} \\ \{u_r\} \end{Bmatrix} = \begin{Bmatrix} \{F\} \\ \{0\} \end{Bmatrix} \quad (4.25)$$

where,  $\{u_f\}$  are the free DOF and  $\{u_r\}$  are the restrained DOF that are excited by random loading,  $\{F\}$  is the nodal force excitation activated by a nonzero value of force. The value of force can be other than unity, allowing for scaling of the participation factors. The free displacements can be decomposed into pseudo-static and dynamic parts as in Eq. (4.26).

$$\{u_f\} = \{u_s\} + \{u_d\} \quad (4.26)$$

The pseudo-static displacements may be obtained from Eq. (4.25) by excluding the first two terms on the left-hand side of the equation and by replacing  $\{u_f\}$  by  $\{u_s\}$ .

$$\{u_s\} = -[K_{ff}]^{-1}[K_{fr}]\{u_r\} = [A]\{u_r\} \quad (4.27)$$

in which  $[A] = -[K_{ff}]^{-1}[K_{fr}]$ . Physically, the elements along the  $i^{th}$  column of  $[A]$  are the pseudo-static displacements due to a unit displacement of the support DOFs excited by  $i^{th}$  the base PSD. Substituting Eqns. (4.26) & (4.27) into (4.25) and assuming light damping yields:

$$[M_{ff}]\{\ddot{u}_d\} + [C_{ff}]\{\dot{u}_d\} + [K_{ff}]\{u_d\} = \{F\} - ([M_{ff}][A] + [M_{fr}])\{\ddot{u}_r\} \quad (4.28)$$

The second term on the right-hand side of the above equation represents the equivalent forces due to support excitations. Using the mode superposition analysis, as described in the Mode Superposition Method section in ANSYS Help, gives the Eq. (4.29)

$$\{u_d(t)\} = [\varphi]\{y(t)\} \quad (4.29)$$

The above equations are decoupled yielding Eq. (4.30)

$$\ddot{y}_j + 2\xi_j\omega_j\dot{y}_j + \omega_j^2 y_j = G_j \quad (j=1,2,3,\dots,n) \quad (4.30)$$

where,  $n$  is the number of modes chosen for the evaluation,  $y_j$  are the generalized displacements,  $\omega_j$  and  $\xi_j$  are the natural circular frequency and modal damping ratio, respectively. The modal loads  $G_j$  are defined by Eq. (4.31)

$$G_j = \{\Gamma_j\}^T \{\ddot{u}_r\} + \gamma_j \quad (4.31)$$

The modal participation factors corresponding to support excitation are given by:

$$\{\Gamma_j\} = -([M_{ff}][A] + [M_{fr}])^T \{\phi_j\} \quad (4.32)$$

and for nodal excitation:

$$\gamma_j = \{\phi_j\}^T \{F\} \quad (4.33)$$

### 4.3.6 Response Power Spectral Densities and Mean Square Response

Using the theory of random vibrations, the response PSDs can be computed from the input PSDs with the help of transfer functions for single DOF systems  $H(\omega)$  and by using mode superposition techniques. The response PSDs for  $i^{th}$  DOF are given by the Dynamic part, Pseudo-static part and Covariance part as described below.

#### Dynamic Part

$$S_{d_i}(\omega) = \sum_{j=1}^n \sum_{k=1}^n \varphi_{ij} \varphi_{ik} \left( \sum_{\ell=1}^{r_1} \sum_{m=1}^{r_1} \gamma_{\ell j} \gamma_{\ell k} H_j^*(\omega) H_k(\omega) S_{\ell m}^-(\omega) + \sum_{\ell=1}^{r_2} \sum_{k=1}^{r_2} \Gamma_{\ell j} \Gamma_{\ell k} H_j^*(\omega) H_k(\omega) \hat{S}_{\ell m}(\omega) \right)$$

#### Pseudo-Static Part

$$S_{s_i}(\omega) = \sum_{\ell=1}^{r_2} \sum_{m=1}^{r_2} A_{i\ell} A_{im} \left( \frac{1}{\omega^4} \hat{S}_{\ell m}(\omega) \right)$$

#### Covariance Part

$$S_{sd_i}(\omega) = \sum_{j=1}^n \sum_{\ell=1}^{r_2} \sum_{m=1}^{r_2} \varphi_{ij} A_{i\ell} \left( -\frac{1}{\omega^2} \Gamma_{mj} H_j(\omega) \hat{S}_{\ell m}(\omega) \right)$$

where,  $n$  is the number of mode shapes chosen for evaluation.  $r_1$  and  $r_2$  are the number of nodal (away from support) and base PSD tables, respectively. The transfer functions for the single DOF system assume different forms depending on the type of the input PSD and the type of response desired. The forms of the transfer functions for displacement as the output are listed below for different inputs in Eq. (4.34), (4.35), and (4.36).

When input as a force or acceleration:

$$H_j(\omega) = \frac{1}{\omega_j^2 - \omega^2 + i(2\xi_j\omega_j\omega)} \quad (4.34)$$

When input as a displacement:

$$H_j(\omega) = \frac{\omega^2}{\omega_j^2 - \omega^2 + i(2\xi_j\omega_j\omega)} \quad (4.35)$$

When input is a velocity:

$$H_j(\omega) = \frac{i\omega}{\omega_j^2 - \omega^2 + i(2\xi_j\omega_j\omega)} \quad (4.36)$$

where  $\omega$  is the forcing frequency and  $\omega_j$  is the natural circular frequency for the  $j^{th}$  mode and  $i = \sqrt{-1}$ . Now, random vibration analysis can be used to show that the absolute value of the mean square response of the  $i^{th}$  free displacement is Eq. (4.37)

$$\sigma_{f_i}^2 = \sigma_{d_i}^2 + \sigma_{s_i}^2 + 2C_v(U_{s_i}, U_{d_i}) \quad (4.37)$$

where,  $\sigma_{d_i}^2$  is the variance of the  $i^{th}$  relative (dynamic) free displacement,  $\sigma_{s_i}^2$  is the variance of the  $i^{th}$  pseudo-static displacement and  $C_v(U_{s_i}, U_{d_i})$  is the covariance between static and dynamic displacements. The general formulation described above gives simplified equations for several situations commonly encountered in practice.

Results from a random vibration analysis are written to the structural results file, which consists of expanded mode shapes from the modal analysis, static solution for base excitation, and the one sigma displacement solution output. These one sigma, or one standard deviation, values follow a Gaussian distribution. The interpretation is that 68.3% of the time the response will be less than the standard deviation value. The results may be reviewed in ANSYS POST1, the general postprocessor, and then response PSDs can be calculated in POST26, the time-history postprocessor.

## 4.4 Harmonic Response Analysis

The harmonic response analysis solves the time-dependent equations of motion for linear structures undergoing steady-state vibration. It is assumed this analysis is valid for structural, fluid, magnetic, and electrical degrees of freedom. Also, the entire structure has constant or frequency-dependent stiffness, damping, and mass effects. Another assumption is that all loads and displacements vary sinusoidally at the same known frequency, although not necessarily in phase. Element loads are assumed to be real (in-phase) only, except for current density and pressures in SURF153 and SURF154 elements.

### 4.4.1 Formulation

Consider the general equation of motion for a structural system with damping.

$$[M]\{\ddot{u}\} + [C]\{\dot{u}\} + [K]\{u\} = \{F^a\} \quad (4.38)$$

where,  $[M]$  is the structural mass matrix,  $[C]$  is the structural damping matrix,  $[K]$  is the structural stiffness matrix,  $\{\ddot{u}\}$  is the nodal acceleration vector,  $\{\dot{u}\}$  is the nodal velocity vector,  $\{u\}$  is the nodal displacement vector and  $\{F^a\}$  is the applied load vector. All the points in the structure are moving at the same known frequency, however, not necessarily in the same phase. Also, it is known that the presence of damping causes phase shifts. Therefore, the displacements may be defined by Eq. (4.39).

$$\{u\} = \{u_{\max} e^{i\phi}\} e^{i\Omega t} \quad (4.39)$$

where,  $u_{\max}$  is the maximum displacement,  $i$  is  $\sqrt{-1}$ ,  $\Omega$  is the imposed circular frequency in (radians/time) or  $2\pi f$ ,  $f$  is the imposed frequency (cycles/time),  $t$  is time, and  $\phi$  is the displacement phase shift (radians).  $u_{\max}$  and  $\phi$  may be different at each degree of freedom. The



use complex notation allows a compact and efficient description of the problem. Eq. (4.39) can be rewritten as:

$$\{u\} = \{u_{\max} (\cos \phi + i \sin \phi)\} e^{i\Omega t} \quad (4.40)$$

$$\text{or as: } \{u\} = (\{u_1\} + i\{u_2\}) e^{i\Omega t} \quad (4.41)$$

where,  $\{u_1\} = \{u_{\max} \cos \phi\}$  which is the real displacement vector and  $\{u_2\} = \{u_{\max} \sin \phi\}$  is the imaginary displacement vector.

The force vector can be described analogously to the displacement:

$$\{F\} = \{F_{\max} e^{i\psi}\} e^{i\Omega t} \quad (4.42)$$

$$\{F\} = \{F_{\max} (\cos \psi + i \sin \psi)\} e^{i\Omega t} \quad (4.43)$$

$$\{F\} = (\{F_1\} + i\{F_2\}) e^{i\Omega t} \quad (4.44)$$

where,  $F_{\max}$  is the force amplitude.  $\psi$  is force phase shift (in radians).  $\{F_1\} = \{F_{\max} \cos \psi\}$  is the real force vector.  $\{F_2\} = \{F_{\max} \sin \psi\}$  is the imaginary force vector.

Substituting Eq. (4.41) and (4.44) into Eq. (4.38) produces Eq. (4.45).

$$(-\Omega^2 [M] + i\Omega [C] + [K]) (\{u_1\} + i\{u_2\}) e^{i\Omega t} = (\{F_1\} + i\{F_2\}) e^{i\Omega t} \quad (4.45)$$

The dependence on time  $e^{i\Omega t}$  from both sides gives Eq. (4.46).

$$(-\Omega^2 [M] + i\Omega [C] + [K]) (\{U_1\} + i\{U_2\}) = (\{F_1\} + i\{F_2\}) \quad (4.46)$$

#### 4.4.2 Complex Displacement Output

The complex displacement output at each degree of freedom may be given in one of two forms: first, the form  $u_1$ , the real displacement vector, and  $u_2$ , the imaginary displacement vector, and second, the form  $u_{\max}$ , the amplitude, and  $\phi$ , the phase angle, computed at each degree of freedom as:

$$u_{\max} = \sqrt{u_1^2 + u_2^2} \quad (4.47)$$

$$\phi = \tan^{-1} \frac{u_2}{u_1} \quad (4.48)$$

#### 4.4.3 Nodal and Reaction Load Computation

Inertia, damping and static loads on the nodes of each element are computed. The real and imaginary inertia load parts of the element output are computed by:

$$\{F_1^m\}_e = \Omega^2 [M_e] \{u_1\}_e \quad (4.49)$$

$$\{F_2^m\}_e = \Omega^2 [M_e] \{u_2\}_e \quad (4.50)$$

where,  $\{F_1^m\}_e$  and  $\{F_2^m\}_e$  are the real and imaginary parts of the vector of element inertia forces, respectively.  $\{u_1\}_e$ ,  $\{u_2\}_e$  are the real and imaginary parts of the element displacement vectors, respectively.  $[M_e]$  is the element mass matrix.

The real and imaginary damping loads, part of the element output, are computed by Eqs. (4.51) and (4.52)

$$\{F_1^c\}_e = -\Omega [C_e] \{u_2\}_e \quad (4.51)$$

$$\{F_2^c\}_e = \Omega [C_e] \{u_1\}_e \quad (4.52)$$

where,  $\{F_1^c\}_e$  is a vector of element damping forces, the real part,  $\{F_2^c\}_e$  is a vector of element damping forces, the imaginary part, and  $[C_e]$  is the element damping matrix. The real static load is computed the same way as in a static analysis using the real part of the displacement solution  $\{u_1\}_e$ . The imaginary static load is computed also the same way, using the imaginary part  $\{u_2\}_e$ . The imaginary part of the element loads is normally zero, except for current density loads. The nodal reaction loads are computed as the sum of all

three types of loads (inertia, damping, and static) over all elements connected to a given fixed displacement node. There are three available methods for the solution of harmonic response analysis: Full Solution Method, Reduced Solution Method, and Mode Superposition Method, which is used in this simulation.

#### 4.4.4 Mode Superposition Method

Three harmonic response analysis methods are available: full, reduced, and mode superposition. The ANSYS Professional program allows only the mode superposition method. In this method a modal analysis is first performed to compute the natural frequencies and mode shapes. Then the mode superposition solution is carried where these mode shapes are combined to arrive at a solution. This method is faster and less expensive than either the reduced or the full method for many problems. The equation of motion can be expressed as in Eq. (4.53).

$$[M]\{\ddot{u}\} + [C]\{\dot{u}\} + [K]\{u\} = \{F\} \quad (4.53)$$

$\{F\}$  is the time-varying load vector, given by Eq. (4.54)

$$\{F\} = \{F^{nd}\} + s\{F^s\} \quad (4.54)$$

where,  $\{F^{nd}\}$  are time varying nodal forces,  $\{F^s\}$  are load vectors from the modal analysis, and  $s$  is the load vector scale factor. The load vector  $\{F^s\}$  is computed when doing a modal analysis and its generation is the same as for a substructure load vector. A set of modal coordinates  $y_i$  is defined, such that:

$$\{u\} = \sum_{i=1}^n \{\phi_i\} y_i \quad (4.55)$$

where,  $\{\phi_i\}$  is the mode shape of mode  $i$ , and  $n$  is the number of modes to be used. The inverse relationship does exist for the case where all the displacements are known, but not when only some are known. Substituting Eq. (4.55) into Eq. (4.53) gives Eq. (4.56).

$$[M] \sum_{i=1}^n \{\phi_i\} \ddot{y}_i + [C] \sum_{i=1}^n \{\phi_i\} \dot{y}_i + [K] \sum_{i=1}^n \{\phi_i\} y_i = \{F\} \quad (4.56)$$

Pre-multiplying by a typical mode shape  $\{\phi_j\}^T$  gives Eq. (4.57).

$$\{\phi_j\}^T [M] \sum_{i=1}^n \{\phi_i\} \ddot{y}_i + \{\phi_j\}^T [C] \sum_{i=1}^n \{\phi_i\} \dot{y}_i + \{\phi_j\}^T [K] \sum_{i=1}^n \{\phi_i\} y_i = \{\phi_j\}^T \{F\} \quad (4.57)$$

The orthogonal condition of the natural modes states that

$$\{\phi_j\}^T [M] \{\phi_i\} = 0 \text{ if } i \neq j \quad (4.58)$$

$$\{\phi_j\}^T [K] \{\phi_i\} = 0 \text{ if } i \neq j \quad (4.59)$$

In the mode superposition method using the Lanczos and other extraction methods, only Rayleigh or constant damping is allowed so that:

$$\{\phi_j\}^T [C] \{\phi_i\} = 0 \text{ if } i \neq j \quad (4.60)$$

Applying these conditions to Eq. (4.57), only the  $i = j$  terms remain:

$$\{\phi_j\}^T [M] \{\phi_j\} \ddot{y}_j + \{\phi_j\}^T [C] \{\phi_j\} \dot{y}_j + \{\phi_j\}^T [K] \{\phi_j\} y_j = \{\phi_j\}^T \{F\} \quad (4.61)$$

The coefficient of  $\ddot{y}_j$ ,  $\dot{y}_j$ , and  $y_j$  are derived as follows:

Coefficient of  $\ddot{y}_j$ : By the normality condition in Eq. (4.5),

$$\{\phi_j\}^T [M] \{\phi_j\} = 1 \quad (4.62)$$

Coefficient of  $y_j$ : The damping term is based on treating the modal coordinate as a single degree of freedom system for which:

$$\{\phi_j\}^T [C] \{\phi_j\} = C_j \phi_j^2 \quad (4.63)$$

$$\{\phi_j\}^T [M] \{\phi_j\} = M_j \phi_j^2 = 1 \quad (4.64)$$

Eq. (4.64) can give a definition of  $\phi_j$ :

$$\phi_j = \frac{1}{\sqrt{M_j}} \quad (4.65)$$

The critical damping constant:

$$C_j = 2\xi_j \sqrt{K_j M_j} \quad (4.66)$$

Where,  $\xi_j$  is the fraction of critical damping for mode  $j$

and,

$$\omega_j = \sqrt{\frac{K_j}{M_j}} \quad (4.67)$$

where,  $\omega_j$  is the natural circular frequency of the mode  $j$ .

Combining Eq. (4.65) thru Eq. (4.62) with Eq. (4.63),

$$\{\phi_j\}^T [C] \{\phi_j\} = 2\xi_j \sqrt{K_j M_j} \left( \frac{1}{\sqrt{M_j}} \right)^2 = 2\xi_j \omega_j \quad (4.68)$$

Coefficient of  $y_j$ :

from Eq. (4.3):

$$[K] \{\phi_j\} = \omega_j^2 [M] \{\phi_j\} \quad (4.69)$$

Pre-multiplying by  $\{\phi_j\}^T$ ,

$$\{\phi_j\}^T [K]\{\phi_j\} = \omega_j^2 \{\phi_j\}^T [M]\{\phi_j\} \quad (4.70)$$

Substituting Eq. (4.70) for the mass term,

$$\{\phi_j\}^T [K]\{\phi_j\} = \omega_j^2 \quad (4.71)$$

For convenient notation, let

$$f_j = \{\phi_j\}^T \{F\} \quad (4.72)$$

represent the right-hand side of Eq. (4.61). Substituting Eq. (4.62), Eq. (4.68), Eq. (4.71) and Eq. (4.72) into Eq. (4.61), the equation of motion of the modal coordinates is obtained in Eq. (4.73).

$$\ddot{y}_j + 2\omega_j \xi_j \dot{y}_j + \omega_j^2 y_j = f_j \quad (4.73)$$

Where,  $y_j$  is modal coordinate,  $\omega_j$  is natural circular frequency of mode  $j$ ,  $\xi_j$  is fraction of critical damping for mode  $j$  and  $f_j$  is force in modal coordinates. Since  $j$  represents any mode, Eq. (4.73) represents  $n$  uncoupled equations in the  $n$  unknowns  $y_j$ . The  $y_j$  are converted back into geometric displacements  $\{u\}$  (the system response to the loading) by using Eq. (4.55). That is, the individual modal responses  $y_j$  are superimposed to obtain the actual response, and hence the name “mode superposition.”

For a steady sinusoidal vibration,  $f_j$  has the form:

$$f_j = f_{jc} e^{i\Omega t} \quad (4.74)$$

where  $f_{jc}$  is the complex force amplitude and  $\Omega$  is the imposed circular frequency.

For Eq. (4.73) to be true at all times,  $y_j$  must have a similar form as  $f_j$ , or

$$y_j = y_{jc} e^{i\Omega t} \quad (4.75)$$

where,  $y_{jc}$  is the complex amplitude of the modal coordinate for mode  $j$ . Differentiating Eq. (4.75), and substituting Eq. (4.74) and Eq. (4.75) into Eq. (4.73),

$$-\Omega^2 y_{jc} e^{i\Omega t} + 2\omega_j \xi_j (i\Omega y_{jc} e^{i\Omega t}) + \omega_j^2 y_{jc} e^{i\Omega t} = f_{jc} e^{i\Omega t} \quad (4.76)$$

Collecting coefficients of  $y_{jc}$  and dividing by  $e^{i\Omega t}$

$$\left(-\Omega^2 + i2\omega_j \Omega \xi_j + \omega_j^2\right) y_{jc} = f_{jc} \quad (4.77)$$

Solving for  $y_{jc}$ ,

$$y_{jc} = \frac{f_{jc}}{\left(\omega_j^2 - \Omega^2\right) + i\left(2\omega_j \Omega \xi_j\right)} \quad (4.78)$$

The contribution from each mode is give by Eq. (4.79)

$$\{C_j\} = \{\phi_j\} y_{jc} \quad (4.79)$$

where,  $\{C_j\}$  is the contribution of mode  $j$  and  $\{\phi_j\}$  is the mode shape for mode  $j$ .

Finally, the complex displacements are obtained from Eq. (4.55) as

$$\{u_c\} = \sum_{j=1}^n \{C_j\} \quad (4.80)$$

where,  $\{u_c\}$  is the vector of complex displacements.

This chapter discusses the three analysis types involved in the FRF: their purpose, and to show a general formulation of the three analysis types. Three analysis types are used in the simulation: mode-frequency, spectrum, and harmonic. The ultimate purpose is to obtain the nodal complex displacements when a single point excitation force is applied at the opposite end to the support on the beam, plate, and cylinder. The order in which the analyses are described is also the order in which they are performed in the

simulation in order to achieve the required objective of the structure simulation. The next chapter applies the method to the beam, plate, and cylindrical shell; the modeling and simulation, numerical differentiation and integration, and the results are discussed.



## **CHAPTER V**

### **MODELING AND SIMULATION**

This chapter describes the process of providing a way to calculate the output charge of a thin piezoelectric film bonded to a shell structure. The method is applied to cases of a cylindrical shell structure, as well as a beam and plate for both generic and shaped piezoelectric films. In Chapters III and IV, different ANSYS verification manuals and analyses are discussed. This process is carried out using ANSYS Parametric Design Language or APDL for short. Techniques for creating the structure, specifying material properties, and specifying boundary conditions are specified. Also discussed are the analyses techniques, and the process of reading ANSYS displacement results in Matlab. Then, the process of numerical differentiation and integration is performed per the requirements of the sensor equation. The results are then discussed.

#### **5.1 ANSYS Parametric Design Language**

More frequently referred to as APDL, is a scripting language which may be used in order to more easily create the desired structure in terms of parameters. Some of the commands include repeating a command, macros, if-then-else branching, do-loops, and scalar, vector, and matrix operations. In this analysis, commands are written in a separate program, commonly used is notepad, and simply either copy-and-pasted into the ANSYS command prompt, or by using the Read Input From option under the File tab. APDL can be understood as a macro language; one can record a frequently used sequence of ANSYS commands in a macro file. A macro enables the creation of custom ANSYS

commands. In addition to executing a series of ANSYS commands, a macro can call GUI functions or pass values into arguments.

## 5.2 Beam Modeling

The method is first applied to a beam with characteristics as described below. The beam is modeled using ANSYS, and the simulation is performed to find the displacement field. Then, numerical differentiation and integration are performed on the displacements in Matlab and inputted into the beam sensor output charge equation as described in the previous chapters. The results are then discussed.

### Beam Modeling and Material Properties

The cantilevered beam is first created using APDL code. The shape of the beam is decided upon standard manufactured materials; the beam geometrical and material properties [21] are shown in Table 5.1.

Table 5.1: Geometrical and Material Properties for Cantilevered Beam

Parameter	Value	Units
Length, $L$	0.3048	$m$
Height, $H$	0.003175	$m$
Width, $B$	0.0508	$m$
Substrate Material	6061-T6 Aluminum	-
Mass density, $\rho$	2700	$Kg / m^3$
Young's modulus, $E$	70E9	$N/m^2$
Poisson ratio, $\nu$	0.33	-

Using the APDL code in Appendix C, the beam substrate is created in ANSYS. The APDL code follows the stepwise process below for the creation of the beam substrate.

1. Assigning of the required length, height, and width.

2. Define frequency, number of load steps, force, and number of nodes to be used.
3. Define element type and material properties.
4. Specify REAL Constants
5. Define number of nodes in the  $x$  direction, as in Figure 5.1.
6. Fill the nodes with elements as depicted in Figure 5.2.

Only the beam substrate is being modeled and simulated, because the PVDF film does not affect the dynamic characteristics of the beam substrate, as described in Chapter II.



Figure 5.1: Node Creation using APDL Code



Figure 5.2: Element Creation using APDL Code

### Element Type

BEAM4 element is selected. The area moment of inertias are calculated in the APDL code outlined in Appendix C. The nodes are generated using the N command which defines a node in the order it was created. Then the E command is used to define an element by node connectivity; this is done for the initial line of nodes. The EGEN command is then used to create more elements from an existing pattern of elements.

### Boundary Conditions

In order to simulate the clamped-free model, all the degrees of freedom are constrained on the left end of the beam. Figure 5.3 shows the boundary conditions on the

FEA model. All nodes are selected as master degrees of freedom; however, this is not illustrated. The input for the command is in Appendix C.



Figure 5.3: Clamped-Free Aluminum Beam

### 5.3 Beam Simulation

A series of analyses are carried out in a specific sequence in order to study the dynamic frequency response of the beam substrate. The sequence of the analyses is Mode Frequency Analysis, Single Point PSD Spectrum Analysis, and Harmonic Response Analysis. A more in depth look at these analyses are presented in Chapter III.

#### 5.3.1 Mode Frequency Analysis

This analysis type is used for natural frequency and mode shape determination. For this particular clamped-free beam, the first three mode shapes are shown in Figures 5.4, 5.5, and 5.6; the first occurring at a natural frequency of 28.057 Hz, the second mode shape occurring at a natural frequency of 175.81 Hz, and the third at 492.18 Hz. In mode frequency analysis, the first six modes are expanded and extracted, with a frequency range of 0 to 1600 Hz. A list of the modes at their respective frequencies is laid out in Table 5.2.



Figure 5.4: First Mode Shape of Cantilevered Beam (28.057 Hz)



Figure 5.5: Second Mode Shape of Cantilevered Beam (175.81 Hz)



Figure 5.6: Third Mode Shape of Cantilevered Beam (492.18 Hz)

Table 5.2: Frequencies at the First Six Modes

Mode	Frequency (Hz)
1	28.057
2	175.81
3	492.18
4	964.19
5	1593.3
6	2378.9

### 5.3.2 Single Point PSD Spectrum Random Vibration Analysis

The next step after mode frequency analysis is to perform a spectrum analysis. The first six modes are included in the spectrum analysis to calculate element stresses. The model is excited in the Y-direction with a force of 600 N and the modal responses are combined using power spectral density mode combination method. The damping ratio is set to 0.02. Lastly, a one-sigma displacement solution output is written to the results file from the PSD analysis.

### 5.3.3 Harmonic Response Analysis

The third analysis is harmonic response using the mode superposition method option which sums factored mode shapes to calculate the harmonic response. A harmonic analysis is performed after a spectrum analysis. The frequency ranges from 1.0 to 1600 Hz. The harmonic output option to print complex displacements as real and imaginary components is turned on, whereas the cluster option is turned off for uniform spacing of frequency solutions. These results are written in binary file \*.rfrq format. This binary file contains all the displacement data for all the nodes at each frequency interval. In Figure 5.7, the frequency response function (FRF) for the clamped-free beam is plotted. The first four modes are easily distinguishable, defined by the peaks; hence, they have a greater effect on the displacement response than the fifth and sixth modes which are not visible.

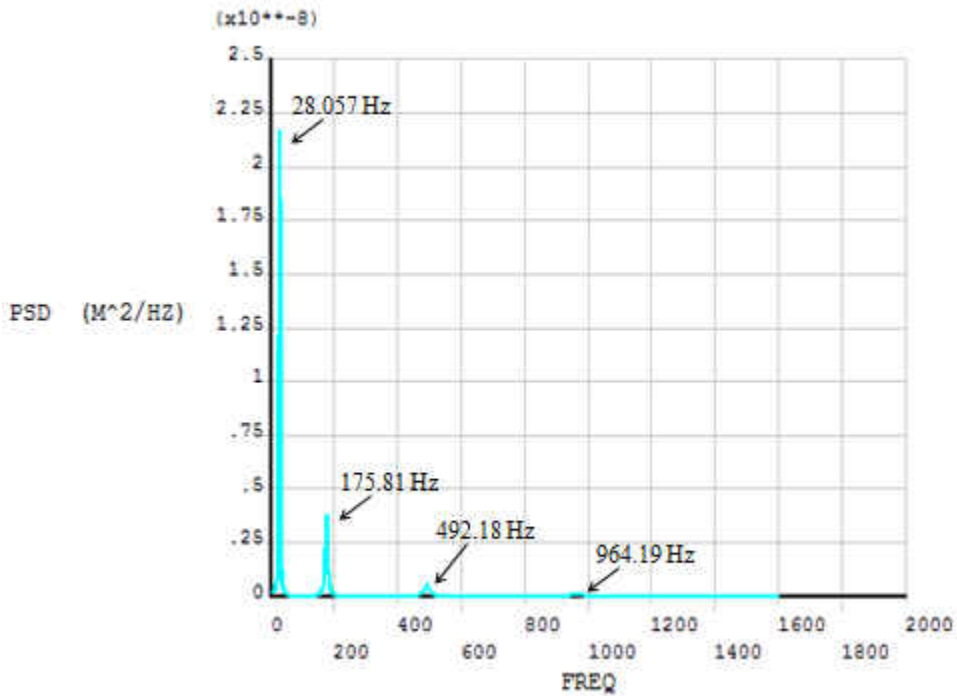


Figure 5.7: FRF Plot of Clamped-Free Beam

## 5.4 Processing of ANSYS Results of Beam in Matlab

The next step is to gather all of the displacement information at each frequency which is done with the harmonic analysis. The information is written to a \*.rfrq file which is an ANSYS output binary file. This information will be imported in Matlab, which requires this data to be in text (ASCII) form. The ANSYS DUMP command converts the binary data into ASCII data. The nodal displacements are listed in ascending node order and then in ascending frequency. The format for this is outlined in Appendix I.

### Stepwise Method of Processing the \*.rfrq Binary File Data in Matlab

1. The ANSYS DUMP command is found in the GUI under Main Menu> List> Files> Binary Files, while choosing All Records to be listed and Entire Record of output per record. The file 'file.rfrq' is selected, creating the 'DUMP.txt' file. This file contains all the complex displacement for the beam for each node at each frequency.
2. The 'FRFResult.txt' file is created from the DUMP.txt file starting after Record 8.
3. An 'NLIST.lis' file is saved, containing all the nodes and their coordinates.
4. The 'FRFProc\_01.m' Matlab file, which is listed in Appendix D as are the other Matlab files for the beam, reads the 'FRFResult.txt' file and places the complex displacements in the  $y$  direction into matrix format for all the nodes and frequencies.
5. The complex displacements are used to calculate the magnitude displacement at each frequency.

- A plot of the FRF of the beam substrate is illustrated in Figure 5.8. This figure is obtained through Matlab; it confirms that the displacements were successfully transferred from ANSYS and organized correctly.

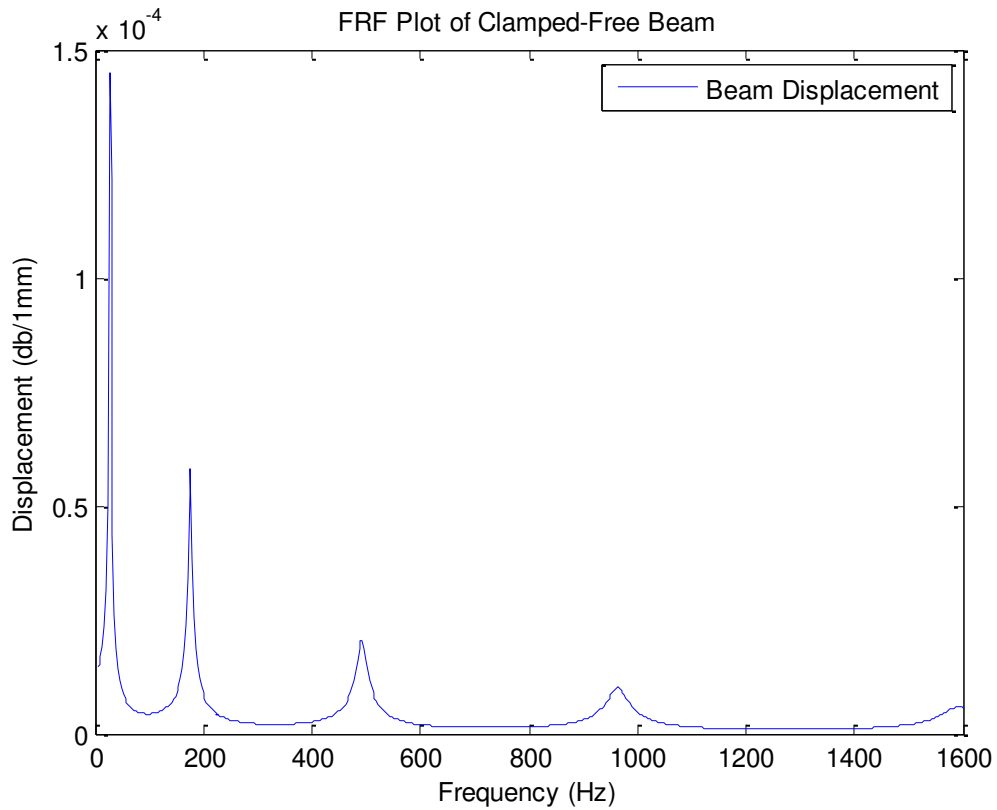


Figure 5.8: FRF Plot of Clamped-Free Beam

- The 'DisplDerivative\_02.m' file is then run in order to obtain the required first derivatives and second derivatives of displacement with respect to the required direction.
- After finding the derivatives, the 'Film\_Shape\_03.m' file is run. This file basically lists the attributes of the sensor and the beam. The end result is the shape of the sensor pictured in Figure 5.9.



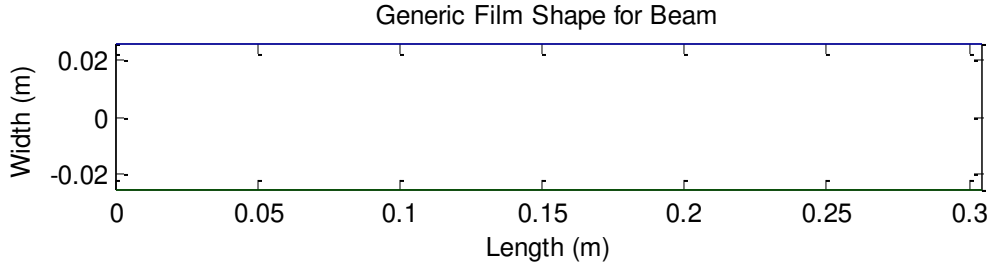


Figure 5.9: Generic Film Shape for Beam

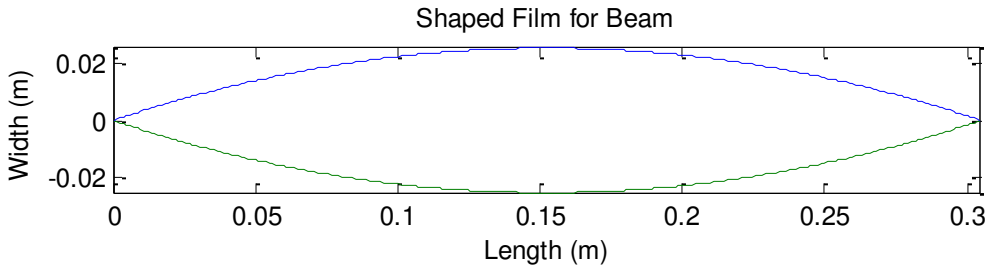


Figure 5.10: Shaped Film for Beam

9. Here, a generic shaped sensor, a sensor which covers the entire surface of the beam as depicted in Figure 5.9, is analyzed. The displacement frequency response of the clamped-free beam and sensor output charge for each frequency is plotted as in Figure 5.11 for the generic sensor output charge equation:

$$\phi^S = -\frac{bh^S}{S^e} \int_x \left( h_{31} r_x^S \frac{\partial^2 u_3}{\partial x^2} \right) dx.$$

10. Running ‘SensorOutput\_Shaped\_05.m’ analyzes the sensor shaped like that of Figure 5.10. The displacement frequency response of the clamped-free beam and sensor output charge for each frequency is plotted as in Figure 5.12 for the sensor

$$\text{output equation with a shaping function: } \phi^S = -\frac{bh^S}{S^e} \int_x W(x) \left( h_{31} r_x^S \frac{\partial^2 u_3}{\partial x^2} \right) dx.$$

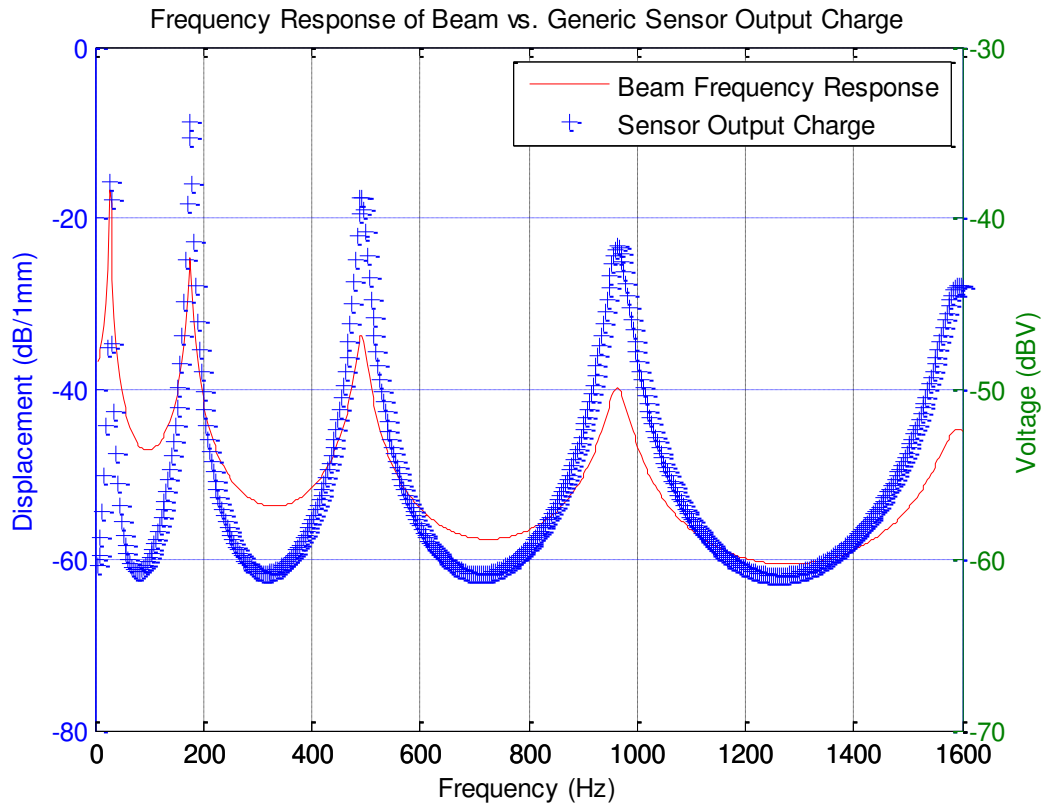


Figure 5.11: Frequency Response of Beam vs. Generic Sensor Output Charge

Electric potential  $\phi$  is equal to the electric potential energy of a charged particle, measured in joules, divided by the charge of the particle, measured in coulombs, which equates to joules per coulomb, or volts.

Suffixes are commonly attached to the basic dB unit in order to indicate the displacement reference level against which the decibel measurement is taken. The units when plotting the FRF are frequency on the horizontal axis and displacement on the vertical axis, whereas the unit for the vertical axis for the sensor voltage FRF output charge is voltage, dBV.

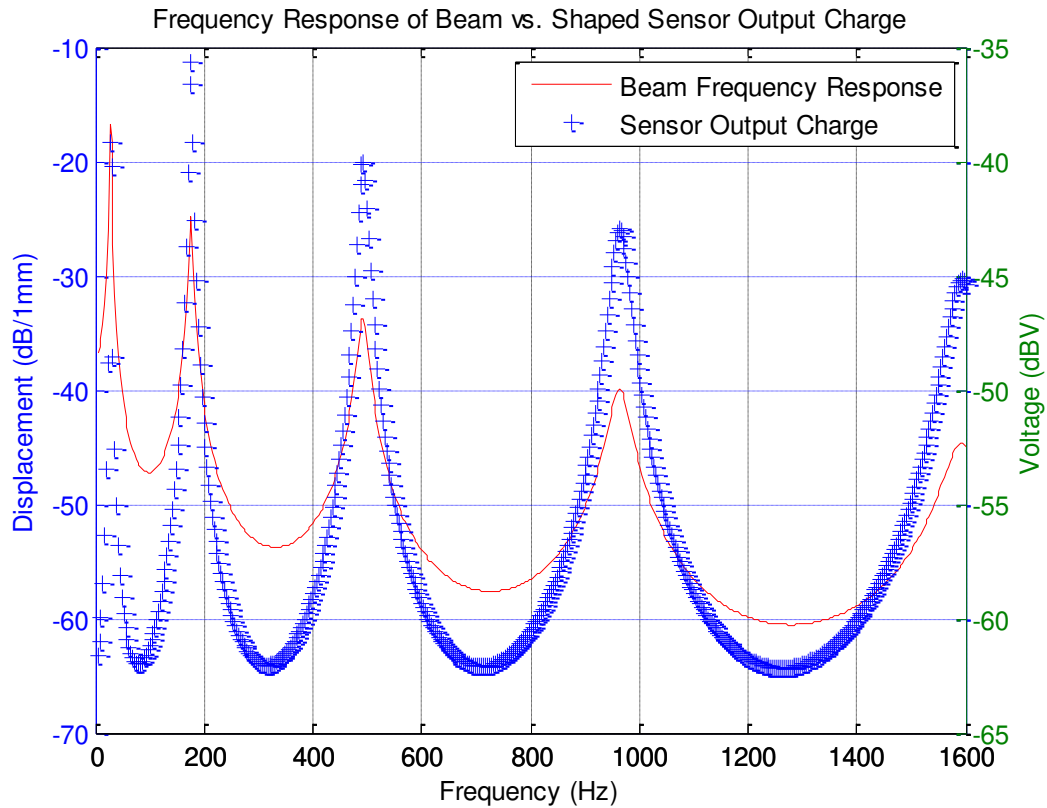


Figure 5.12: Frequency Response of Beam vs. Shaped Sensor Output Charge

It can be shown in both Figure 5.11 and Figure 5.12 that the films can correctly capture the natural frequencies of the beam.

### 5.5 Plate Modeling

The method is then applied to a plate with characteristics as described below. The plate is modeled using ANSYS, and the simulation is performed to find the displacement field. Then, numerical differentiation and integration are performed on the displacements in Matlab and inputted into the plate sensor output charge equation as described in previous chapters. The results are then discussed.

## Plate Modeling and Material Properties

The cantilevered plate is first created using APDL code. The shape of the plate is decided upon standard manufactured materials; the plate geometrical and material properties [21] are shown in Table 5.3.

Table 5.3: Geometrical and Material Properties for Cantilevered Plate

Parameter	Value	Units
Length, $L$	0.6096	$m$
Height, $H$	0.381	$m$
Width, $B$	0.0047625	$m$
Substrate Material	6061-T6 Aluminum	
Mass density, $\rho$	2700	$Kg / m^3$
Young's modulus, $E$	70E9	$N/m^2$
Poisson ratio, $\nu$	0.33	-

Using the APDL code in Appendix E, the plate substrate is created in ANSYS. The APDL code follows the stepwise process below for the creation of the plate substrate.

1. Assigning of the required length, height, and width.
2. Define frequency, number of load steps, force, and number of nodes to be used.
3. Define element type and material properties.
4. Specify REAL Constants.
5. Define number of nodes in the  $x$  and  $y$  directions, as in Figure 5.13.
6. Fill the nodes with elements as depicted in Figure 5.14.

Only the plate substrate is being modeled and simulated, because the PVDF film does not affect the dynamic characteristics of the plate substrate, as described in Chapter II.

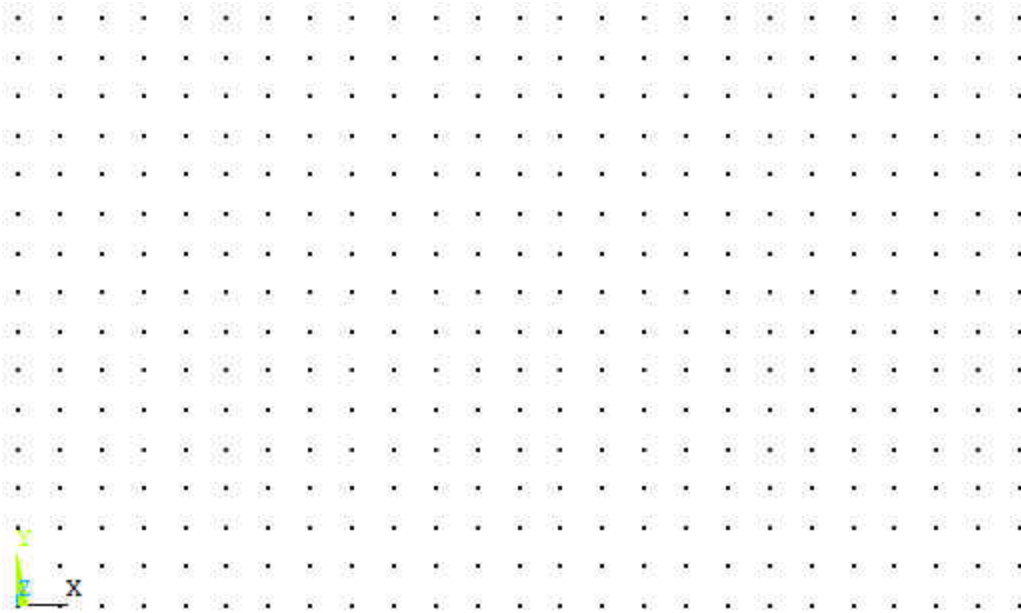


Figure 5.13: Node Creation using APDL Code

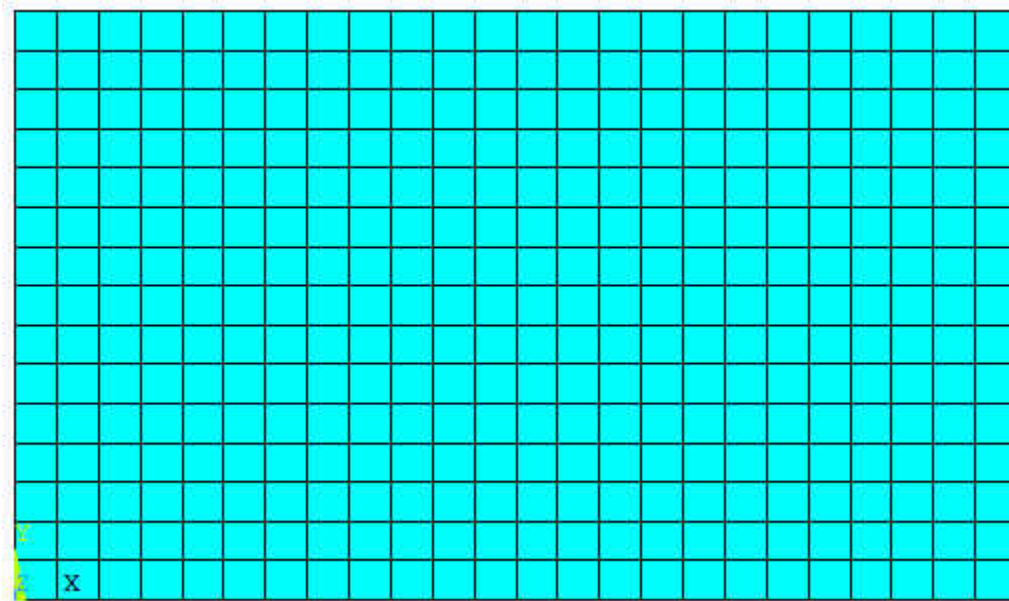


Figure 5.14: Element Creation using APDL Code

**Element Type**

SHELL63 element is selected. The area moment of inertias are calculated in the APDL code outlined in Appendix E. The nodes are generated using the N command which defines a node in the order it is created. The NGEN command is then used to

create more nodes from a pattern of nodes; in this case, a line is copied and generated in a linear pattern. Then the E command is used to define an element by node connectivity; this is done for the initial line of nodes. The EGEN command is then used to create more elements from an existing pattern of elements.

### **Boundary Conditions**

In order to simulate the clamped-free model, all the degrees of freedom are constrained on the left end of the plate. Figure 5.15 shows the boundary conditions on the FEA model. All nodes are selected as master degrees of freedom; however, only in the Z direction. The input for the command is in Appendix E.

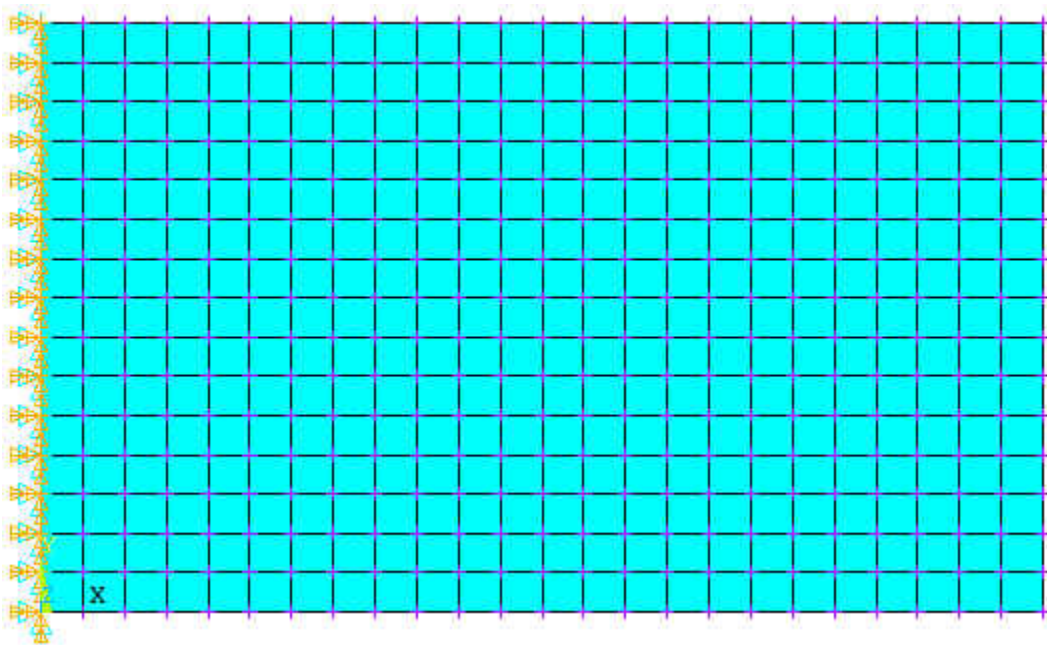


Figure 5.15: Clamped-Free Aluminum Plate

### **5.6 Plate Simulation**

A series of analyses are carried out in a specific sequence in order to study the dynamic frequency response of the plate substrate. The sequence of the analyses is Mode

Frequency Analysis, Single Point PSD Spectrum Analysis, and Harmonic Response Analysis. A more in depth look at these analyses are presented in Chapter III.

### 5.6.1 Mode Frequency Analysis

This analysis type is used for natural frequency and mode shape determination. For this particular clamped-free plate, the first four mode shapes are shown in Figures 5.16, 5.17, 5.18, and 5.19; the first occurring at a natural frequency of 10.881 Hz, the second mode shape occurring at a natural frequency of 40.363 Hz, the third at 67.644 Hz, and the fourth at 134.34 Hz. In mode frequency analysis, the first six modes are expanded and extracted, with a frequency range of 0 to 250 Hz. A list of the modes at their respective frequencies is laid out in Table 5.4.



Figure 5.16: First Mode Shape of Cantilevered Plate (10.881 Hz)

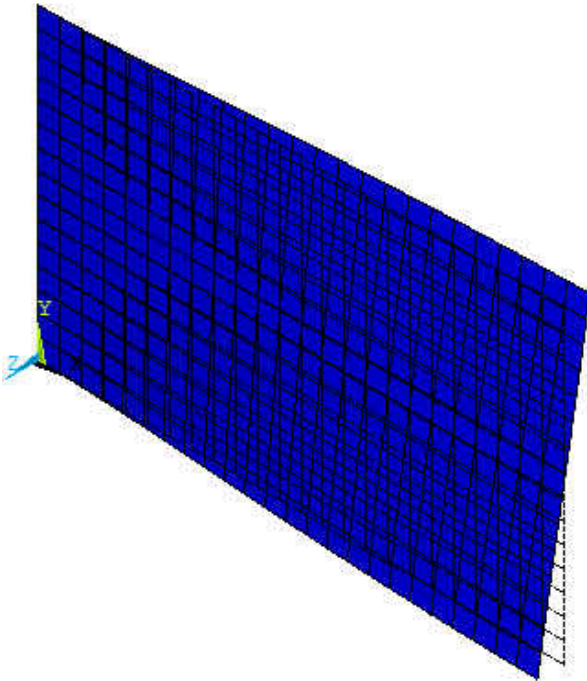


Figure 5.17: Second Mode Shape of Cantilevered Plate (40.363 Hz)



Figure 5.18: Third Mode Shape of Cantilevered Plate (67.644 Hz)

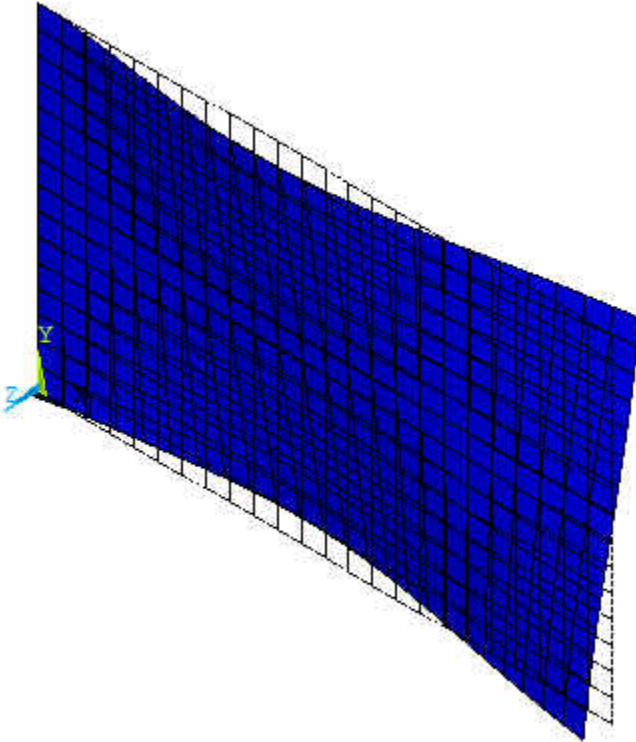





Figure 5.19: Fourth Mode Shape of Cantilevered Plate (134.34 Hz)

Table 5.4: Frequencies at the First Six Modes

Mode	Frequency (Hz)	Mode Shape
1	10.881	
2	40.363	
3	67.644	



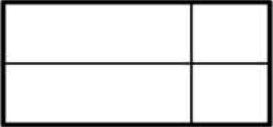


Mode	Frequency (Hz)	Mode Shape
4	134.34	
5	187.98	
6	221.46	

Table 5.5: Natural Frequency Convergence

Number of Elements	35	105	171	253	360	713	1457	1989	2961
Mode 1 Freq. (Hz)	10.87	10.87	10.87	10.87	10.88	10.88	10.88	10.88	10.88
2	44.77	42.84	41.80	41.14	40.36	39.62	39.26	39.05	38.91
3	68.15	67.66	67.64	67.63	67.64	67.62	67.62	67.62	67.62
4	147.7	141.6	138.5	136.6	134.3	132.1	131.1	130.5	130.1
5	192.8	189.4	188.9	188.5	187.9	186.8	186.1	185.6	185.2
6	273.3	250.1	237.7	230.1	221.4	213.7	210.3	208.4	207.2

It can be observed from Table 5.5 that at mode six, the natural frequency converges to 207 Hz. In this thesis, using 360 elements is a beneficial number for reducing computation time and an adequate number for the accuracy of the natural frequency of mode six; therefore, 360 elements are used in this thesis for the simulation of a clamped-free plate.

### 5.6.2 Single Point PSD Spectrum Random Vibration Analysis

The next step after mode frequency analysis is to perform a spectrum analysis. The first six modes are included in the spectrum analysis to calculate element stresses. The model is excited in the Z-direction with a force of 50 N and the modal responses are

combined using power spectral density mode combination method. The damping ratio is set to 0.02. Lastly, a one-sigma displacement solution output is written to the results file from the PSD analysis.

### **5.6.3 Harmonic Response Analysis**

The third analysis is harmonic response using the mode superposition method option which sums factored mode shapes to calculate the harmonic response. A harmonic analysis is performed after a spectrum analysis. The frequency ranges from 1.0 to 250 Hz. The harmonic output option to print complex displacements as real and imaginary components is turned on, whereas the cluster option is turned off for uniform spacing of frequency solutions. These results are written in binary file \*.rfrq format. This binary file contains all the displacement data for all the nodes at each frequency interval. A plot of the FRF of the clamped-free plate is presented in Figure 5.20. The second and fourth modes are torsional; hence, they do not have as great of an effect as the bending modes, modes one and three, on the displacement response of the plate.

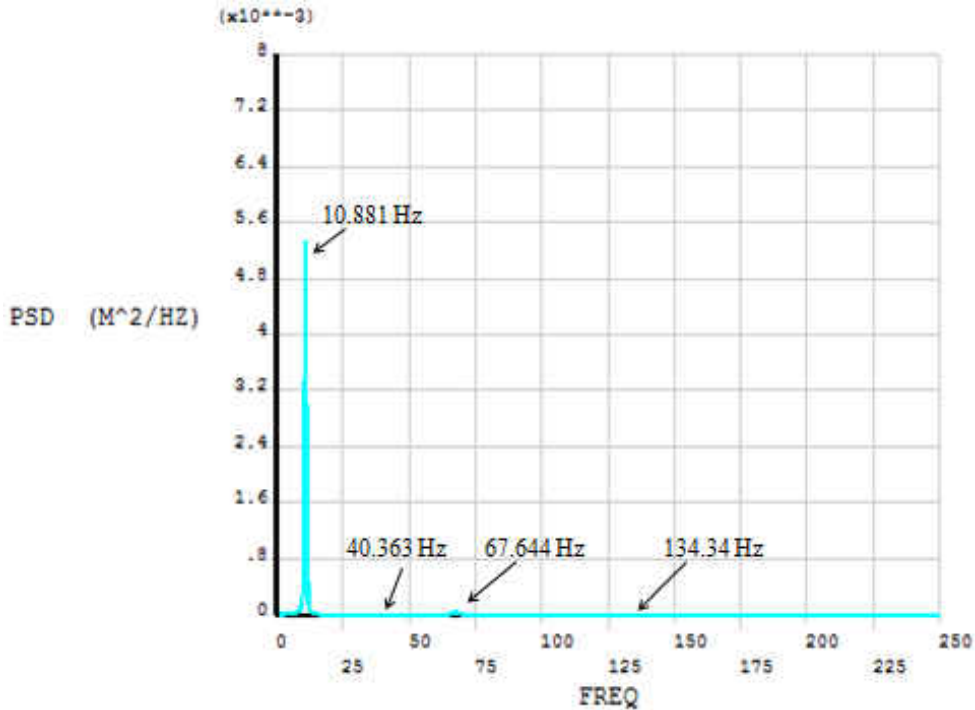


Figure 5.20: FRF Plot of Clamped-Free Plate

### 5.7 Processing of ANSYS Results of Plate in Matlab

As was with the beam, the next step is to gather all of the displacement information at each frequency which is done with the harmonic analysis. The information is written to a \*.rfrq file which is an ANSYS output binary file. This information will be imported in Matlab, which requires this data to be in text (ASCII) form. The ANSYS DUMP command converts the binary data into ASCII data. The nodal displacements are listed in ascending node order and then in ascending frequency. The format for this is outlined in Appendix I.

#### Stepwise Method of Processing the \*.rfrq Binary File Data in Matlab

1. The ANSYS DUMP command is found in the GUI under Main Menu> List> Files> Binary Files, while choosing All Records to be listed and Entire Record of output per record. The file 'file.rfrq' is selected, creating the 'DUMP.txt' file.

This file contains all the complex displacement for the plate for each node at each frequency.

2. The 'FRFResult.txt' file is created from the DUMP.txt file starting after Record 8.
3. An 'NLIST.lis' file is saved, containing all the nodes and their coordinates.
4. The 'FRFProc\_01.m' Matlab file, which is listed in Appendix F along with the subsequent Matlab files for the plate, reads the 'FRFResult.txt' file and places the complex displacements in the  $z$  direction into matrix format for all the nodes and frequencies.
5. The complex displacements for each individual node at each frequency are then combined to create a displacement magnitude.
6. A plot of the FRF of the plate substrate is illustrated in Figure 5.21. This figure is obtained through Matlab; it confirms that the displacements were successfully transferred from ANSYS and organized correctly.

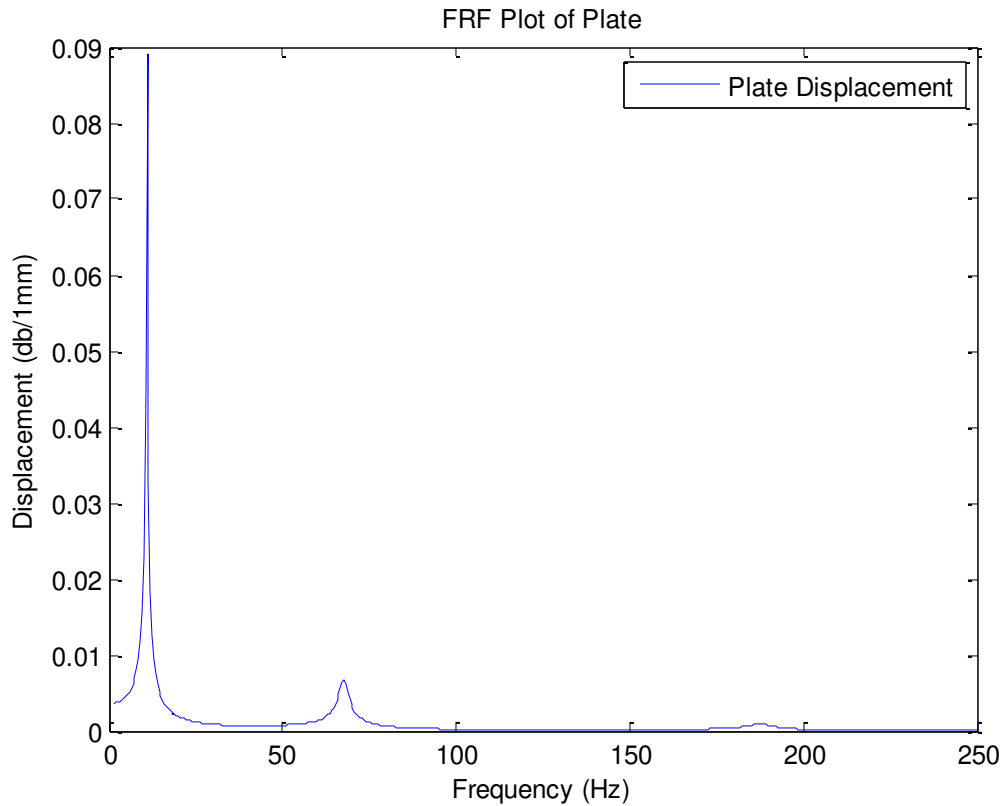


Figure 5.21: FRF Plot of Plate

7. The 'DisplDerivative\_02.m' file is then run in order to obtain the required first derivatives and second derivatives of displacement with respect to the required direction. This is required for the sensor output charge equation.
8. After finding the derivatives, the 'PLATEreadcoord\_02.m' file is run. This file reads the 'NLIST.lis' file to extract the nodal coordinates of the plate. Running this file essentially gives a [16 x 25] matrix of the x or y coordinates of each node to be used as an input for the charge output equation.
9. After finding the derivatives, the 'Film\_Shape\_03.m' file is run. This file basically lists the attributes of the sensor and the plate. The end result is the shape of the sensor pictured in Figure 5.22, also in matrix format, depicted in Figure 5.23 for calculations. During calculations, the matrix represents the sensor shape

function  $W_s(\alpha_1, \alpha_2)$  in the sensor output charge equation for a plate. Unlike a shaped sensor, a generic sensor would still have this matrix, only it would be filled with all 1s, representing the shape of the sensor. The sensor shape function matrix gets multiplied by the corresponding second derivatives in the sensor output charge equation. Wherever there is a “1” means that the sensor is covering that location; conversely, wherever there is a “0” means that there is not a sensor at that location.

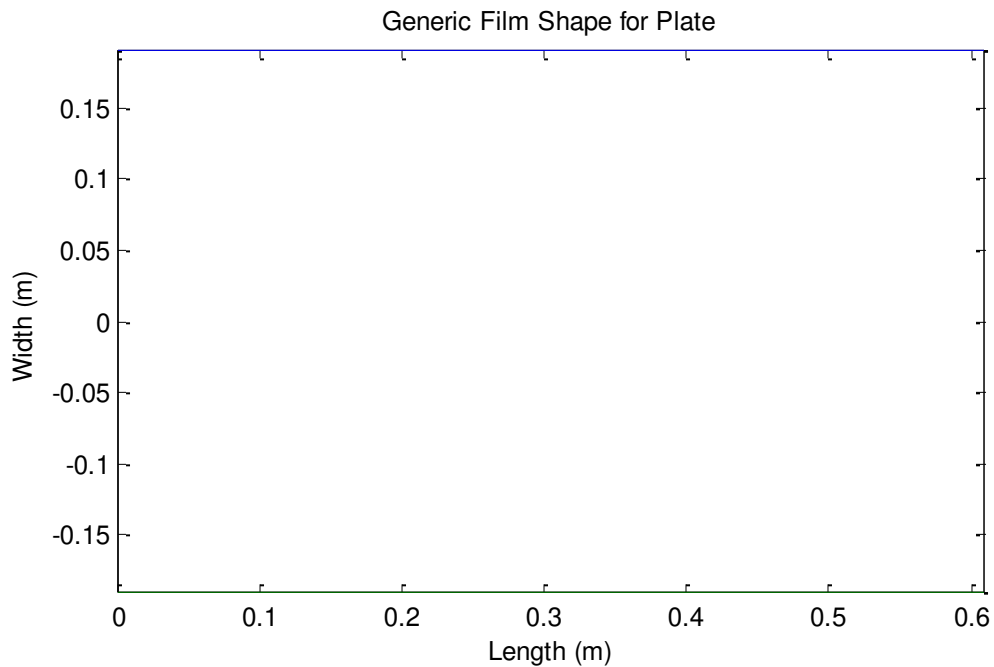


Figure 5.22: Generic Film Shape for Plate

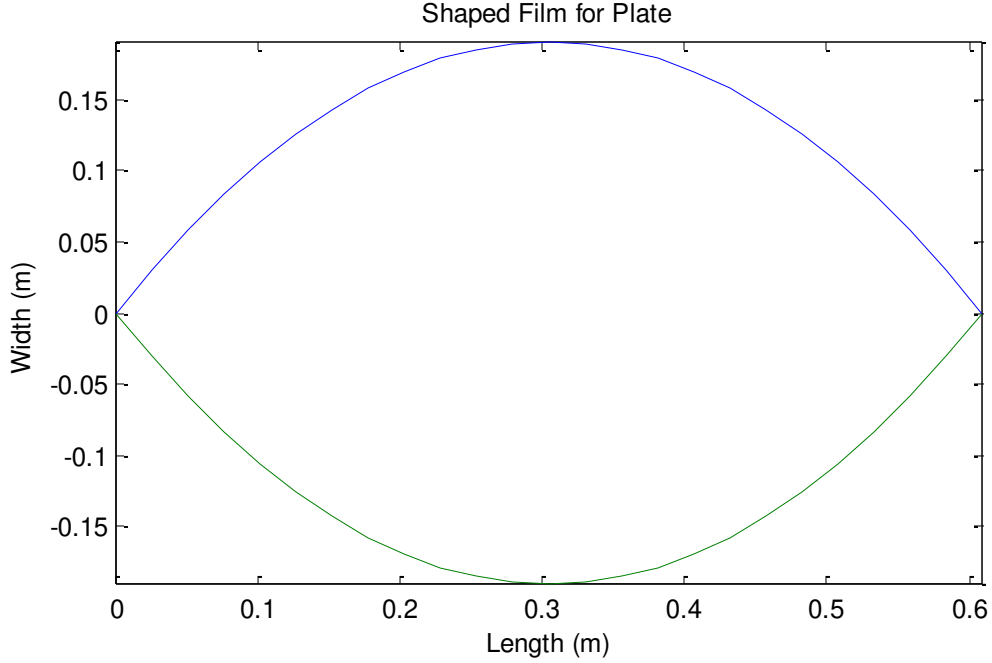


Figure 5.23: Shaped Film for Plate

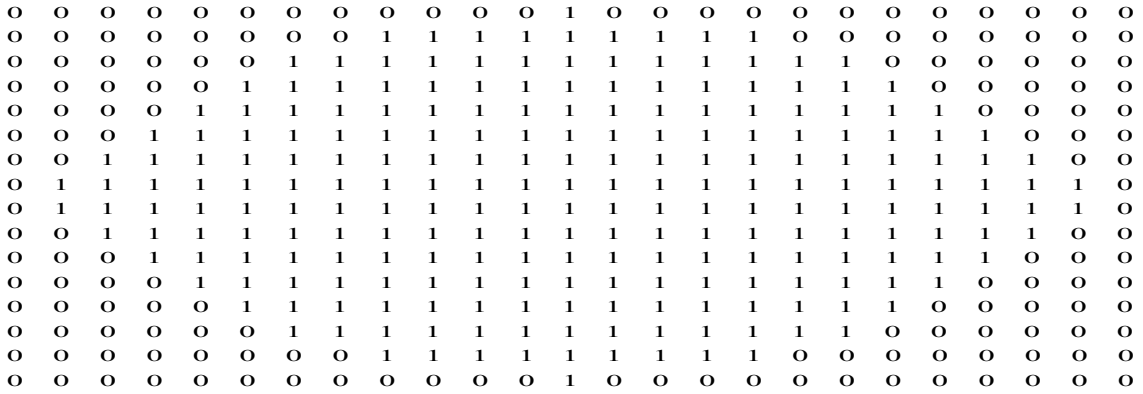


Figure 5.24: Shaped Film in Matrix Form

10. Here, a generic shaped sensor, a sensor which covers the entire surface of the plate as depicted in Figure 5.22, is analyzed. The displacement frequency response of the clamped-free plate and sensor output charge for each frequency is plotted as in Figure 5.25 for the generic sensor output charge equation:

$$\phi^S = -\frac{h^S}{S^e} \int_{S^e} \left[ h_{31} r_x^S \frac{\partial^2 u_3}{\partial x^2} + h_{32} r_y^S \frac{\partial^2 u_3}{\partial y^2} \right] dS^e .$$

11. Running ‘SensorOutput\_Shaped\_05.m’ analyzes the sensor shaped like that of Figure 5.23. The displacement frequency response of the clamped-free plate and sensor output charge for each frequency is plotted as in Figure 5.26 for the sensor output charge equation with a shaping function:

$$\phi^S = -\frac{h^S}{S^e} \int_{S^e} W_S(x, y) \left[ h_{31} r_x^S \frac{\partial^2 u_3}{\partial x^2} + h_{32} r_y^S \frac{\partial^2 u_3}{\partial y^2} \right] dS^e .$$

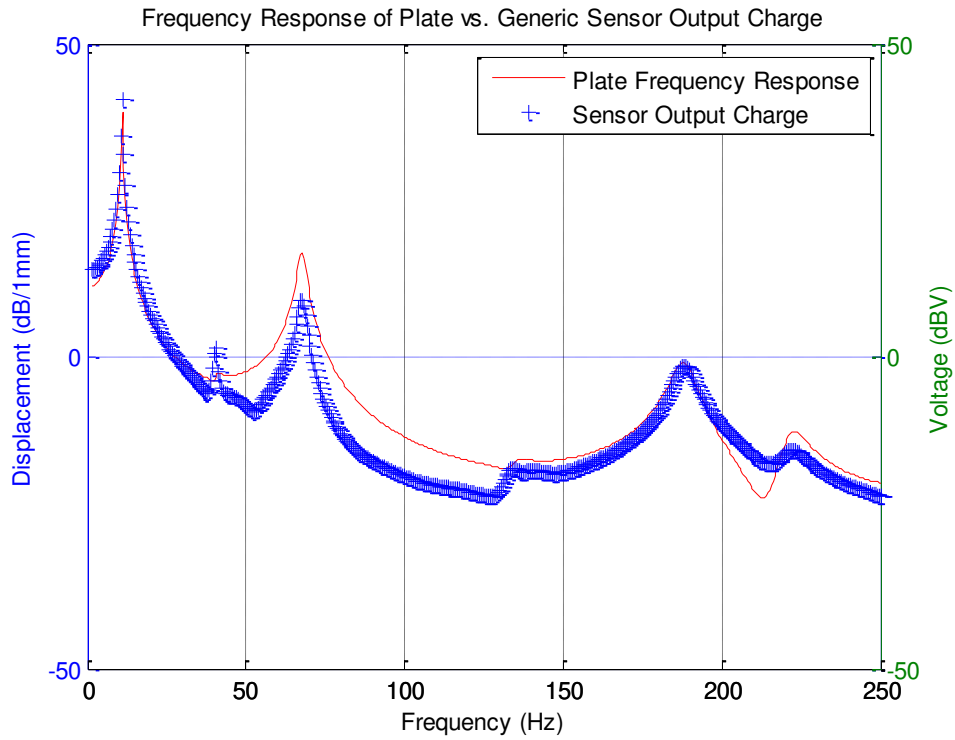


Figure 5.25: Frequency Response of Plate vs. Generic Sensor Output Charge



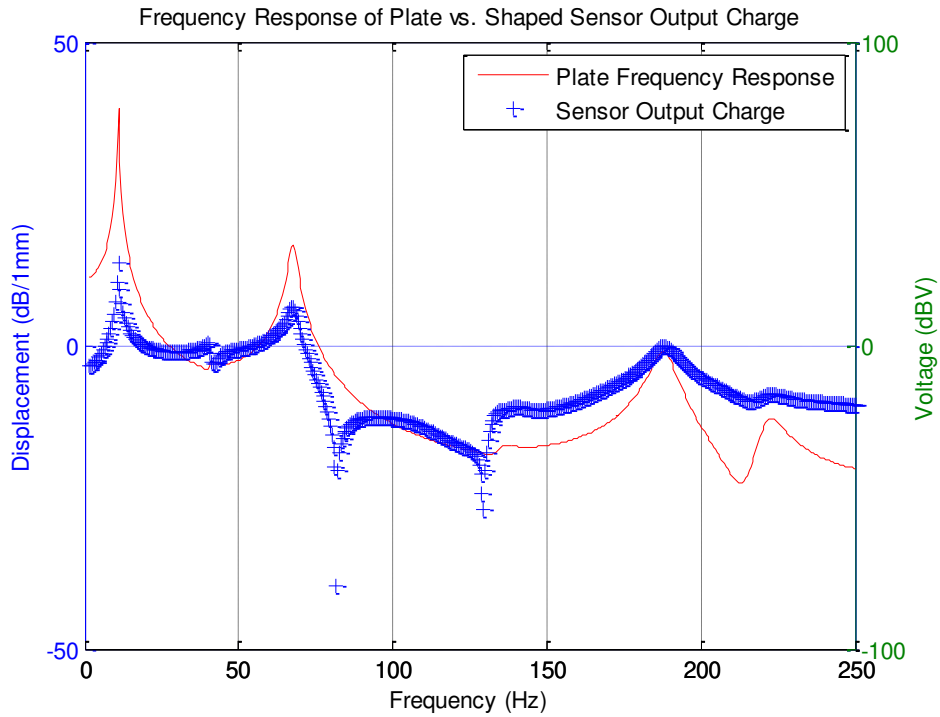


Figure 5.26: Frequency Response of Plate vs. Shaped Sensor Output Charge

It can be shown in both Figure 5.25 and Figure 5.26 that the films can correctly capture the natural frequency of the plate. The discrepancies in resonant frequencies between the sensor output charge and the frequency response of the plate can be accounted for by the following explanation. The output charge equation integrates “strains” over the whole surface of the sensor; it is the summation of the derivatives of displacements. The displacement frequency response function shown on the figure only takes into account one point on the substrate; this point may not see certain modes. For instance, in the case of the beam in Figure 5.27, the particular point considered is a node and will not correctly capture the third mode of the beam. The sensor output charge equation, however, captures all the modes and therefore will show more modes than the substrate point considered.



Figure 5.27: Node on a Beam Example

As an example, an accelerometer attached to the substrate at a node of a mode will not measure that mode, because it will remain “still” at excitation coinciding with that mode. In surface shaping sensor design, the objective is to design a sensor which monitors those modes which need to be controlled. Hence, the FRF of a point may show fewer modes than the FRF of the sensor output charge.

### 5.8 Cylindrical Shell Modeling

Lastly, the method is applied to a cylindrical shell with characteristics as described below. The cylindrical shell is modeled using ANSYS, and the simulation is performed to find the displacement field. Then, numerical differentiation and integration are performed on the displacements in Matlab and inputted into the cylindrical shell sensor output charge equation as described in previous chapters. The results are then discussed.

#### Shell Modeling and Material Properties

The cylindrical shell substrate is first created using APDL code. The shape of the cylinder is decided upon standard manufactured materials; the cylinder geometrical and material properties [21] are shown in Table 5.6.

Table 5.6: Geometrical and Material Properties for Aluminum Cylindrical Shell

Parameter	Value	Units
Length, $L$	0.3048	$m$

Parameter	Value	Units
Outside Radius, $R$	0.022225	$m$
Thickness, $h_b$	0.000889	$m$
Substrate Material	6061-T6 Aluminum	-
Mass density, $\rho$	2700	$Kg / m^3$
Young's modulus, $E$	68.9E9	$N / m^2$
Poisson ratio, $\nu$	0.33	-

Using the APDL code in Appendix G, the shell substrate is created in ANSYS. The APDL code follows the stepwise process below for the creation of the shell substrate.

1. Assigning of the required length, radius, and thickness.
2. Define frequency, number of load steps, force, and number of nodes to be used.
3. Define element type and material properties.
4. Specify cylindrical coordinates
5. Define number of nodes in the  $z$  direction and number of nodes in the  $\theta$  direction, as in Figure 5.28.
6. Fill the nodes with elements as depicted in Figure 5.29.

Only the shell substrate is being modeled and simulated, because the PVDF film does not affect the dynamic characteristics of the shell substrate, as described in Chapter II.

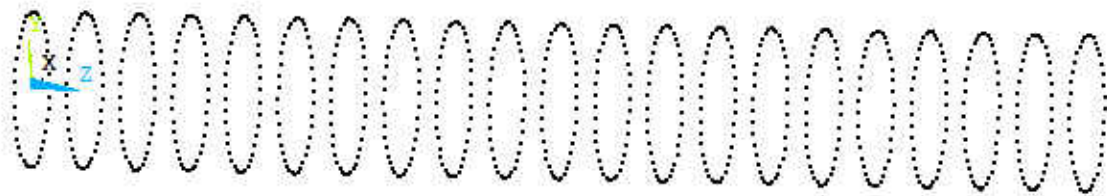


Figure 5.28: Node Creation using APDL Code

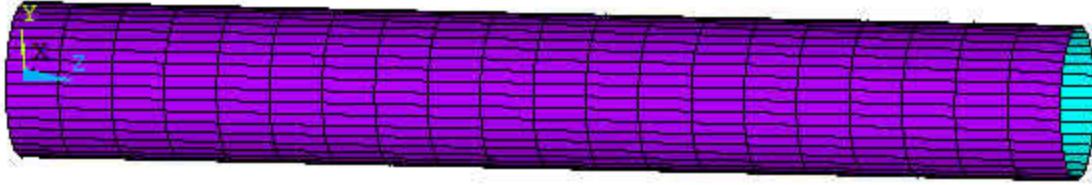


Figure 5.29: Element Creation using APDL Code

### Element Type and Meshing

SHELL63 element with bending and membrane element stiffness option is selected. The nodes are generated using the N command which defines a node in the order it is created. The NGEN command is then used to create more nodes from a pattern of nodes; in this case, a line is copied and generated in a circular pattern. Then the E command is used to define an element by node connectivity; this is done for the initial line of nodes. The EGEN command is then used to create more elements from an existing pattern of elements. This is how the mesh is created.

### Boundary Conditions

In order to simulate the clamped-free model, all the degrees of freedom are constrained on the left end of the shell. Figure 5.30 shows the boundary conditions on the FEA model. The input for the command is Appendix G.

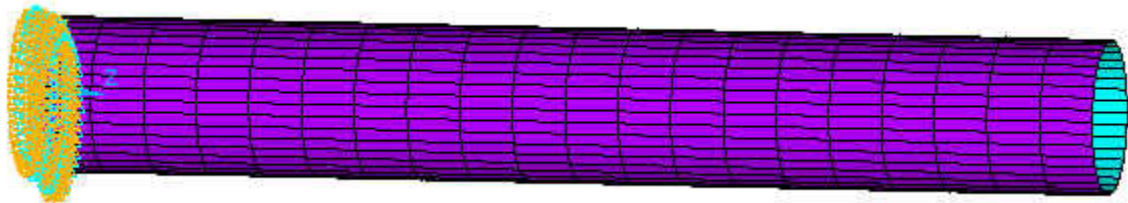


Figure 5.30: Clamped-Free Aluminum Cylindrical Shell

## 5.9 Cylindrical Shell Simulation

A series of analyses are carried out in a specific sequence in order to study the dynamic frequency response of the cylindrical shell substrate. The sequence of the analyses is Mode Frequency Analysis, Single Point PSD Spectrum Analysis, and Harmonic Response Analysis. A more in depth look at these analyses are presented in Chapter III.

### 5.9.1 Mode Frequency Analysis

This analysis type is used for natural frequency and mode shape determination. For this particular clamped-free cylindrical shell, the first six mode shapes are shown in Figures 5.31, 5.32, 5.33, 5.34, 5.35, 5.36; the first and second occurring at a natural frequency of 452.46 Hz, the third and fourth mode shapes occurring at a natural frequency of 1247.6 Hz, and the fifth and sixth at 1550.7 Hz. It is noted that the first and second, third and fourth, and the fifth and sixth modes occur at the same frequency. In mode frequency analysis, the first six modes are expanded and extracted, with a frequency range of 0 to 1600 Hz, with the element calculation key turned OFF. A list of the modes at their respective frequencies is laid out in Table 5.7.

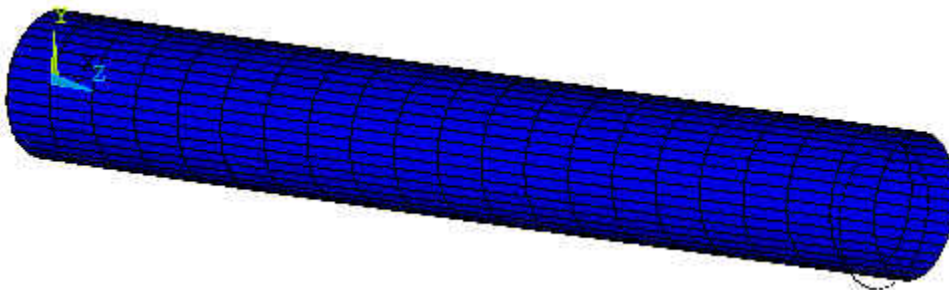


Figure 5.31: First Mode Shape of Cantilevered Cylinder (452.46 Hz)

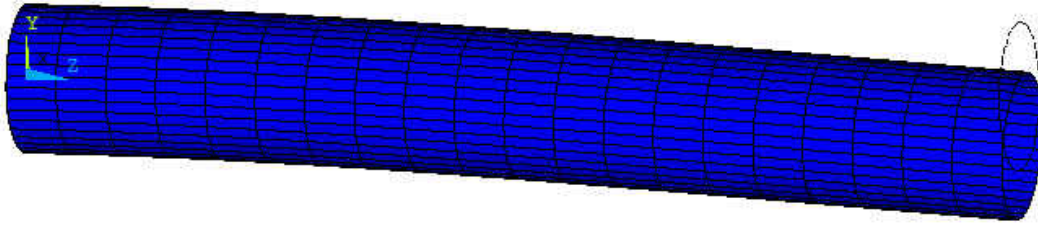


Figure 5.32: Second Mode Shape of Cantilevered Cylinder (452.46 Hz)

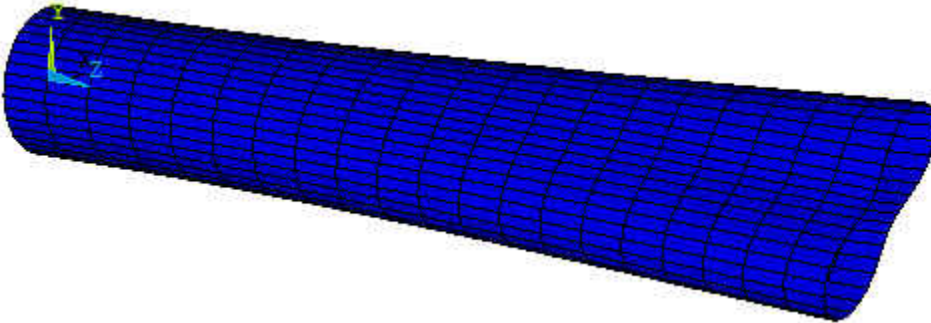


Figure 5.33: Third Mode Shape of Cantilevered Cylinder (1247.6 Hz)

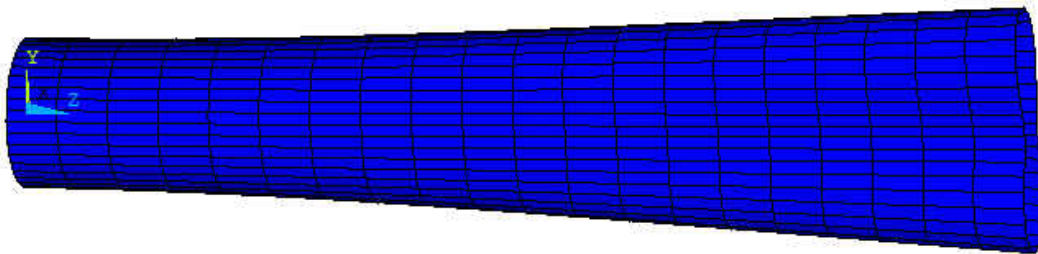


Figure 5.34: Fourth Mode Shape of Cantilevered Cylinder (1247.6 Hz)

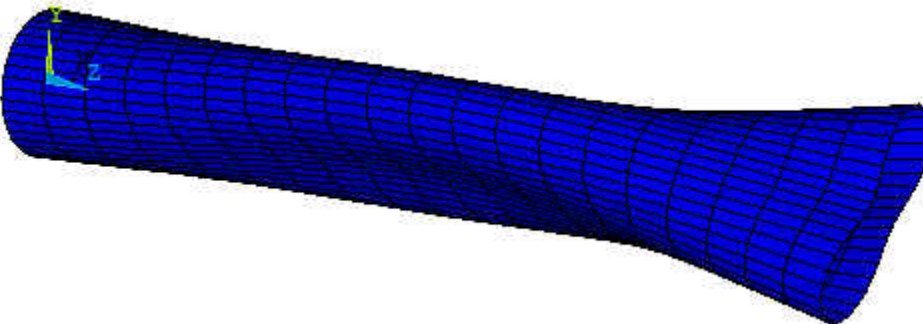


Figure 5.35: Fifth Mode Shape of Cantilevered Cylinder (1550.7 Hz)

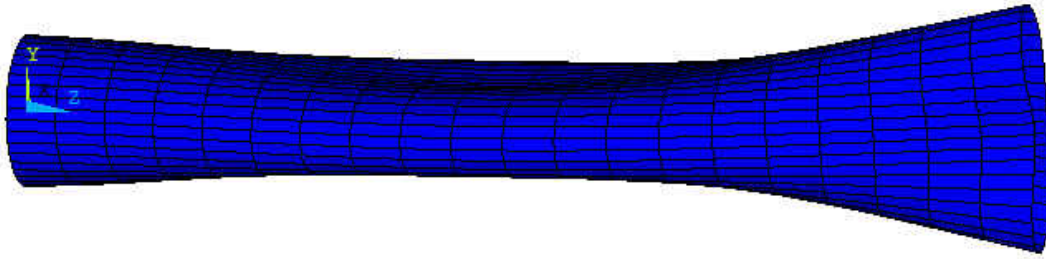


Figure 5.36: Sixth Mode Shape of Cantilevered Cylinder (1550.7 Hz)

Table 5.7: Frequencies at the First Six Modes

Mode	Frequency (Hz)
1	452.46
2	452.46
3	1247.6
4	1247.6
5	1550.7
6	1550.7

### 5.9.2 Single Point PSD Spectrum Random Vibration Analysis

The next step after mode frequency analysis is to perform a spectrum analysis. The first six modes are included in the spectrum analysis to calculate element stresses. The model is excited in the Y-direction with a force of 200 N and the modal responses are combined using power spectral density mode combination method. The damping ratio is set to 0.02. Lastly, a one-sigma displacement solution output is written to the results file from the PSD analysis.

### 5.9.3 Harmonic Response Analysis

The third analysis is harmonic response using the mode superposition method option which sums factored mode shapes to calculate the harmonic response. A harmonic

analysis is performed after a spectrum analysis. The frequency ranges from 1.0 to 1600 Hz. The harmonic output option to print complex displacements as real and imaginary components is turned on, whereas the cluster option is turned off for uniform spacing of frequency solutions. These results are written in binary file \*.rfrq format. This binary file contains all the displacement data for all the nodes at each frequency interval. A plot of the FRF of the clamped-free cylinder is presented in Figure 5.37. The third, fourth, fifth, and sixth modes are not purely bending; hence, they do not have as great of an effect as the purely bending modes, modes one and two, on the displacement response of the cylindrical shell.

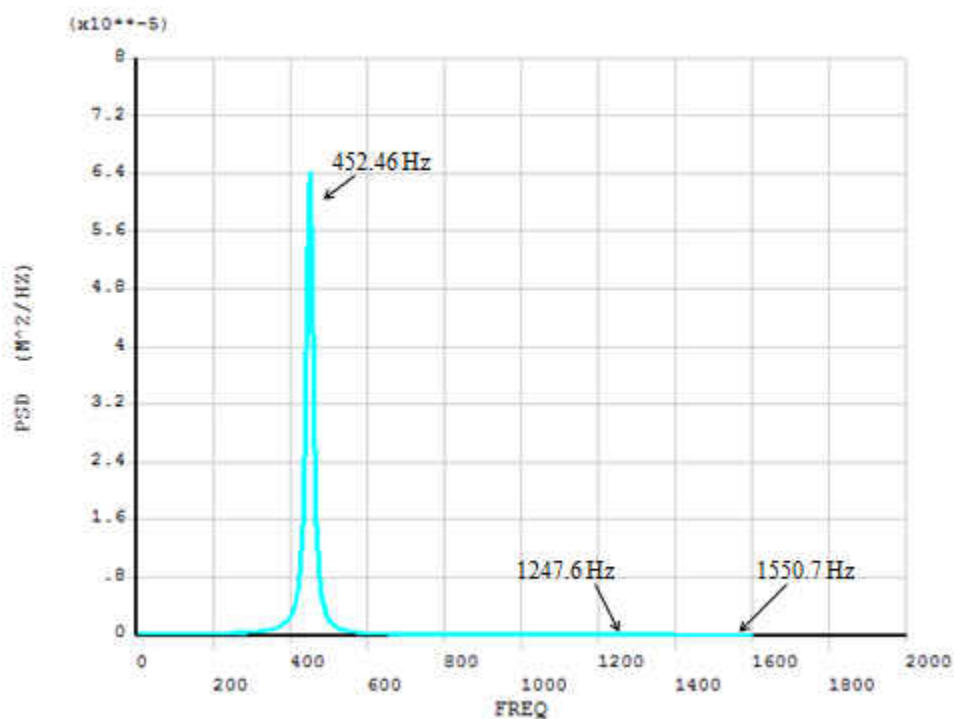


Figure 5.37: FRF Plot of Clamped-Free Cylindrical Shell

### 5.10 Processing of ANSYS Results of Cylindrical Shell in Matlab

The next step is to gather all of the displacement information at each frequency which is done with the harmonic analysis. The information is written to a \*.rfrq file



which is an ANSYS output binary file. This information will be imported in Matlab, which requires this data to be in text (ASCII) form. The ANSYS DUMP command converts the binary data into ASCII data. The nodal displacements are listed in ascending node order and then in ascending frequency. The format for this is outlined in Appendix I.

### **Stepwise Method of Processing the \*.rfrq Binary File Data in Matlab**

1. The ANSYS DUMP command is found in the GUI under Main Menu> List> Files> Binary Files, while choosing All Records to be listed and Entire Record of output per record. The file 'file.rfrq' is selected, creating the 'DUMP.txt' file. This file contains all the complex displacement for the cylindrical shell for each node at each frequency.
2. The 'FRFResult.txt' file is created from the DUMP.txt file starting after Record 8.
3. An 'NLIST.lis' file is saved, containing all the nodes and their coordinates.
4. The 'FRFProc\_01.m' Matlab file, which is listed in Appendix H along with the subsequent Matlab files for the cylinder, reads the 'FRFResult.txt' file and places the complex displacements in the  $x$ ,  $y$ , and  $z$  directions into matrix format for all the nodes and frequencies. However, only the top half of the shell is taken into account for ease of computation.
5. The complex displacements for each individual node at each frequency are then combined to create a displacement magnitude.
6. Then the 'NLIST.lis' file is read into Matlab to give the node numbers in order and their coordinates.

7. Since the displacements are in Cartesian coordinates, they are first converted to cylindrical coordinates, and then consolidated into one matrix. These are then placed into “Shell Coordinates”, three different [21x21x250] matrices representing the shell as if it was laid out with displacements of each node at each frequency. A plot of the FRF of the cylindrical shell substrate is illustrated in Figure 5.38. This figure is obtained through Matlab; it confirms that the displacements were successfully transferred from ANSYS and organized correctly. The plot illustrates the proposed assumption that the transverse direction exhibits a much greater displacement than that of the other two directions. Displacement in the X direction is negligible, whereas displacement in the Z is less than 22 % of that in the Y at the first mode, 10 % at the second mode, and negligible at the third mode.

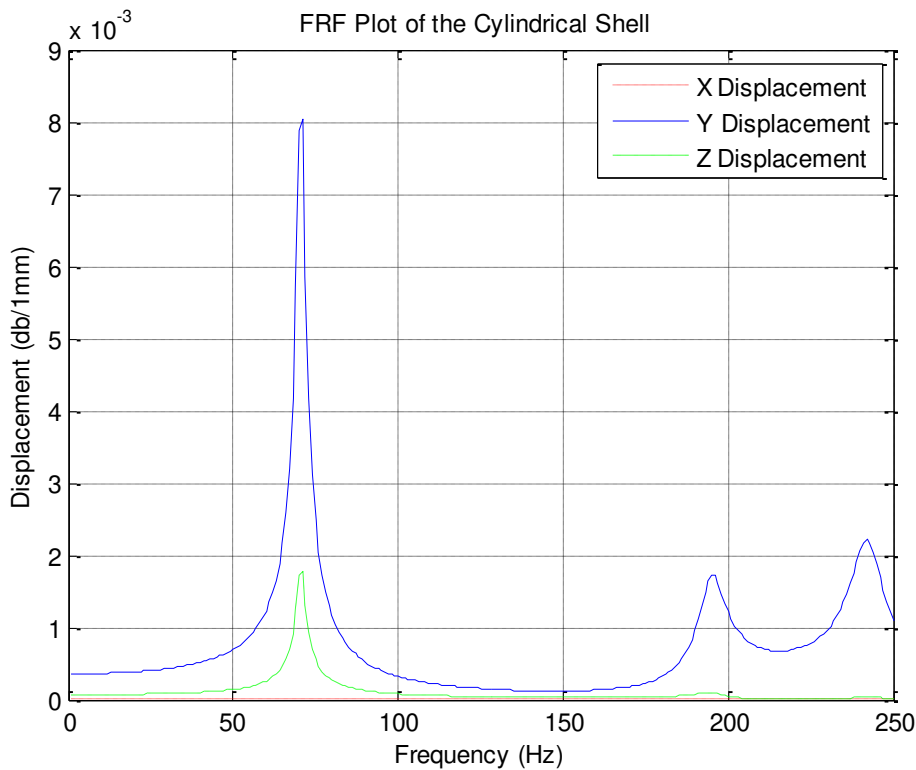


Figure 5.38: FRF Plot of the Cylindrical Shell

8. The 'DisplDerivative\_02.m' file is then run in order to obtain the required first derivatives and second derivatives of displacement with respect to the required direction.
9. After finding the derivatives, the 'Film\_Shape\_03.m' file is run. This file basically lists the attributes of the sensor and the cylindrical shell. The end result is the shape of the sensor pictured in Figure 5.40, also in matrix format, depicted in Figure 5.41 for calculations. During calculations, the matrix represents the sensor shape function  $W_s(\alpha_1, \alpha_2)$  in the sensor output charge equation for a cylindrical shell. Unlike a shaped sensor, a generic sensor would still have this matrix, only it would be filled with all 1s, representing the shape of the sensor. The sensor shape function matrix gets multiplied by the corresponding second derivatives in the sensor output charge equation. Wherever there is a "1" means that the sensor is covering that location; conversely, wherever there is a "0" means that there is not a sensor at that location.

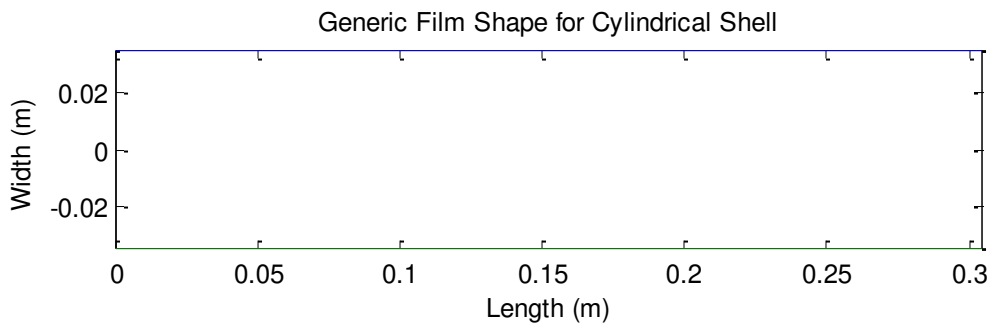


Figure 5.39: Generic Film Shape for Cylindrical Shell

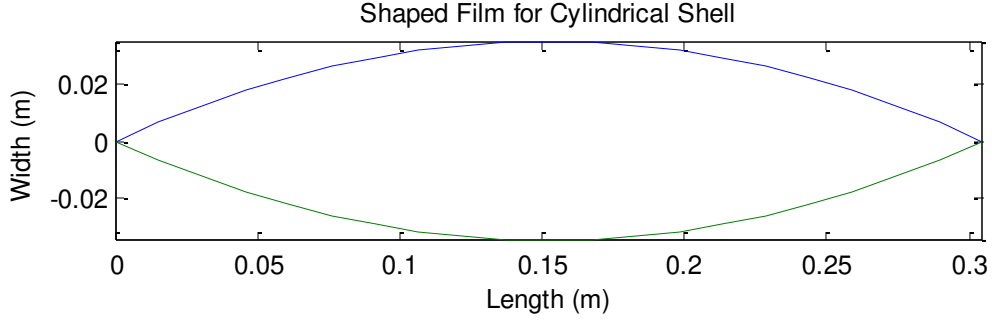


Figure 5.40: Shaped Film for Cylindrical Shell

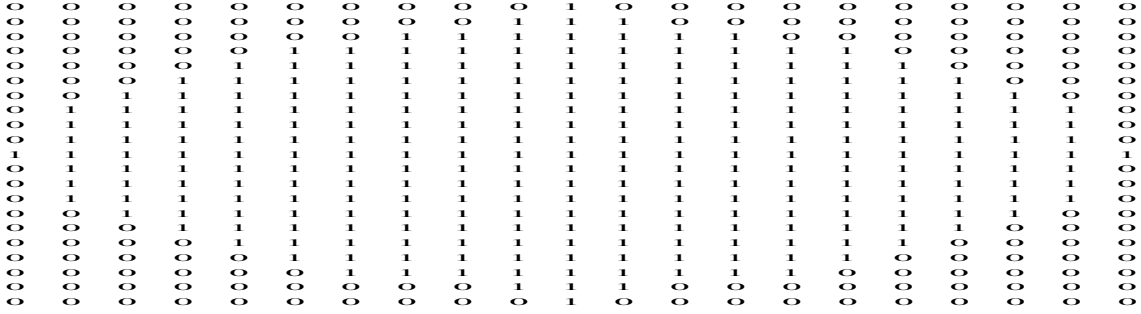


Figure 5.41: Film Shape in Matrix Form

10. Figure 5.39 shows a generic shaped sensor, a sensor which covers the entire surface of the cylindrical shell, is analyzed. The displacement frequency response of the clamped-free cylindrical shell and sensor output charge for each frequency is plotted as in Figure 5.42 for the generic sensor output charge equation:

$$\phi^s(z, \theta) = \frac{-e_{31}h^s}{e_{33}S^e} \int_{S^e} \left\{ e_{31} \left( \frac{\partial u_z}{\partial z} - r_z^s \frac{\partial^2 u_R}{\partial z^2} \right) + e_{32} \left( \frac{\partial u_\theta}{R \partial \theta} + \frac{u_R}{R^2} + r_\theta^s \frac{\partial u_\theta}{R^2 \partial \theta} - r_\theta^s \frac{\partial^2 u_R}{R^2 \partial \theta^2} \right) \right\} dS^e$$

11. Running ‘SensorOutput\_Shaped\_05.m’ analyzes the sensor shaped like that of Figures 5.40 and utilizes the values in Figure 5.41 in its calculations. The displacement frequency response of the clamped-free cylindrical shell and sensor output charge for each frequency is plotted as in Figure 5.43 for the sensor output

charge equation with a shaping function:

$$\phi^s(z, \theta) = \frac{-e_{31}h^s}{e_{33}S^e} \int_{S^e} W_s(z, \theta) \left\{ e_{31} \left( \frac{\partial u_z}{\partial z} - r_z^s \frac{\partial^2 u_R}{\partial z^2} \right) + e_{32} \left( \frac{\partial u_\theta}{R \partial \theta} + \frac{u_R}{R^2} + r_\theta^s \frac{\partial u_\theta}{R^2 \partial \theta} - r_\theta^s \frac{\partial^2 u_R}{R^2 \partial \theta^2} \right) \right\} dS^e$$

Here, the graphs of the displacement frequency response of the clamped-free cylindrical shell and sensor output charge for each frequency of the generic sensor and the shaped sensor are shown.

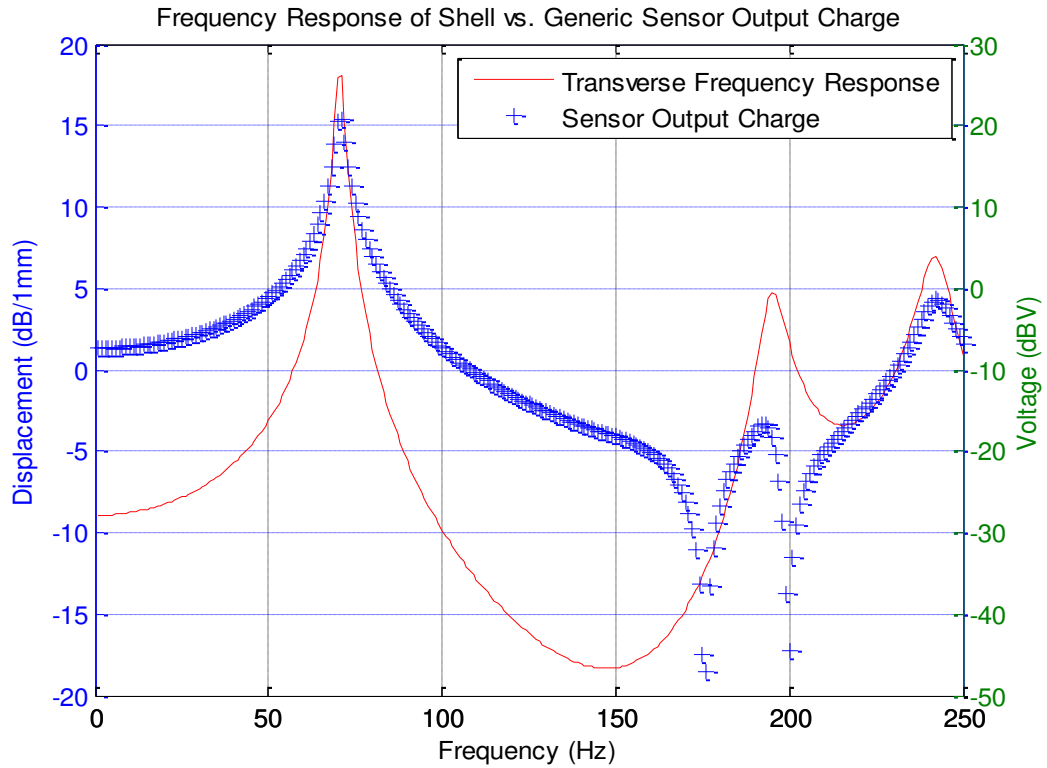


Figure 5.42: Frequency Response of Shell vs. Generic Sensor Output Charge

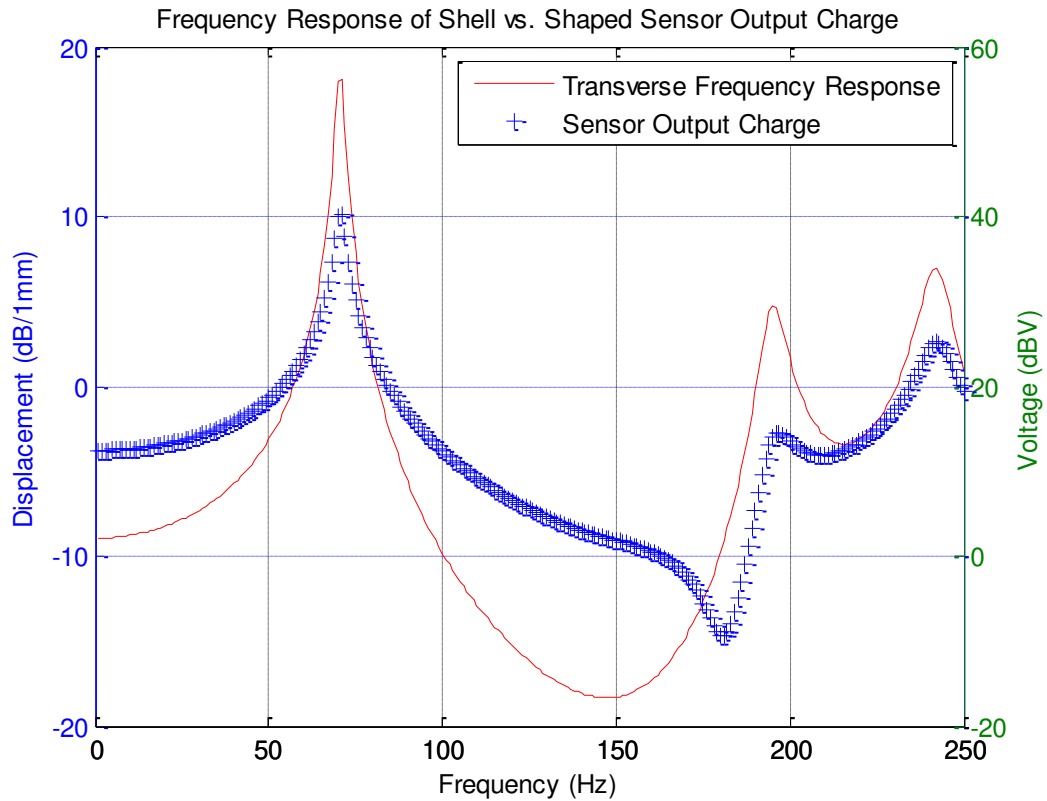


Figure 5.43: Frequency Response of Shell vs. Shaped Sensor Output Charge

It can be observed in both Figure 5.42 and Figure 5.43 that the films can correctly capture the mode shapes of the displacement frequency response of the substrate; however, they experience some discrepancies between the sensor output charge and the frequency response of the cylindrical shell. The discrepancies in resonant frequencies between the sensor output charge and the frequency response of the cylindrical shell can be accounted for by the same explanation as for the plate. The output charge equation integrates “strains” over the whole surface of the sensor; it is the summation of the derivatives of displacements. The displacement frequency response function shown on the figure only takes into account one point on the substrate; this point may not see certain modes. For instance, in the case of the beam in Figure 5.27, the particular point considered is a node and will not correctly capture the third mode of the beam. The

sensor output charge equation, however, captures all the modes and therefore will show more modes than the substrate point considered. As an example, an accelerometer attached to the substrate at a node of a mode will not measure that mode, because it will remain “still” at excitation coinciding with that mode. In surface shaping sensor design, the objective is to design a sensor which monitors those modes which need to be controlled. Hence, the FRF of a point may show fewer modes than the FRF of the sensor output charge.

## **5.11 Conclusions and Future Scope**

### **Conclusions**

This work shows that a mix of finite element and numerical differentiation and integration methods can be used in order to calculate the output charge of a thin piezoelectric film bonded to a shell structure. The method was applied to cases of a cylindrical shell structure, as well as a beam and plate for both the generic and shaped piezoelectric film. The method can be applied to cases where the required input variables such as film shape and shell vibration profile are in discrete form. Therefore, experimentally obtained input variables can be used with the herein described method to calculate the piezoelectric film output charge and thus, design a sensor for desired output. The results indicate that sensor output captures the behavior of the structures as far as the modes are concerned. The proposed method can be applied to calculate the output charge of films attached to complex structures or structures with complex boundary conditions. This can also be applied in cases where close form equations cannot be derived and the only data available are discrete or experimental. Moreover, in sensor design applications

where the film is often shaped so that its output charge corresponds to a specific structural dynamic property, the proposed method greatly simplifies the design process.

### **Future Scope**

After the simulation of the beam, plate, and cylindrical shell and finding the output charge of their sensors, the next step would be to develop an actuator and use it in the same control system as the sensor. After that, an experiment should be performed to verify the findings. A possible change could be to apply the method to more complex structures, and a possible improvement could be to use an increased number of nodes for all three structures for increased resolution; this may decrease errors in numeric computing.



## **APPENDICES**

## APPENDIX A

### ANSYS INPUT LOG FILE FOR VM19

```
/COM,ANSYS MEDIA REL. 120 (02/19/2009) REF. VERIF. MANUAL: REL. 120  
  
/VERIFY,VM19  
  
/PREP7  
  
/TITLE, VM19, RANDOM VIBRATION ANALYSIS OF A DEEP SIMPLY-  
SUPPORTED BEAM  
  
/COM REFERENCE: NAFEMS FORCED VIBRATION BENCHMARKS TEST 5R  
  
ET,1,BEAM4          ! DEFINE ELEMENT TYPE  
  
MP,EX,1,200E9      ! DEFINE MATERIAL PROPERTIES  
  
MP,NUXY,1,0.3  
  
MP,ALPX,1,0.1E-5  
  
MP,DENS,1,8000  
  
R,1,4,1.333,1.333,2,2,0    ! DEFINE REAL CONSTANTS  
  
RMORE,0,2.2496,1.177,1.177  
  
N,1,0  
  
N,11,10  
  
FILL  
  
E,1,2  
  
EGEN,10,1,1  
  
FINISH
```

```

/SOLU

ANTYPE,MODAL          ! DEFINE ANALYSIS TYPE

MXPAND,9,,,YES      ! EXPAND 9 MODES, CALC. STRESS VALUES

MODOPT,REDUC

D,1,UX,0,0,1,1,UY,UZ,ROTX    ! APPLY CONSTRAINTS

D,11,UY,0,0,11,1,UZ

M,2,UY,10,1

SOLVE

*GET,FREQ,MODE,1,FREQ

FINISH

/COPY,,tri,,mode,tri

/SOLU

ANTYPE,SPECTR        ! PREFORM SPECTRUM PSD ANALYSIS

SPOPT,PSD,9,ON      ! CALC. STRESS RESPONSE FOR FIRST 9 MODES

PSDUNIT,1,FORCE

DMPRAT,0.02

F,1,FY,-0.5E6        ! SCALE LOADS

F,11,FY,-0.5E6

F,2,FY,-1E6,,10,1

PSDFRQ,1,1,0.1,70.

PSDVAL,1,1,1        ! IN N**2/HZ

PFACT,1,NODE

PSDRES,DISP,REL

```

PSDCOM

SOLVE

FINISH

/POST26

STORE,PSD,10

NSOL,2,6,U,Y

RPSD,8,2

PRTIME,42.640,42.641

PRVAR,8

\*GET,P1,VARI,8,RTIME,42.64

PM=P1\*1000000

FINISH

/POST26

STORE,PSD,10

ESOL,3,5,6,LS,7

RPSD,9,3

PRTIME,42.640,42.641

PRVAR,9

\*GET,P2,VARI,9,RTIME,42.64

PM2=P2/(1E12)

\*DIM,LABEL,CHAR,3,2

```

*DIM,VALUE,,3,3

LABEL(1,1) = 'FREQ1','PEAK d','PSD(N/mm'

LABEL(1,2) = '(Hz)',' mm^2/Hz','^2)^2/Hz'

*VFILL,VALUE(1,1),DATA,42.65,180.9,58515.6

*VFILL,VALUE(1,2),DATA,FREQ,PM,PM2

*VFILL,VALUE(1,3),DATA,ABS(FREQ/42.65) ,ABS(PM/180.9 ),ABS(PM2/58515.6 )

FINISH

/COM

/OUT,vm19.vrt

/COM,----- VM19 RESULTS COMPARISON -----

/COM,

/COM,          | TARGET | ANSYS | RATIO

/COM,

*VWRITE,LABEL(1,1),LABEL(1,2),VALUE(1,1),VALUE(1,2),VALUE(1,3)

(1X,A8,A8,' ',F10.2,' ',F10.2,' ',1F5.2)

/COM,-----

/COM,

/COM,-----

/COM,NOTE: THERE ARE VERIFIED RESULTS IN VM19 NOT CONTAINED IN

/COM,THIS TABLE

/COM,-----

/OUT

*LIST,vm19.vrt

```

## APPENDIX B

### ANSYS INPUT LOG FILE FOR VM203

```
/VERIFY,VM203

/PREP7

/TITLE, VM203, DYNAMIC LOAD EFFECT ON SIMPLY-SUPPORTED THICK
SQUARE PLATE

/COM REFERENCE: NAFEMS FORCED VIBRATION BENCHMARKS, TEST 21R

C***      USING SHELL281 ELEMENTS

ET,1,SHELL281      ! DEFINE ELEMENT TYPE

SECTYPE,1,SHELL

SECDATA,1,1,0,5      ! THICKNESS

MP,EX,1,200E9      ! DEFINE MATERIAL PROPERTIES

MP,NUXY,1,0.3

MP,ALPX,1,0.1E-5

MP,DENS,1,8000

N,1,0,0,0      ! DEFINE MODEL

N,9,0,10,0

FILL

NGEN,5,40,1,9,1,2.5

N,21,1.25,0,0

N,29,1.25,10,0
```

```

FILL,21,29,3
NGEN,4,40,21,29,2,2.5
EN,1,1,41,43,3,21,42,23,2
EGEN,4,2,1
EGEN,4,40,1,4
FINISH
SAVE,MODEL
*CREATE,SOLVIT,MAC
/SOLU
ANTYPE,MODAL      ! DEFINE ANALYSIS TYPE AS MODAL VIBRATION
MODOPT,REDUC
MXPAND,16,,YES
SFE,ALL,,PRES,,-1E6    ! PRESS LOAD OF 1000,000 N/M**2
D,ALL,UX,0,,,UY,ROTZ    ! APPLY CONSTRAINTS
D,1,UZ,0,0,9,1,ROTX
D,161,UZ,0,0,169,1,ROTX
D,1,UZ,0,0,161,20,ROTY
D,9,UZ,0,0,169,20,ROTY
NSEL,S,LOC,X,.1,9.9
NSEL,R,LOC,Y,.1,9.9
M,ALL,UZ      ! SELECT MASTERS
NSEL,ALL
SOLVE

```

```

*GET,F,MODE,1,FREQ

FINISH

/SOLU

/TITLE, VM203, RANDOM VIBRATION , RESPONSE TO UNIFORM PSD FORCE

ANTYPE,SPECTR          ! DEFINE ANALYSIS TYPE

SPOPT,PSD,2,ON        ! USE FIRST 2 MODES, CALC ELEM. STRESSES

PSDUNIT,1,PRES        ! DEFINE TYPE OF PSD AS A PRESSURE SPECTRUM

DMPRAT,0.02

PSDFRQ,1,1,1.0,80.0

PSDVAL,1,1.0,1.0      ! IN N**2/HZ

SFEDELE,ALL,,PRES,,

LVSCALE,1             ! USE AND SCALE THE LOAD VECTOR GENERATED

AT MODAL ANALYSIS

PFACT,1,NODE

PSDRES,DISP,REL

PSDCOM

SOLVE

FINISH

/POST1

SET,3,1               ! ONE SIGMA DISPLACEMENT SOLUTION RESULTS

/VIEW,1,2,3,4

PLNSOL,U,Z

PRNSOL,U,Z

```



```

L2=NODE(2,8,0)
*GET,SIGEL2,NODE,L2,S,EQV
NSEL,,NODE,,L2
PRNSOL,S,COMP
NSEL,ALL
FINISH

/SOLUTION
ANTYPE,HARMIC           ! REDEFINE ANALYSIS TYPE AND SOLVE AGAIN
HROPT,MSUP             ! USING MODE SUPERPOSITION HARMONIC
ANALYSIS
HROUT,OFF,ON          ! PRINT AMPLITUDE & PHASE, CLUSTER
FREQUENCIES
KBC,1
HARFRQ,1,80
DMPRAT,0.02
NSUBSTEP,10
SOLVE
FINISH

/POST26
FILE,,rfrq
PRCPLX,1
NSOL,2,85,U,Z
PSDDAT,6,1,1.0,80,1.0

```

```
PSDTYP,2
PSDCAL,7,2
PSDPRT
PRVAR,2,7
*GET,P,VARI,7,EXTREM,VMAX
*STATUS,PARM
/AXLAB,Y,PSD (M^2/HZ)
PLVAR,7
*DIM,LABEL,CHAR,2,2
*DIM,VALUE,,2,3
LABEL(1,1) = 'f','PSD '
LABEL(1,2) = 'Hz','SQmmS/Hz'
*VFILL,VALUE(1,1),DATA,45.9,3.4018E-3
*VFILL,VALUE(1,2),DATA,F,P
*VFILL,VALUE(1,3),DATA,ABS(F/45.9),ABS(P/(3.4018E-3))
FINISH
*END
SOLVIT
SAVE,TABLE_1
/NOPR
RESUME,TABLE_1
/COM
/OUT,vm203,vrt
```

```

/COM,----- VM203 RESULTS COMPARISON -----
/COM,
/COM,      | TARGET | ANSYS | RATIO
/COM,
/COM, SHELL281
/COM,
*VWRITE,LABEL(1,1),LABEL(1,2),VALUE(1,1),VALUE(1,2),VALUE(1,3)
(1X,A8,A8,' ',F11.6,' ',F11.6,' ',1F6.3)
/COM,
/COM,
/COM,-----
/COM,
/OUT
FINISH
*LIST,vm203,vrt
/DELETE,MODEL
/DELETE,SOLVIT,MAC
/DELETE,TABLE_1

```

## APPENDIX C

### ANSYS INPUT LOG FILE FOR SIMULATION OF BEAM

```
FINISH
/CLEAR,ALL
/CONFIG, NRES, 15000 ! Maximum number of results sets(subsets) allowed on the
results file.
/CWD,'j:\BeamPSD Verify'
/TITLE, Dynamic Analysis
/PREP7

! Define variables for problem:
!-----
! INCHES TO METRIC
*set,L,12*2.54/100
*set,H,1/8*2.54/100
*set,B,2*2.54/100
*set,MYFRQ,1600
*set,MyLoadStep,500
*set,MYFORCE,-600
*set,NODES,251
A=B*H
Izz=B*H**3/12
Iyy=H*B**3/12

! Define elements and material properties:
!-----
ET,1,BEAM4           ! DEFINE ELEMENT TYPE
MP,EX,1,70E9         ! DEFINE MATERIAL PROPERTIES
MP,NUXY,1,0.33
MP,DENS,1,2710
R,1,A,Izz,Iyy,H,B,0 ! DEFINE REAL CONSTANTS

! Geometry:
!-----
N,1,0
N,NODES,L
FILL
E,1,2
```

```

EGEN,NODES-1,1,1                !Generates elements from an existing pattern
including pattern

! BC and master nodes:
!-----
D,1,ALL ! Constrain left end
NSEL,S,,,1,NODES, ! select nodes 1 - LAST
M,ALL,UY, , , ! Define Master DOFs
NSEL,ALL ! Reselect all nodes
FINISH

/SOLU
ANTYPE,MODAL                    ! DEFINE ANALYSIS TYPE AS MODAL VIBRATION
MODOPT,REDUC
MXPAND,6,,,YES
NSEL,ALL
SOLVE
FINISH

/POST1
SET,LIST !List mode frequencies

/SOLU
ANTYPE,SPECTR                   ! DEFINE ANALYSIS TYPE
SPOPT,PSD,4,ON                 ! USE FIRST 4 MODES, CALC ELEM. STRESSES
PSDUNIT,1,FORCE                ! DEFINE TYPE OF PSD AS A FORCE SPECTRUM
DMPRAT,0.02                    ! DMPRAT, RATIO
F,2,FY,MYFORCE
PSDFRQ,1,1,1.0,MYFRQ
PSDVAL,1,1.0,1.0              ! IN N**2/HZ
LVSCALE,1                      ! USE AND SCALE THE LOAD VECTOR GENERATED
AT MODAL ANALYSIS
PFACT,1,NODE                   ! Calculates participation factors
PSDRES,DISP,REL
PSDCOM
SOLVE
FINISH

/POST1
SET,3,1                        ! ONE SIGMA DISPLACEMENT SOLUTION RESULTS
/VIEW,1,2,3,4
PLNSOL,U,Y !Displays results as continuous contours.
PRNSOL,U,Y !Prints the nodal solution results.
FINISH

/SOLUTION

```

```
ANTYPE,HARMIC      ! REDEFINE ANALYSIS TYPE AND SOLVE AGAIN
HROPT,MSUP        ! USING MODE SUPERPOSITION HARMONIC ANALYSIS
HROUT,ON,OFF      ! PRINT AMPLITUDE & PHASE, CLUSTER FREQUENCIES
KBC,1
HARFRQ,1,MYFRQ
DMPRAT,0.02
NSUBST,MyLOadStep
SOLVE
FINISH
```

```
/POST26
FILE,,rfreq
PRCPLX,0 !Defines the output form for complex variables
NSOL,2,NODES,U,Y
PSDDAT,6,1,1.0,MYFRQ,1.0
PSDTYP,2
PSDCAL,7,2
PSDPRT
PRVAR,2,7
*GET,P,VARI,7,EXTREM,VMAX
*STATUS,PARM
/AXLAB,Y,PSD (M^2/HZ)
PLVAR,7
```

**APPENDIX D**  
**MATLAB CODE FOR BEAM**

**FRFProc\_01.m Matlab Code**

```
clc
clear all
close all
%
% Data
LoadStep=500;
Wy = fopen('FRFResult2.txt','r');
%junk1=fscanf(Wy,'%s',2651);
for j=1:LoadStep;%LoadStep % Total dispload
    for i=1:102 % 102 line per record
        WyTmp=fscanf(Wy,'%g',[1 5]);
        Junk2=fscanf(Wy,'%s',2);
        RawData(i,:j)=WyTmp;
    end
    Junk3=fscanf(Wy,'%s',26);
end
% Extract frequency
for i=1:LoadStep
```

```

Freq(i)=RawData(101,1,i);
end

% Extract UY with column per load
for j=1:LoadStep
    RawDataV1=RawData(1:100, :,j)';
    RawDataV(:,j)=RawDataV1(:);
end

% Extract UY per load
for j=1:LoadStep
    k=0;
    for i=1:2:499
        k=k+1;
        UyReal=RawDataV(i,j);
        UyIm=RawDataV(i+1,j);
        Uy(:,k,j)=[UyReal;UyIm];
    end
end

% Check
for j=1:LoadStep
    Uplot(:,j)=Uy(:,250,j); %Last node 250
    UplotMag(j)=sqrt(Uplot(1,j)^2+Uplot(2,j)^2);
end

```



```

% Create U of magnitude
for j=1:500
    for i=1:250
        Um(1,i,j)=sqrt(Uy(1,i,j)^2+Uy(2,i,j)^2);
    end
end

save DispData Uy Um Freq UplotMag
plot(Freq,UplotMag)
title('FRF Plot of Clamped-Free Beam')
legend('Beam Displacement')
xlabel('Frequency (Hz)')
ylabel('Displacement (db/1mm)')

```

### **DisplDerivative\_02.m Matlab Code**

```

clc
clear all
%
load DispData
N=size(Uy);
L=12*2.54/100;
dx=L/250;
x=0:dx:L;
%

```

```

for j=1:N(3)
    tmp1(1,2:251)=Um(1,.,j);
    Dpp(1,.,j)=diff(tmp1,2,2)/dx;
end
%
save DisplDerivative Dpp Freq UplotMag

```

### **Film\_Shape\_03.m Matlab Code**

```

close all
clear all
clc
%
hb=1/8*2.54/100;
hs=28e-6;
e31=7.25;
b=2*2.54/100;
L=12*2.54/100;
k=-b/(2*e31*(hb+hs));
dx=L/250;
x=0:dx:L;
N=length(x);
Fones=ones(N,1);

```

```

F=Fones*b/2;
%Fs=k*(x-L).^2;
Fs=k*(x.^2-L*x);
save FilmShape F Fs e31 hb hs
plot(x,Fs,x,-Fs)
title('Shaped Film for Beam')
xlabel('Length (m)')
ylabel('Width (m)')
axis equal
axis([0 L -b/2 b/2])

%plot(x,F,x,-F)
%title('Generic Film Shape for Beam')
xlabel('Length (m)')
ylabel('Width (m)')
axis equal
axis([0 L -b/2 b/2])

```

#### **SensorOutput\_Generic\_04**

```

close all
clear all
clc
%
```

```

load DisplDerivative
load FilmShape
L=12*2.54/100;
dx=L/250;
x=0:dx:L;
%
N=size(Dpp);
F=F(1:end-2);
NewCoord=x(1:end-2);
for j=1:500
    Itmp=-e31*(hs+hb)*F'.*Dpp(1,,:j);
    q(j)=trapz(Itmp,NewCoord);
end
%
[ax,h1,h2]=plotyy(Freq,20*log10(UplotMag/1e-3),Freq,20*log10(1e1*q/1e-
3),'plot','plot');
set(h1,'color','red');
set(h2,'color','blue','linestyle','+');
set(get(ax(1), 'Ylabel'), 'String', 'Displacement (dB/1mm)');
set(get(ax(2), 'Ylabel'), 'String', 'Voltage (dBV)');
grid
title('Frequency Response of Beam vs. Generic Sensor Output Charge')
xlabel('Frequency (Hz)')

```

```
legend('Beam Frequency Response','Sensor Output Charge')  
axis square
```

### SensorOutput\_Shaped\_05.m Matlab Code

```
close all  
clear all  
clc  
%  
load DisplDerivative  
load FilmShape  
L=12*2.54/100;  
dx=L/250;  
x=0:dx:L;  
%  
N=size(Dpp);  
Fs=Fs(1:end-2);  
%Fones=ones(249,1);  
NewCoord=x(1:end-2);  
for j=1:500  
    Itmp=-e31*(hs+hb)*Dpp(1,:,j);  
    %Itmp=-e31*(hs+hb)*Fs.*Dpp(1,:,j);  
    q(j)=trapz(Itmp,NewCoord);  
end
```

```
%  
  
[ax,h1,h2]=plotyy(Freq,20*log10(UplotMag/1e-3),Freq,20*log10(.22*q/1e-  
3),'plot','plot');  
  
set(h1,'color','red');  
  
set(h2,'color','blue','linestyle','+');  
  
set(get(ax(1), 'Ylabel'), 'String', 'Displacement (dB/1mm)');  
  
set(get(ax(2), 'Ylabel'), 'String', 'Voltage (dBV)');  
  
grid  
  
title('Frequency Response of Beam vs. Shaped Sensor Output Charge')  
  
xlabel('Frequency (Hz)')  
  
legend('Beam Frequency Response','Sensor Output Charge')
```

## APPENDIX E

### ANSYS INPUT LOG FILE FOR SIMULATION OF PLATE

```
FINISH
/CLEAR,ALL
/CONFIG, NRES, 15000 ! Maximum number of results sets(subsets) allowed on the
results file.
/CWD,'j:\PlatePSD Verify'
/TITLE, Dynamic Analysis
/PREP7

! Define variables for problem:
!-----
*set,H,15*2.54/100
*set,L,24*2.54/100
*set,B,3/16*2.54/100
*set,MYFRQ,250
*set,MyLoadStep,500
*set,MYFORCE,-50
*set,NODES,400

! Define elements and material properties:
!-----
ET,1,SHELL63           ! Element Type
MP,EX,1,70E9           ! Young's Modulus
MP,PRXY,1,0.33         ! Poisson's Ratio
MP,DENS,1,2710         ! Density
R,1,B,B,B,B,0,0       ! Thickness

! Geometry:
!-----
N,1,0,0,0
N,25,L,0,0
FILL
NGEN,16,25,1,25,1,,H/16
EN,1,1,2,27,26
EGEN,24,1,1
EGEN,15,25,1,25

! BC and master nodes:
```

```

!-----
D,1,ALL,,376,25 ! Constrain left end
NSEL,S,,1,NODES, ! select nodes 1 - LAST
M,ALL,UZ, , , ! Define Master DOFs
NSEL,ALL ! Reselect all nodes
FINISH

/SOLU
ANTYPE,MODAL          ! DEFINE ANALYSIS TYPE AS MODAL VIBRATION
MODOPT,REDUC
MXPAND,6,,YES
NSEL,ALL
SOLVE
FINISH

/POST1
SET,LIST !List mode frequencies

/SOLU
ANTYPE,SPECTR        ! DEFINE ANALYSIS TYPE
SPOPT,PSD,6,ON      ! USE FIRST 6 MODES, CALC ELEM. STRESSES
PSDUNIT,1,FORCE     ! DEFINE TYPE OF PSD AS A FORCE SPECTRUM
DMPRAT,0.02         ! DMPRAT, RATIO
!
F,200,FZ,MYFORCE
!
PSDFRQ,1,1,1.0,MYFRQ
PSDVAL,1,1.0,1.0    ! IN N**2/HZ
LVSCALE,1           ! USE AND SCALE THE LOAD VECTOR GENERATED
AT MODAL ANALYSIS
PFACT,1,NODE        ! Calculates participation factors
PSDRES,DISP,REL
PSDCOM
SOLVE
FINISH

/POST1
SET,3,1             ! ONE SIGMA DISPLACEMENT SOLUTION RESULTS
/VIEW,1,2,3,4
!
PLNSOL,U,Z !Displays results as continuous contours.
PRNSOL,U,Z !Prints the nodal solution results.
!
FINISH

/SOLUTION

```



```

ANTYPE,HARMIC      ! REDEFINE ANALYSIS TYPE AND SOLVE AGAIN
HROPT,MSUP        ! USING MODE SUPERPOSITION HARMONIC ANALYSIS
HROUT,ON,OFF      ! PRINT AMPLITUDE & PHASE, CLUSTER FREQUENCIES
KBC,1
HARFRQ,1,MYFRQ
DMPRAT,0.02
NSUBST,MyLoadStep
SOLVE
FINISH

/POST26
FILE,,rfrq
PRCPLX,0 !Defines the output form for complex variables
!
NSOL,2,110,U,Z
!
PSDDAT,6,1,1.0,MYFRQ,1.0
PSDTYP,2
PSDCAL,7,2
PSDPRT
PRVAR,2,7
*GET,P,VARI,7,EXTREM,VMAX
*STATUS,PARM
/AXLAB,Y,PSD (M^2/HZ)
PLVAR,7

```

**APPENDIX F**  
**MATLAB CODE FOR PLATE**

**FRFProc\_01.m Matlab Code**

```
clc

clear all

close all

%

% Data

LoadStep=500;

Wy = fopen('FRFResult.txt','r');

%junk1=fscanf(Wy,'%s',2651);

for j=1:LoadStep;%LoadStep % Total displrecord

    for i=1:155 % 303 line per record

        WyTmp=fscanf(Wy,'%g',[1 5]);

        Junk2=fscanf(Wy,'%s',2);

        RawData(i,:j)=WyTmp;

    end

    Junk3=fscanf(Wy,'%s',29);

end

% extract frequency

for i=1:LoadStep
```

```

    Freq(i)=RawData(154,4,i);
end

% Extract UZ with column per load
for j=1:LoadStep
    RawDataV1=RawData(1:154,:,j)';
    RawDataV(:,j)=RawDataV1(:);
end

% Extract UZ per load
for j=1:LoadStep
    k=0;
    for i=1:2:768
        k=k+1;
        UzReal=RawDataV(i,j);
        UzIm=RawDataV(i+1,j);
        Uz(:,k,j)=[UzReal;UzIm];
    end
end

% Check
for j=1:LoadStep
    Uplot(:,j)=Uz(:,200,j); % at node 200
    UplotMag(j)=sqrt(Uplot(1,j)^2+Uplot(2,j)^2);
end

% Create U of magnitude

```

```

for j=1:500
    for i=1:384
        Um(1,i,j)=sqrt(Uz(1,i,j)^2+Uz(2,i,j)^2);
    end
end

% Place Um in Plate Coordinates
Umt=zeros(16,24,500); %16 by 24 nodes, subtracted left end due to constraints
j=16;k=24;
while j>=1
    ii=1:500;
    Umt(j,:,ii)=Um(:,k-23:k,ii);
    k=k+24;
    j=j-1;
end

save DispData Uz Umt Freq UplotMag
plot(Freq,UplotMag)
title('FRF Plot of Plate')
legend('Plate Displacement')
xlabel('Frequency (Hz)')
ylabel('Displacement (db/1mm)')

```

**DisplDerivative\_02.m Matlab Code**

```

close all

clear all

clc

%

load DispData

N=size(Umt);

L=24*2.54/100;

dx=L/24;

x=0:dx:L;

H=15*2.54/100;

dy=H/15;

y=0:dy:H;

% 2nd Derivatives

NewD=zeros(16,25,500);

NewD(:,2:end,:)=Umt(:,:,:); % add constrained end of plate

for j=1:N(3)

[X,Y]=gradient(NewD(:,:,j));

[XX,Junk1]=gradient(X/dx);

[Junk2,YY]=gradient(Y/dy);

end

save DisplDerivative XX YY NewD Freq UplotMag N X Y dx dy

```

## PLATEreadcoord\_02.m Matlab Code

```
close all

clear all

clc

%

% Data

NumberOfPoint=400;%From ANSYS file *DO LOOP ON

%PARAMETER= ICOUNT FROM 0.0000 TO 400.00

%Tf=20; %Must be bigger than the final time from ANSYS file

Np=0;

k=0;

kk=1;

jj=1;

%

Wy = fopen('NLIST.lis','r');

junk1=fscanf(Wy,'%s',16);

while Np < NumberOfPoint

    for j=1:20

        if Np < NumberOfPoint

            k=k+1;

            CoTmp=fscanf(Wy,'%g',[1 4]);

            Coord(k,:,kk)=CoTmp;
```

```

        Np=Coord(k,1);
    end
end
junk2=fscanf(Wy,'%s',4);
end
fclose(Wy);
% For Dxx
NewCoordx=zeros(16,25);
j=16;k=25;
while j>=1
    NewCoordx(j,:)=Coord(k-24:k,2);
    k=k+25;
    j=j-1;
end
% For Dyy
NewCoordy=zeros(16,25);
j=1;k=25;
while j<=16
    NewCoordy(j,:)=Coord(k-24:k,3);
    k=k+25;
    j=j+1;
end
save PLATECoord NewCoordx NewCoordy Coord

```

### Film\_Shape\_03.m Matlab Code

```
close all

clear all

clc

%

load PLATECoord

load DisplDerivative

%Calculate Film Shape Outline

hb=3/16*2.54/100;

hs=50e-6;

e31=9.65;

L=24*2.54/100;

b=15*2.54/100/2;

k=-b/(2*e31*(hb+hs));

dx=L/24;

x=0:dx:L;

F=k*(x.^2-L*x);

plot(x,F,x,-F)

%title('Shaped Film for Plate')

%xlabel('Length (m)')

%ylabel('Width (m)')
```



```

%Create Film on Plate

y=b:-b/7.5:-b;

for i=1:25

    Y(:,i)=y;

end

W=ones(16,25);

for j=1:25

    for k=1:16

        if F(1,j)' < Y(k,j)

            W(k,j)=0;

        end

        if -F(1,j)' > Y(k,j)

            W(k,j)=0;

        end

    end

end

end

save FilmShape e31 hb hs F y Y W

%

Fones=ones(25,1);

F1=Fones*b;

%

plot(x,F1,x,-F1)

title('Generic Film Shape for Plate')

```

```
xlabel('Length (m)')
```

```
ylabel('Width (m)')
```

```
axis equal
```

```
axis([0 L -b b])
```

### **SensorOutput\_Generic\_04**

```
close all
```

```
clear all
```

```
clc
```

```
%
```

```
load PLATECoord
```

```
load DispData
```

```
load DisplDerivative
```

```
load FilmShape
```

```
L=24*2.54/100;
```

```
dx=L/24;
```

```
x=0:dx:L;
```

```
H=15*2.54/100;
```

```
dy=H/15;
```

```
y=0:H/24:H; % needs to be <1x24> to match dx
```

```
%
```

```
N=size(NewD);
```

```
Xt=X'; Yt=Y; % Use with trapz
```

```

X=Xt(:,1); Y=Yt(1,:); % Use with trapz

Fnew=ones(16,25);

%Fnew or NewCoordy or else?

for i=1:500

    [X1,Y1]=gradient(NewD(:,i));

    [XX,Junk1]=gradient(X1/dx);

    [Junk2,YY]=gradient(Y1/dy);

    [Yn,Xn]=meshgrid(Y,X);

    Itmp=-e31*(hs+hb)*Fnew*(XX+YY); % XX = d^2F/dx^2 and YY = d^2F/dy^2

    %Y2=[0 .005 .01 .015 .02 .025 .03 .035 .04 .045 .05 .055 .06 .065 .07 .075 .08 .085 .09
.095 .1];

    X2=[0 .02 .04 .06 .08 .1 .12 .14 .16 .18 .2];

    %q(i)=trapz(Y2,trapz(X',Itmp.'.'); % Y2 needs to be [1 x 21] vector

    q(i)=trapz(y,trapz(NewCoordx(1,:),Itmp.'.');

end

%

[ax,h1,h2]=plotyy(Freq,20*log10(UplotMag/1e-3),Freq,20*log10(3*q/1e-3),'plot','plot');

set(h1,'color','red');

set(h2,'color','blue','linestyle','+');

set(get(ax(1), 'Ylabel'), 'String', 'Displacement (dB/1mm)');

set(get(ax(2), 'Ylabel'), 'String', 'Voltage (dBV)');

grid

title('Frequency Response of Plate vs. Generic Sensor Output Charge')

```

```
xlabel('Frequency (Hz)')
```

```
legend('Plate Frequency Response','Sensor Output Charge')
```

### **SensorOutput\_Shaped\_05.m Matlab Code**

```
close all
```

```
clear all
```

```
clc
```

```
%
```

```
load PLATECoord
```

```
load DispData
```

```
load DisplDerivative
```

```
load FilmShape
```

```
L=24*2.54/100;
```

```
H=15*2.54/100/2;
```

```
dx=L/24;
```

```
x=0:dx:L;
```

```
dy=H/24;
```

```
y=0:dy:H;
```

```
%
```

```
for i=1:500
```

```
    [X1,Y1]=gradient(NewD(:,:,i));
```

```
    [XX,Junk1]=gradient(X1/dx);
```

```
    [Junk2,YY]=gradient(Y1/dy);
```

```

[Yn,Xn]=meshgrid(Y,X);

Itmp=-e31*(hs+hb)*W*(XX+YY); % XX = d^2F/dx^2 and YY = d^2F/dy^2

q(i)=trapz(y,trapz(x,Itmp).');

end

%

[ax,h1,h2]=plotyy(Freq,20*log10(UplotMag/1e-3),Freq,20*log10(1e1*q/1e-
3),'plot','plot');

set(h1,'color','red');

set(h2,'color','blue','linestyle','+');

set(get(ax(1), 'Ylabel'), 'String', 'Displacement (dB/1mm)');

set(get(ax(2), 'Ylabel'), 'String', 'Voltage (dBV)');

grid

title('Frequency Response of Plate vs. Shaped Sensor Output Charge')

xlabel('Frequency (Hz)')

legend('Plate Frequency Response','Sensor Output Charge')

```

## APPENDIX G

### ANSYS INPUT LOG FILE FOR SIMULATION OF CYLINDER

```
FINISH
/CLEAR,ALL
/CONFIG, NRES, 15000 ! Maximum number of results sets(subsets) allowed on the
results file.
/CWD,'f:\ShellPSD Verify2'
/TITLE, Dynamic Analysis
/PREP7

! Define variables for problem:
!-----
! INCHES TO METERS
*set,R,1.715/2*2.54/100
*set,Z,12*2.54/100
*set,B,0.035*2.54/100
*set,MYFRQ,1600
*set,MyLoadStep,250
*set,MYFORCE,-200
*set,NODES,861

! Define elements and material properties:
!-----
ET,1,SHELL63           ! Element Type
MP,EX,1,68.9E9         ! Young's Modulus
MP,PRXY,1,0.33        ! Poisson's Ratio
MP,DENS,1,2700         ! Density
R,1,B,B,B,B,0,0,      ! Thickness

! Geometry:
!-----
CSYS,1 ! Cylindrical Coordinates
N,1,R,0,0
N,21,R,0,Z
FILL
NGEN,41,21,1,21,1,,90/10
EN,1,1,2,23,22
EGEN,20,1,1
EGEN,40,21,1,21
```

```

! Boundary Conditions:
!-----
D,1,ALL,,841,21 ! Constrain left end
NSEL,S,,1,NODES, ! select nodes 1 - LAST
NSEL,ALL ! Reselect all nodes

NUMMRG,NODE
FINISH

/SOLU
ANTYPE,MODAL          ! DEFINE ANALYSIS TYPE AS MODAL VIBRATION
MODOPT,LANB,1500,0,MYFRQ, ,OFF
EQSLV,SPAR
MXPAND,6,,0
LUMPM,0
PSTRES,0
!OUTRES,NSOL,ALL
!MODOPT,LANB,6,0,750, ,OFF
SOLVE
FINISH

/POST1
SET,LIST !List mode frequencies
!rsys,1

/SOLU
ANTYPE,SPECTR          ! DEFINE ANALYSIS TYPE
SPOPT,PSD,6,ON          ! USE FIRST 6 MODES, CALC ELEM. STRESSES
PSDUNIT,1,FORCE          ! DEFINE TYPE OF PSD AS A FORCE SPECTRUM
DMPRAT,0.02              ! DMPRAT, RATIO
F,231,FY,MYFORCE
PSDFRQ,1,1,1.0,MYFRQ
PSDVAL,1,1.0,1.0        ! IN N**2/HZ
LVSCALE,1              ! USE AND SCALE THE LOAD VECTOR GENERATED
AT MODAL ANALYSIS
PFACT,1,NODE            ! Calculates participation factors
PSDRES,DISP,REL
PSDCOM
SOLVE
FINISH

/POST1
SET,3,1                ! ONE SIGMA DISPLACEMENT SOLUTION RESULTS
/VIEW,1,2,3,4
!rsys,1
!

```

```

!PLNSOL,U,X !Displays results as continuous contours.
!PRNSOL,U,X !Prints the nodal solution results.
!
PLNSOL,U,Y !Displays results as continuous contours.
PRNSOL,U,Y !Prints the nodal solution results.
!
!PLNSOL,U,Z !Displays results as continuous contours.
!PRNSOL,U,Z !Prints the nodal solution results.
!
FINISH

/SOLUTION
ANTYPE,HARMIC      ! REDEFINE ANALYSIS TYPE AND SOLVE AGAIN
HROPT,MSUP        ! USING MODE SUPERPOSITION HARMONIC ANALYSIS
HROUT,ON,OFF      ! PRINT AMPLITUDE & PHASE, CLUSTER FREQUENCIES
KBC,1
HARFRQ,1,MYFRQ
DMPRAT,0.02
NSUBST,MyLoadStep
SOLVE
FINISH

/POST26
FILE,,rfrq
PRCPLX,0 !Defines the output form for complex variables
!
NSOL,2,410,U,Y      !!!!!!!!!!!!!!!!!!!!!X or Y, node number,
!
PSDDAT,6,1,1.0,MYFRQ,1.0
PSDTYP,2
PSDCAL,7,2
PSDPRT
PRVAR,2,7
*GET,P,VARI,7,EXTREM,VMAX
*STATUS,PARM
/AXLAB,Y,PSD (M^2/HZ)
PLVAR,7
/GROPT,VIEW,ON

```



## APPENDIX H

### MATLAB CODE FOR CYLINDER

#### FRFProc\_01.m Matlab Code

```
clc

clear all

close all

%

% Data

LoadStep=250;

NumberOfPoints=441; %Actually 861 nodes,

    %21 overlap @ 0 and 360 degrees

Wy = fopen('FRFResult.txt','r');

for j=1:LoadStep;%LoadStep % Total displrecord

    for i=1:2018 % 303 line per record

        WyTmp=fscanf(Wy,'%g',[1 5]);

        Junk2=fscanf(Wy,'%s',2);

        RawData(i,:j)=WyTmp;

    end

    Junk3=fscanf(Wy,'%s',8);

end

% Extract Frequency
```

```

for i=1:LoadStep
    Freq(i)=RawData(2017,4,i);
end

% Extract U with column per load

for j=1:LoadStep
    RawDataV1=RawData(1:2017, :,j)';
    RawDataV(:,j)=RawDataV1(:);
end

% Extract UX per load

for j=1:LoadStep
    k=0;
    for i=1:12:10084
        k=k+1;
        UxReal=RawDataV(i,j);
        UxIm=RawDataV(i+1,j);
        Ux(:,k,j)=[UxReal;UxIm];
    end
end

% Extract UY per load

for j=1:LoadStep
    k=0;
    for i=3:12:10084
        k=k+1;

```

```

    UyReal=RawDataV(i,j);
    UyIm=RawDataV(i+1,j);
    Uy(:,k,j)=[UyReal;UyIm];
end
end
% Extract UZ per load
for j=1:LoadStep
    k=0;
    for i=5:12:10084
        k=k+1;
        UzReal=RawDataV(i,j);
        UzIm=RawDataV(i+1,j);
        Uz(:,k,j)=[UzReal;UzIm];
    end
end
end
% Check UX
for j=1:LoadStep
    Uplotx(:,j)=Ux(:,410,j); % at node 410
    UplotMagx(j)=sqrt(Uplotx(1,j)^2+Uplotx(2,j)^2);
end
% Check UY
for j=1:LoadStep
    Uploty(:,j)=Uy(:,410,j); % at node 410

```

```

    UplotMagy(j)=sqrt(Uploty(1,j)^2+Uploty(2,j)^2);
end
% Check UZ
for j=1:LoadStep
    Uplotz(:,j)=Uz(:,410,j); % at node 410
    UplotMagz(j)=sqrt(Uplotz(1,j)^2+Uplotz(2,j)^2);
end
% Create UX of magnitude
for j=1:LoadStep
    for i=1:NumberOfPoints
        Umx(1,i,j)=sqrt(Ux(1,i,j)^2+Ux(2,i,j)^2);
    end
end
% Create UY of magnitude
for j=1:LoadStep
    for i=1:NumberOfPoints
        Umy(1,i,j)=sqrt(Uy(1,i,j)^2+Uy(2,i,j)^2);
    end
end
% Create UZ of magnitude
for j=1:LoadStep
    for i=1:NumberOfPoints
        Umz(1,i,j)=sqrt(Uz(1,i,j)^2+Uz(2,i,j)^2);
    end
end

```

```

    end

end

% Organize Cartesian

Np=0;

k=0;

kk=1;

jj=1;

%

Wy = fopen('NLIST.lis','r');

junk1=fscanf(Wy,'%s',16);

while Np < NumberOfPoints

    for j=1:20

        if Np < NumberOfPoints

            k=k+1;

            CoTmp=fscanf(Wy,'%g',[1 4]);

            Coord(k,;,kk)=CoTmp;

            Np=Coord(k,1);

        end

    end

    junk2=fscanf(Wy,'%s',4);

end

fclose(Wy);

Cartesian=zeros(NumberOfPoints,6,LoadStep); % [X Y Z UX UY UZ]

```

```

for j=1:LoadStep
    Cartesian(:,1:3,j)=Coord(:,2:4);
    Cartesian(:,4,j)=Umx(1,,:j)';
    Cartesian(:,5,j)=Umy(1,,:j)';
    Cartesian(:,6,j)=Umz(1,,:j)';
end

% Convert to Cylindrical Coordinates
[Theta,R,Z]=cart2pol(Coord(:,2),Coord(:,3),Coord(:,4));
Cylindrical=zeros(NumberOfPoints,6,LoadStep);
for j=1:LoadStep
    for i=1:NumberOfPoints
        A=[cos(Theta(i,1)) sin(Theta(i,1)) 0;-sin(Theta(i,1)) cos(Theta(i,1)) 0;0 0 1];
        B=[Umx(1,i,j);Umy(1,i,j);Umz(1,i,j)];
        C(:,i,j)=A*B;
    end
end

for j=1:LoadStep
    Cylindrical(:,1,j)=R(:,1);
    Cylindrical(:,2,j)=Theta(:,1);
    Cylindrical(:,3,j)=Z(:,1);
    Cylindrical(:,4,j)=C(1,,:j)';

```

```

    Cylindrical(:,5,j)=C(2,,:j)';
    Cylindrical(:,6,j)=C(3,,:j)';
end

% Place into "Shell Coordinates"
NewDr=zeros(21,21,LoadStep);
i=1;k=21;
while i<=21
    j=1:LoadStep;
    NewDr(i,1:21,j)=Cylindrical(k-20:k,4,j); %for UR
    k=k+21;
    i=i+1;
end

NewDt=zeros(21,21,LoadStep);
i=1;k=21;
while i<=21
    j=1:LoadStep;
    NewDt(i,1:21,j)=Cylindrical(k-20:k,5,j); %for UT
    k=k+21;
    i=i+1;
end

```

```

NewDz=zeros(21,21,LoadStep);
i=1;k=21;
while i<=21
    j=1:LoadStep;
    NewDz(i,1:21,j)=Cylindrical(k-20:k,5,j); %for UZ
    k=k+21;
    i=i+1;
end
save DispData Cylindrical Cartesian NewDr NewDt NewDz Freq UplotMagx
UplotMagy UplotMagz
plot(Freq,UplotMagx,'r',Freq,UplotMagy,'b',Freq,UplotMagz,'g--')
grid
Title('FRF Plot of the Cylindrical Shell ')
xlabel('Frequency (Hz)')
ylabel('Displacement (db/1mm)')
legend('X Displacement','Y Displacement','Z Displacement')

```

### **DisplDerivative\_02.m Matlab Code**

```

clc
clear all
load DispData
%
N=size(NewDr);

```



```

L=12*2.54/100;

dz=L/20;

z=0:dz:L;

T=pi;

dtheta=T/20;

theta=0:dtheta:T;

% 2nd Derivatives

for j=1:N(3)

[Z,Theta]=gradient(NewDr(:,j)); % NewD in Cylindrical Coordinates

[ZZ,Junk1]=gradient(Z/dz);

[Junk2,ThetaTheta]=gradient(Theta/dtheta);

end

for j=1:N(3)

[Zt,dUT]=gradient(NewDt(:,j)); % NewD in Cylindrical Coordinates

end

for j=1:N(3)

[dUZ,Thetaz]=gradient(NewDz(:,j)); % NewD in Cylindrical Coordinates

end

save DisplDerivative ThetaTheta ZZ dUT dUZ NewDr NewDt NewDz N Theta Z dtheta

dz

```

### **Film\_Shape\_03.m Matlab Code**

```
close all
```

```

clear all

clc

%

load DispData

load DisplDerivative

%Calculate Film Shape Outline

hb=0.035*2.54/100;

hs=50e-6;

e31=12.367;

L=12*2.54/100;

r=1.75/2*2.54/100;

b=pi*r/2;

dx=L/20;

x=0:dx:L;

k=-b/(2*e31*(hb+hs));

F=k*(x.^2-L*x);

plot(x,F,x,-F)

title('Shaped Film for Cylindrical Shell')

xlabel('Length (m)')

ylabel('Width (m)')

axis equal

axis([0 L -b b])

```

```

%Create Film on Plate

y=b:-b/10:-b;

for i=1:21

    Y(:,i)=y;

end

W=ones(21,21);

for j=1:21

    for k=1:21

        if F(1,j)' < Y(k,j)

            W(j,k)=0;

        end

        if -F(1,j)' > Y(k,j)

            W(j,k)=0;

        end

    end

end

end

%Matchup Coordinate #s

save FilmShape e31 hb hs F y Y W

Fones=ones(21,1);

F1=Fones*b;

%plot(x,F1,x,-F1)

```

```
%title('Generic Film Shape for Cylindrical Shell')  
xlabel('Length (m)')  
ylabel('Width (m)')  
axis equal  
axis([0 L -b b])
```

#### **SensorOutput\_Generic\_04**

```
close all  
clear all  
clc  
%  
load DispData  
load DisplDerivative  
load FilmShape  
L=12*2.54/100;  
dz=L/20;  
z=0:dz:L;  
R=1.75/2*2.54/100;  
T=pi;  
dtheta=T/20;  
t=0:dtheta:T;  
%  
e33=0.06;
```

```

e32=0.06;

Se=T*R*L; %effective sensor electrode surface

rzs=R+hs/2+hb/4; %sensor location from neutral surface

rts=rzs;

%for trapz

zcoord=Cylindrical(1:21,3,1);

tcoord=zeros(1,21);

%for cos(theta)^2

k=1;

for i=1:21

Newtheta(i,:)=Cylindrical(k:k+20,2,1);

k=k+21;

end

i=1;k=1;

while i<=21

    tcoord(1,i)=Cylindrical(k,2,1);

    k=k+21;

    i=i+1;

end

%

for i=1:N(3)

[Z,Theta]=gradient(NewDr(:, :, i)); % NewD in Cylindrical Coordinates

[ZZ,Junk1]=gradient(Z/dz);

```

```

[Junk2,ThetaTheta]=gradient(Theta/dtheta);

%

[Zt,dUT]=gradient(NewDt(:, :, i)); % NewD in Cylindrical Coordinates

%

[dUZ,Thetaz]=gradient(NewDz(:, :, i)); % NewD in Cylindrical Coordinates

%

Itmp=-(e31*hs)/(e33*Se)*(e31*(dUZ-
rzs*ZZ)+e32*(dUT/R+NewDr(:, :, i)/R^2+rts*dUT/R^2-
rts*ThetaTheta/R^2))*(R^2*cos(Newtheta).^2);

% NewDr=UR

q(i)=trapz(tcoord,trapz(zcoord,Itmp.'.');

end

%q(z,t)=-(e31*hs)/(e33*Se)*INT {e31(dUz/dz-rzs*d^2Ur/dz^2)
    % +e32(dUt/Rdt+UR/R^2+rts*dUt/R^2dt-rts*d^2Ur/R^2dt^2)} dSe

[ax,h1,h2]=plotyy(Freq,20*log10((UplotMagy)/1e-3),Freq,20*log10(2*q/1e-
4),'plot','plot');

Title('Frequency Response of Shell vs. Generic Sensor Output Charge')

xlabel('Frequency (Hz)')

set(h1,'color','red');

set(h2,'color','blue','linestyle','+');

set(get(ax(1), 'Ylabel'), 'String', 'Displacement (dB/1mm)');

set(get(ax(2), 'Ylabel'), 'String', 'Voltage (dBV)');

```

```
grid
```

```
legend('Transverse Frequency Response','Sensor Output Charge')
```

### **SensorOutput\_Shaped\_05.m Matlab Code**

```
close all
```

```
clear all
```

```
clc
```

```
%
```

```
load DispData
```

```
load DisplDerivative
```

```
load FilmShape
```

```
L=12*2.54/100;
```

```
dz=L/20;
```

```
z=0:dz:L;
```

```
R=1.75/2*2.54/100;
```

```
T=2*pi;
```

```
dtheta=T/20;
```

```
%
```

```
e33=0.06;
```

```
e32=0.06;
```

```
Se=T*R*L; %effective sensor electrode surface
```

```
rzs=R+hs/2+hb/4; %sensor location from neutral surface
```

```
rts=rzs;
```

```

%for trapz

zcoord=Cylindrical(1:21,3,1);

tcoord=zeros(1,21);

%for cos(theta)^2

k=1;

for i=1:21

Newtheta(i,:)=Cylindrical(k:k+20,2,1);

k=k+21;

end

i=1;k=1;

while i<=21

    tcoord(1,i)=Cylindrical(k,2,1);

    k=k+21;

    i=i+1;

end

%

for i=1:N(3)

[Z,Theta]=gradient(NewDr(:, :, i)); % NewD in Cylindrical Coordinates

[ZZ,Junk1]=gradient(Z/dz);

[Junk2,ThetaTheta]=gradient(Theta/dtheta);

%

[Zt,dUT]=gradient(NewDt(:, :, i)); % NewD in Cylindrical Coordinates

%

```



```

[dUZ,Thetaz]=gradient(NewDz(:,:,i)); % NewD in Cylindrical Coordinates
%
Itmp=-((e31*hs)/(e33*Se))*W*((e31*(dUZ-
rzs*ZZ)+e32*(dUT/R+NewDr(:,:,i)/R^2+rts*dUT/R^2-
rts*ThetaTheta/R^2))*(R^2*cos(Newtheta).^2);
% NewDr=UR
q(i)=trapz(tcoord,trapz(zcoord,Itmp.'));
end
%q(z,t)=-((e31*hs)/(e33*Se))*INT{e31(dUZ/dz-rzs*d^2Ur/dz^2)
% +e32(dUt/Rdt+UR/R^2+rts*dUt/R^2dt-rts*d^2Ur/R^2dt^2)}dSe

[ax,h1,h2]=plotyy(Freq,20*log10((UplotMagy)/1e-3),Freq,20*log10(2.5*q/1e-
4),'plot','plot');
xlabel('Frequency (Hz)')
set(h1,'color','red');
set(h2,'color','blue','linestyle','+');
set(get(ax(1), 'Ylabel'), 'String', 'Displacement (dB/1mm)');
set(get(ax(2), 'Ylabel'), 'String', 'Voltage (dBV)');
grid
legend('Transverse Frequency Response','Sensor Output Charge')
Title('Frequency Response of Shell vs. Shaped Sensor Output Charge')

```

## APPENDIX I

### \*.RFRQ BINARY FILE FORMAT

#### SET 1: STANDARD ANSYS FILE HEADER

Each of the ANSYS program's binary files contains a standard, 100-integer file header that describes the file contents. The header contains the items listed below, always in the order shown below.

- |             |  |
|-------------|--|
| Item 1      | The file number  |
| Item 2      | The file format. This item has a value of 0 if the file is internal, or 1 if the file is external. |
| Item 3      | The time, in compact form  |
| Item 4      | The date, in compact form  |
|             | The units of measurement used. The value of this item is as follows:                               |
|             | · 0 for user-defined units   |
|             | · 1 for SI units   |
| Item 5      | · 2 for CSG units  |
|             | · 3 for British units (feet)   |
|             | · 4 for British units (inches)   |
| Item 10     | The ANSYS release level in integer form ("5.4" in character form)                                  |
| Item 11     | The date of the ANSYS release  |
| Items 12-14 | The machine identifier in integer form (three four-character strings)                              |
| Items 15-16 | The Jobname in integer form (two four-character strings)   |
| Items 17-18 | The ANSYS product name in integer form (two four-character strings)                                |
| Item 19     | The ANSYS special version label in integer form (one four-character string)                        |
| Items 20-22 | The user name in integer form (three four-character strings)                                       |
| Items 23-25 | The machine identifier in integer form (three four-character strings)                              |
| Item 26     | The system record size   |
| Item 27     | The maximum file length  |
| Item 28     | The maximum record number  |
| Item 29     | The number of processors assigned to this task   |

Items 41-60 The main analysis title in integer form (20 four-character strings)

Items 61-80 The first subtitle in integer form (20 four-character strings)

**SET 2 - RFRQ FILE HEADER**

- Record ID: N/A
- Type: Integer
- Number of Records: 1
- Record Length: 40

fun10	nmrow	nmatrx	nmode	numdof
maxn	wfmax	lenbac	0	ncumit
kan	0	0	0	0
0	0	0	0	0
ptrDOF	ptrDNC	ptrSTF	ptrMAS	ptrDMP
ptrFRQ	ptrDSP	0	0	0
0	0	0	0	0
0	0	0	0	0

where:

- fun10 - unit number (rfrq file is 10)
- nmrow - number of rows/columns in matrices
- nmatrx - number of reduced matrices on file
- nmode - number of modes extracted during modal analysis (or nmrow if reduced method)
- numdof - number of dofs per node
- maxn - maximum node number
- wfmax - maximum wavefront
- lenbac - number of nodes
- 0 - position not used
- ncumit - total number of iterations done during analysis
- kan - analysis type = 6 - reduced harmonic
- 0 - position not used
- 0 - position not used
- 0 - position not used
- 0 - position not used
- 0 - position not used
- 0 - position not used
- 0 - position not used
- 0 - position not used
- 0 - position not used
- ptrDOF - pointer to degree of freedom set used in model
- ptrDNC - pointer to nodal constraints
- ptrSTF - pointer to the reduced stiffness matrix
- ptrMAS - pointer to the reduced mass matrix
- ptrDMP - pointer to the reduced damping matrix or mode shapes

- ptrFRQ - pointer to the frequencies
- ptrDSP - pointer to the calculated displacements
- 0 - position not used
- 0 - position not used
- 0 - position not used
- 0 - position not used
- 0 - position not used
- 0 - position not used
- 0 - position not used
- 0 - position not used
- 0 - position not used
- 0 - position not used
- 0 - position not used
- 0 - position not used
- 0 - position not used

**SET 3 - ANALYSIS INFORMATION**

**Group 1 - Degrees Of Freedom Per Node** The following define the degree of freedom reference numbers:

UX = 1	UY = 2	UZ = 3	ROTX= 4
ROTY= 5	ROTZ= 6	AX = 7	AY = 8
AZ = 9	VX =10	VY =11	VZ =12
13-18 are spares	PRES=19	TEMP=20	VOLT=21
MAG =22	ENKE=23	ENDS=24	EMF =25
CURR=26	27-32 are spares		

**Group 2 - Nodal Equivalence Table**

- Record ID: N/A
- Type: Integer
- Number of Records: 1
- Record Length: lenbac

This table equates the actual node number to the number used for storage. (baclst (i),i=1,lenbac)

**Group 3 - Unused Record**

- Record ID: N/A
- Type: Double-precision
- Number of Records: 1
- Record Length: 10

The record contents are as follows:

1.0 0.0 0.0 0.0 0.0  
0.0 0.0 0.0 0.0 0.0

**Group 4 - Degree Of Freedom Set Used**

- Record ID: DOF
- Type: Integer

- Number of Records: 1
- Record Length: nmrow

The DOFs are calculated as  $(N-1)*\text{numdof}+\text{DOF}$ , where N is the position number of the node in the nodal equivalence table and DOF is the DOF reference number given above.

If the analysis uses the reduced method, the original DOF order (see next record) is rearranged so that DOFs having nodal constraints are listed first.

If the analysis uses the mode superposition method (using the reduced mode extraction technique), the DOF order is the same as the original order (see next record).  
(l(i),i=1,nmrow)

#### **Group 5 - Original Reduced Set Of Degrees Of Freedom Used**

- Record ID: N/A
- Type: Integer
- Number of Records: 1
- Record Length: nmrow+1

The DOFs are calculated as  $(N-1)*\text{numdof}+\text{DOF}$ , where N is the position number of the node in the nodal equivalence table and DOF is the DOF reference number given above.

If the analysis uses the reduced method, the original DOF order, plus the number of nodal constraints (nbcdsp), is stored. If the analysis uses the mode superposition method (using the reduced mode extraction technique), this record matches the previous record. The nmrow+1 entry will be zero. (lorig(i),i=1,nmrow),nbcds

#### **Group 6 - DOF of Nodal Constraints**

- Record ID: DNC
- Type: Integer
- Number of Records: 1
- Record Length: nbcdsp

This record is present only if the analysis uses the reduced method and nbcdsp > 0 (see record at ptrDOF). These numbers are the positions in the previous record of dofs with a nodal constraint. These are nodal constraints only on nodes that also are masters.  
(na(i),i=1,nbcdsp)

### **SET 4 - REDUCED MATRICES DATA**

#### **Group 1 - Reduced Stiffness Matrix**

- Record ID: STF
- Type: Double-precision
- Number of Records: 1
- Record Length: nbcdsp

Each row of the matrix is stored as a record. The matrix is present only if nmatrx > 0 and analysis is not using mode superposition method (using the subspace mode extraction method). Row order is the same as the DOF order in record at ptrDOF.  
(ak(i,j),i=1,nmrow)

#### **Group 2 - Reduced Mass Matrix**

- Record ID: MAS
- Type: Double-precision
- Number of Records: nmrow
- Record Length: nmrow

Each row of the matrix is stored as a record. The matrix is present only if nmatrx > 1 and analysis is not using mode superposition method (using the subspace extraction technique). Row order is the same as the DOF order in record at ptrDOF. (am(i,j),i=1,nmrow)

### **Group 3 - Reduced Damping Matrix Or Mode Shapes**

- Record ID: DMP
- Type: Double-precision
- Number of Records: varies
- Record Length: varies

If the analysis uses the reduced method, each record will be nmrow items in length. The reduced damping matrix is present only if nmatrx > 2. There will be nmrow records of this type stored here. Row order is the same as the DOF order in record at ptrDOF.

If the analysis uses the mode superposition method (using the reduced mode extraction technique), each record will be nmode items in length. These records contain mode shapes (eigenvectors) of the frequencies (eigenvalues) actually used in the harmonic analysis. There will be nmode records of this type stored here, with the first N records containing the mode shapes and the other records containing zeros, where N is the number of modes actually used in the harmonic analysis. Order corresponds to the DOF order given in record at ptrDOF. If the analysis uses the mode superposition method (using the subspace mode extraction technique), this record will not be present. (psi(i,j),i=1,nmrow) (or ac)

### **Group 4 - Frequencies Extracted From Modal Analysis**

- Record ID: FRQ
- Type: Double-precision
- Number of Records: 1
- Record Length: nmrow

This record is present only for analyses using the mode superposition method (using the reduced mode extraction technique). (freq(i),i=1,nmrow)

### **Set 5 - Calculated Displacements**

Located by the PTRDSP variable defined in Set 2.

Set 5 is repeated NCUMIT times.

### **Group 1 - Calculated Complex Displacements**

- Record ID: DSP
- Type: cmp
- Number of Records: ncumit
- Record Length: nmrow+5

The first nmrow entries are the displacements in the same order as the original set of DOFs (see record AFTER ptrDOF). For the last five entries:

**Real part**

1. frequency for these values
2. load step number
3. cumulative iteration number
4. zero
5. scale factor (zero if the analysis uses the reduced method)

**Imaginary part**

- frequency increment
- substep number
- zero
- zero
- zero

## REFERENCES

- [1] "Piezoelectricity." *Encyclopedia Britannica. Encyclopedia Britannica Online.*  
Encyclopedia Britannica Inc., 2012. Web. 01 Feb. 2012.  
<<http://www.britannica.com/EBchecked/topic/460053/piezoelectricity>>.
- [2] Kawai, H. "Piezoelectricity of Polyvinylidene Fluoride." Jap. J. Appl. Phys. 8 (1969):  
975-976.
- [3] Mason, W. P. "Piezoelectricity, Its history and Applications." J. Acoustics. Soc. Am.  
70. 6 (1981): 1561-1566.
- [4] Gautschi, G. Piezoelectric Sensorics. New York: Springer, 2006.
- [5] Hurlebaus, S., Stobener, U., and Gaul, L. "Vibration Reduction of Curved Panels by  
Active Modal Control." Computers and Structures 86 (2008): 251-257.
- [6] Xu, J., Dapino, M.J., Gallego-Perez, D., and Hansford, D. "Microphone Based on  
Polyvinylidene Fluoride (PVDF) Micro-Pillars and Patterned Electrodes." Sensors  
and Actuators A: Physical 153 (2009): 24-32.
- [7] Choi, Seung-Chan, Park, Jae-Sang, and Kim, Ji-Hawn "Active Damping of Rotating  
Composite Thin-Walled Beams using MFC Actuators and PVDF Sensors." Composite Structures 76 (2006): 362-374.
- [8] Song, Zhi-Guang, and Li, Feng-Ming "Active Aeroelastic Flutter Analysis and  
Vibration Control of Supersonic Composite Laminated Plate." Composite  
Structures 94 (2012): 702-713.



- [9] Zhao, Zhan, Li, Yaoming, Liang, Zhenwei, and Chen, Yi “Optimum Design of Grain Impact Sensor Utilising Polyvinylidene Fluoride Films and a Floating Raft Damping Structure.” Biosystems Engineering 112 (2012): 227-235.
- [10] Saviz, M. R., and Mohammadpourfard, M. “Dynamic Analysis of a Laminated Cylindrical Shell with Piezoelectric Layers under Dynamic Loads.” Finite Elements in Analysis and Design 46 (2010): 770-781.
- [11] Benedetti, I., Aliabadi, M. H., and Milazzo, A. “A Fast BEM for the Analysis of Damaged Structures with Bonded Piezoelectric Sensor.” Computer Methods in Applied Mechanics and Engineering 199 (2010): 490-501.
- [12] Alibeigloo, A., and Kani, A. M. “3D Free Vibration Analysis of Laminated Cylindrical Shell Integrated Piezoelectric Layers using the Differential Quadrature Method.” Applied Mathematical Modelling 34 (2010): 4123-4137.
- [13] Tzou, Horn S. Piezoelectric Shells: Distributed Sensing and Control of Continua. New York, New York: Springer, 1993.
- [14] Soedel, W. Vibrations of Shells and Plates, 3<sup>rd</sup> Edition. New York, New York: Marcel Dekker, 2004.
- [15] Tzou, H.S., Bergman, L.A. Dynamics and Control of Distributed Systems. Cambridge, New York: Cambridge University Press, 1998.
- [16] Lee, C. K., and Moon, F. C. “Modal Sensors/Actuators.” Trans. ASME 57 (1990): 434-441.
- [17] Zahui, Marcellin, and Wendt, Ron. “Development of Local Volume Displacement Sensors for Vibrating Plates.” Journal of Acoustical Society of America 116 (2004): 1-7.

- [18] Johnson, M. E., and Elliott, S. J. "Volume Velocity Sensors for Active Control." Proc. of the Institute of Acoustics 15 (1993): 411-420.
- [19] Rex, J. The Use of Integrated Transducers for the Active Control of Structural Vibration. M. Sc. Thesis, University of South Hampton, 1991.
- [20] ANSYS, Inc. (2007) ANSYS (Version 11.0) [Computer Program].
- [21] Aluminum 6061-T6; 6061-T651. MatWeb.com. MatWeb LLC. 3 September 2011.  
<http://www.matweb.com/search/DataSheet.aspx?MatGUID=1b8c06d0ca7c456694c7777d9e10be5b>
- [22] Bower, Allan F. "Vectors and Tensor Operations in Polar Coordinates." Applied Mechanics of Solids. 2008. 27 July, 2011  
<<http://solidmechanics.org/text/AppendixD.htm>>.
- [23] Zahui , Marcellin, and Cierzan, Marc "Computations of the Response of Thin Piezoelectric Films." *18<sup>th</sup> Congress on Sound & Vibration*.